UNIVERSIDAD COMPLUTENSE DE MADRID
FACULTAD DE CIENCIAS FÍSICAS
Departamento de Física de la Tierra y Astrofísica

TESIS DOCTORAL

The role of ice-ocean interactions in the past evolution of the Greenland Ice Sheet

El papel de la interacción hielo-océano en la evolución pasada del manto de hielo de Groenlandia

MEMORIA PARA OPTAR AL GRADO DE DOCTOR

PRESENTADA POR

Ilaria Tabone

Directores

María Luisa Montoya Redondo
Alexander Robinson

Madrid
Ed. electrónica 2019

The role of ice-ocean interactions in the past evolution of the Greenland Ice Sheet

El papel de la interacción hielo-océano en la evolución pasada del manto de hielo de Groenlandia

Memoria que presenta

Ilaria Tabone

para optar al grado de

Doctor en Ciencias Físicas

Directores:

Dra. María Luisa Montoya Redondo

Dr. Alexander Robinson

Departamento de Física de la Tierra y Astrofísica
Facultad de Ciencias Físicas
Universidad Complutense de Madrid

2019

This thesis was funded by the Spanish National Programme for the Promotion of Talent and Its Employability (grant no. BES-2015-074097) of the Spanish Ministry of Science and Innovation under the project MOCCA (Modelling Abrupt Climate Change, grant no. CGL2014-59384-R). All model simulations analysed in this thesis were performed in EOLO, the High-Performance computing of Climate Change of the International Campus of Excellence of Moncloa, funded by MECD (Ministerio de Eucación, Cultura y Deporte) and MICINN (Ministerio de Ciencias, Innovación y Universidades). Special thanks go to Catherine Ritz for providing the original ice-sheet-shelf model GRISLI (GRenoble Ice Shelf and Land Ice model), subsequently extended by our research group (PalMA) and named as GRISLI-UCM model to be used in this thesis.

A mamma e a papà

"Si...può...fare!!"

Dr. Frederick Frankenstein
in the italian dubbed version
of *Young Frankenstein* (1974)

Contents

Agradecimientos

En estos tres años he partido mi corazón, mente y cuerpo en tres lugares diferentes, a veces dos de los tres en el mismo sitio, pero nunca juntos a la vez. Ha sido ir y volver, despedirme y saludar, regar plantas y dejarlas morir. Pero ahí, en el medio, ha ocurrido algo que difícilmente olvidaré. Difícilmente me olvidaré de como pronto me sentí acogida cuando llegué a Madrid, con mis dos palabras de español que conocía y con una paella en familia a los tres días en España (y por eso, y por mucho más, Susana, gracias!). Difícilmente olvidaré tanto la extraordinaria tenacidad en el trabajo como el profundo cariño de la persona que más ha creído en mi y que ha sido un constante guía, científico y no, en esta aventura (sí, se puede, Marisa! Vaya poder de las mujeres!). Difícilmente olvidaré la pasión investigadora de Alex y Jorge, cada uno con su manera de mirar hacia lo desconocido, cada uno enseñándome lo bonito de hacer preguntas y ponerse en tela de juicio, siempre. Difícilmente olvidaré las infinitas experiencias que he compartido con mi compi de mesa, contestador personal de dudas e indispensable acompañante en este viaje madrileño. Aunque a veces parecimos a una pareja refunfuñona de 80 años, nada, nada de verdad habría sido igual sin ti, Javi, y tú lo sabes.

Difícilmente olvidaré las estupendas personas que han compartido esta aventura (y el mismo laboratorio) conmigo. Cris (R.), eres una crack, tienes el poder mágico de sacar lo bueno de cada situación y tienes una garra increíble. Nadie y nada te parará! Camilo, como lo he pasado bien con un par de cervezas hablando

de nuestros futuros y de nuestras vidas. Quizá que un día no te lleve a ver el giro de Italia! Elena, las charlas de las 8.30 al subir las persianas han sido un bálsamo para el alma. Eres una mujer increíble. Rubén, aunque últimamente no se te ve por el pasillo, nunca me olvidaré de tu espíritu sonriente y de la gran ayuda que me diste a lo largo de la tesis. Ha sido un pasaje de testimonio muy agradable. Etor, siempre disponible en ayudarte, gracias sobre todo por los últimos tiempos, tu apoyo ha sido indispensable para llegar aquí. Norman, tu pasión en el trabajo ha sido ejemplar. Has sido mi conexión entre dos países muy distintos y quizás que algún día no empecemos nuevamente nuestro tándem de idiomas (pero esta vez te enseño un poco de italiano!). Cris (V.), tu sonrisa alegra todo el despacho, eres un sol y me alegro de que el grupo pueda contar en ti. Jorge, gracias porqué con tus risas has sido una alegre presencia a mi lado, siempre disponible para distribuir un cacho de pan (jiji). Y fuera del laboratorio, gracias a Fidel, por transmitir tu inagotable curiosidad y por enseñar que siempre se puede ir más allá de la primera capa de cortinas, explorando con humildad y pasión.

En fin, difícilmente me olvidaré del apoyo de mis padres, porqué sin vosotros nada de todo esto habría sido posible. Gracias por haberme ayudado en milliones de maneras y, sobre todo, por haberme sujetado en los momentos más dificiles. Sé que dejarme volar fuera del nido no ha sido fácil.

Y difícilmente me olvidaré de ti, que eres el motor de esta locura. Desde cuando has cogido asiento en este viaje, has estado a mi lado, siempre, también cuando los 2000 km en el medio se ponían duros. Pero que dices, tal vez habrá llegado el momento de reducir nuestra huella de CO_2, no?

List of acronyms

AIS	Antarctic Ice Sheet
AMOC	Atlantic Meridional Overturning Circulation
BP	Before Present
D-O	Dansgaard-Oeschger (events)
EIS	Eurasian Ice Sheet
ELRA	Elastic Litosphere-Relaxing Asthenosphere
EMIC	Earth system Model of Intermediate Complexity
FIS	Fennoscandian Ice Sheet
GCM	Global Circulation Model
GHG	Greenhouse Gas
GI	Greenland Interstadial
GIA	Glacial Isostatic Adjustment
GrIS	Greenland Ice Sheet
HE	Heinrich Event
IRD	Ice-rafted debris
ka	Thousand years
LE	Large Ensemble
LGM	Last Glacial Maximum
LGP	Last Glacial Period
LHS	Latin Hypercube Sampling

LIG	Last Interglacial
LIS	Laurentide Ice Sheet
Ma	Million years
MIS	Marine Isotope Stage (e.g. MIS-3, Marine Isotope Stage 3)
MPT	Mid-Pleistocene Transition
NADW	North Atlantic Deep Water
NEEM	North Greenland Eemian Ice Drilling
NEGIS	North East Greenland Ice Stream
NGRIP	North Greenland Ice Core Project
NH	Northern Hemisphere
NSW	Northern Sourced Water
PD	Present Day
PDD	Positive Degree-Day
RMSD	Root Mean Square Deviation
SH	Southern Hemisphere
SIA	Shallow Ice Approximation
SLE	Sea Level Equivalent
SSA	Shallow Shelf Approximation
SST	Sea Surface Temperature
SSW	Southern Sourced Water

List of parameters

A_0	Arrhenius Law constant (3.985 $10^{-13}\, s^{-1}\, Pa^{-3}$ for T $\leq$ 263.15 K; 1.916 $10^{-13}\, s^{-1}\, Pa^{-3}$ for T $>$ 263.15 K))
b	Base of the ice sheet
B_{ref}	Reference submarine melting rate, assumed at the present-day
B	Basal melt (B_{gl}, at the grounding line; B_{sh}, below the ice shelf)
c	Heat capacity of ice (146.3 + 7.253 T[K]) J $kg^{-1}\, K^{-1}$)
g	Gravitational acceleration (9.81 $m\, s^{-2}$)
H	Ice thickness
M	Surface mass balance
n	Flow law stress exponent
N_{eff}	Effective pressure between ice and water pressure
p	Pressure
P_{ann}	Annual precipitation
Q	Activation energy (60 kJ mol^{-1} for T $\leq$ 263.15 K; 139 kJ mol^{-1} for T $>$ 263.15 K)
R	Universal gas constant (8.314 J $mol^{-1}\ K^{-1}$)
S	Ice surface elevation
T	Temperature
T_{f}	Temperature at the freezing point
T_{atm}	Atmospheric temperature
T_{ocn}	Oceanic temperature
t	time

U	Vertically-integrated ice horizontal velocity (=(U_x,U_y))
U_x	Vertically-integrated ice velocity u
U_y	Vertically-integrated ice velocity v
$\mathbf{v}$	Ice velocity (=(u, v, w))
α	Orbital climatic index
β	Millennial climatic index
ΔT_{atm}	Atmospheric temperature anomaly
ΔT_{ocn}	Oceanic temperature anomaly ($\Delta T_{\mathrm{ocn}}^{\mathrm{mil}}$, interstadial-stadial anomaly; $\Delta T_{\mathrm{ocn}}^{\mathrm{orb}}$, glacial-interglacial anomaly)
ϵ_{ij}	Strain rate
η	Ice viscosity
κ	Ice-ocean heat-flux coefficient (oceanic sensitivity)
κ_i	Heat conductivity of ice (9.828 exp(-0.0057 T[K]) W $m^{-1}\,K^{-1}$)
ρ	Density of the ice (910 kg m^{-3})
ρ_w	Density of seawater (1028 kg m^{-3})
$\boldsymbol{\sigma}$	Cauchy stress tensor
τ_{ij}	Deviatoric stress
τ_{b}	Basal drag term
τ_{d}	Driving stress

The role of ice-ocean interactions in the past evolution of the Greenland Ice Sheet - Summary

Introduction

Assessing the response of the Greenland Ice Sheet (GrIS) to climate variations is crucial to understand its past and constrain its future evolution under a changing climate. On one hand, the evidence of atmospheric warming observed since the last century has strongly demanded a major understanding of the sensitivity of the GrIS to atmospheric temperature variations, leading to extensive investigation of this topic in the past. On the other hand, only recent evidence connecting GrIS mass loss to warming North Atlantic waters has driven the attention to the potential role of a changing ocean on the GrIS evolution, an aspect that has been overlooked for a long time. Starting from this evidence, several studies have been dedicated to understanding the interactions between the current GrIS evolution and the surrounding ocean. However, although we are now aware that the ocean plays a non-negligible role in shaping the configuration of the present-day GrIS, many uncertainties remain about its role in the past. This lack of knowledge is mainly due to the scarcity of paleo records evidencing the interactions between the ocean and the GrIS in the past, and to the fact that for a long time the majority of modelling studies have considered these mechanisms as irrelevant in the GrIS paleo evolution. Therefore, whether, and to what extent, the ocean influenced the GrIS evolution in the past is still unclear and a further understanding of this issue is highly needed.

Aim of this thesis

This thesis aims to assess the role of past oceanic changes in the evolution of the GrIS throughout the last glacial cycle. Particularly, the goal of this study is to investigate the sensitivity of the GrIS to past temperature variations in the surrounding ocean at long (orbital) and short (millennial) timescales from a modelling perspective. To this end, paleoclimatic simulations of the GrIS are performed for the last glacial cycle using a three-dimensional, hybrid, thermo-mechanical ice-sheet-shelf model. The model includes a parameterisation of the submarine melting at the ice-ocean interface that specifically allows the study of the effect of changing oceanic temperatures on the GrIS paleo evolution. Through this parameterisation, paleo temperature variations used to force the model are transformed into melting at the marine margins. Investigating the GrIS response to these melting fluctuations facilitates assessment of the role of the ocean in the past evolution of the GrIS.

Results

A first study addresses the sensitivity of the GrIS to oceanic variations at glacial-interglacial timescales. Paleoclimate reconstructions suggest that the GrIS strongly responded to orbital-driven climate changes, expanding and retreating its margins throughout the glacial cycles. Moreover, the fact that the GrIS margins were fully in contact with the ocean during the last glacial period leads to the hypothesis that the ocean may have played a non-negligible role in the past. Starting from this assumption, transient simulations of the last glacial cycle are performed forcing the model by glacial-interglacial oceanic variations. Results suggest that the ocean forcing is a primary driver of the GrIS paleo evolution at glacial-interglacial timescales. Particularly, modelling the past GrIS evolution without considering the ocean limits the agreement between model simulations and paleo reconstructions, strongly suggesting the need for including oceanic variations in paleo ice-sheet modeling. A second study investigates the influence

of the ocean on the evolution of the North East Greenland Ice Stream (NEGIS) during the Last Glacial Period (LGP). The motivation of this work is found in a recent study suggesting that the NEGIS margin heavily fluctuated throughout the LGP and specifically retreated by more than 200 km during the Marine Isotope Stage (MIS) 3 from its maximum glacial position. This strong retreat was attributed to changes in the orbital and atmospheric conditions, however the potential role of the ocean was not taken into account. Here, high-resolution paleo simulations of the ice-sheet-shelf model are performed to investigate the effect that orbital-driven variations in the oceanic conditions may have had on this retreat. Results suggest that forcing the model with an active ocean not only allows the NEGIS margin position to fluctuate during the LGP, but triggers the NEGIS retreat during MIS-3 similarly to that suggested by reconstructions. Therefore, changes in the oceanic temperatures are fundamental in driving the NEGIS margin evolution through the past. A third study investigates the effect of millennial-scale oceanic variability on the GrIS evolution throughout the LGP. Proxy data from Greenland ice cores are in agreement suggesting about 25 abrupt warming events that the GrIS underwent during the LGP. These strong and rapid atmospheric temperature increases, named as Dansgaard-Oeschger (D-O) events, are associated with abrupt oceanic temperature changes. However, due to the scarcity of marine records reconstructing the GrIS evolution during D-O events, their limited interval of time within the LGP in which the data are available, and the almost-total absence of modelling studies tackling this issue, the response of the GrIS to these events is still unclear. Here, the effect of abrupt oceanic temperature changes during the LGP on the GrIS evolution is investigated from a modelling perspective. Model results suggest a strong senstivity of the GrIS to millenial-scale oceanic variations, indicating a potential ice volume fluctuation of more than 1.5 m in Sea Level Equivalent (SLE) during the most abrupt events associated with strong ice discharge into the ocean. These results therefore suggest a high influence of millennial-scale oceanic variability associated with D-O events on the evolution of the GrIS during the LGP.

Main conclusions

All the studies carried out for this thesis point at the ocean as a fundamental driver of the GrIS evolution throughout the past, at different timescales and spatial distances. Therefore, this thesis suggests that considering the ocean as an active forcing should be an essential requirement for those ice-sheet modelling studies that aim to investigate the GrIS paleo evolution.

El papel de la interacción hielo-océano en la evolución pasada del manto de hielo de Groenlandia - Resumen

Introducción

Comprender la respuesta del manto de hielo de Groenlandia (del inglés, Greenland Ice Sheet, GrIS) a las variaciones del clima es crucial para entender la evolución pasada de dicho manto así como para constreñir su evolución futura en un clima cambiante. Por un lado, la evidencia del calentamiento global observado desde el siglo pasado ha exigido una mejor comprensión de la sensibilidad del GrIS frente a las variaciones de la temperatura del aire, lo que ha llevado a investigar ampliamente este asunto en el pasado. Por otra parte, recientemente las observaciones han permitido relacionar la pérdida masiva de hielo del GrIS con el calentamiento del Atlántico Norte. Ello ha puesto el foco en el posible papel del océano en la evolución del GrIS, aspecto que se ha pasado por alto durante mucho tiempo. Desde entonces se ha hecho un esfuerzo importante por tratar de comprender mejor las interacciones entre el GrIS y el océano en la actualidad. Sin embargo, aunque ahora somos conscientes de que el océano desempeña un papel importante en la configuración actual del GrIS, subsisten todavía incertidumbres importantes acerca de su papel en el pasado. Este desconocimiento se debe principalmente a la escasez de registros paleoclimáticos que proporcionen evidencia acerca de las interacciones pasadas entre el océano y el GrIS, y al hecho de que durante mucho tiempo la mayoría de los estudios de modelización han considerado el papel de estos mecanismos como irrelevantes en la evolución

pasada del GrIS. Por lo tanto, aún no está claro en qué medida el océano influyó en la evolución pasada del GrIS.

Objetivo de la tesis

Esta tesis tiene por objeto evaluar el papel de los cambios oceánicos pasados en la evolución del GrIS a lo largo del último ciclo glacial. En particular, el objetivo es investigar la sensibilidad del GrIS a las variaciones de temperatura pasadas en el océano tanto a escalas de tiempo orbitales como milenarias, desde la perspectiva de la modelización. Para ello se realizan simulaciones paleoclimáticas del GrIS para el último ciclo glacial utilizando un modelo tridimensional, híbrido y termomecánico del manto de hielo. Este modelo cuenta con una parametrización de la fusión basal en la interfaz hielo-océano que, al ser función de la temperatura oceánica, permite estudiar el efecto de la variación de éstas en la evolución pasada del GrIS. La investigación de la respuesta del GrIS a estas fluctuaciones de fusión basal permite evaluar el papel del océano en la evolución pasada del GrIS.

Resultados

En primer lugar se aborda la sensibilidad del GrIS a las variaciones oceánicas en escalas de tiempo orbitales (ciclos glaciales). Las reconstrucciones paleoclimáticas sugieren que el GrIS respondió fuertemente a los cambios climáticos orbitales, sufriendo la expansión y retroceso de sus márgenes a lo largo de los ciclos glaciales. Además, el hecho de que los márgenes del GrIS estuvieran totalmente rodeados por océano en los periodos glaciales corrobora la hipótesis de que el océano pudo haber desempeñado un papel no despreciable en la evolución pasada del GrIS. Los resultados de las simulaciones transitorias del último ciclo glacial sugieren que el forzamiento oceánico es uno de los principales impulsores de la evolución pasada del GrIS a escala temporal glacial-interglacial. En particular, la modelización de la evolución del GrIS sin tener en cuenta el océano limita el acuerdo entre las

simulaciones y las reconstrucciones paleoclimáticas, lo que sugiere la necesidad de incluir variaciones oceánicas en la modelización del GrIS en el pasado.

En segundo lugar, se investiga la influencia del océano en la evolución del así llamado North East Greenland Ice Stream (NEGIS) durante el último periodo glacial (del inglés, Last Glacial Period, LGP). La motivación de este estudio procede de un trabajo reciente que sugiere que el margen del NEGIS fluctuó fuertemente a lo largo del LGP y específicamente retrocedió más de 200 km durante la Etapa Isotópica Marine (del inglés, Marine Isotopic Stage, MIS)-3 desde su posición glacial máxima. Este fuerte retroceso se atribuyó a cambios en las configuraciones orbital y atmosférica. Sin embargo el papel potencial del océano no se tuvo en cuenta. En el marco de esta tesis se han realizado simulaciones paleoclimaticas con alta resolución espacial para investigar el efecto que las variaciones orbitales en las condiciones oceánicas pueden haber tenido en este retroceso. Los resultados sugieren que forzar el modelo con un océano activo no sólo permite que la posición del margen del NEGIS fluctúe durante el LGP, sino que desencadena la retirada del NEGIS durante el MIS-3 de manera similar a la sugerida por las reconstrucciones. Por lo tanto, los cambios en las temperaturas oceánicas son fundamentales para impulsar la evolución pasada del margen de NEGIS.

Por último, se estudia el efecto de la variabilidad oceánica a escala milenaria en la evolución del GrIS a lo largo del LGP. Los datos procedentes de los núcleos de hielo de Groenlandia sugieren que el GrIS sufrió varios calentamientos abruptos durante el LGP, denominados eventos Dansgaard-Oeschger (D-O). Los eventos D-O están asociados a variaciones en la temperatura oceánica. Sin embargo, debido a la escasez de registros marinos que reconstruyan la evolución del GrIS durante los eventos D-O, y a la casi total ausencia de estudios de modelización que aborden este tema, la respuesta del GrIS a estos eventos aún no está clara. Aquí se investiga el efecto de los cambios abruptos de temperatura oceánica durante el LGP en la evolución del GrIS desde la perspectiva de la modelización. Las simulaciones sugieren una fluctuación del volumen de hielo de más de 1,5 m en Equivalente del Nivel del Mar (del inglés, Sea Level Equivalent, SLE) durante los eventos más abruptos, lo que indica una fuerte sensibilidad del GrIS a

las variaciones oceánicas a escala milenaria. Estos resultados demuestran que la variabilidad oceánica a escala milenaria asociada a los eventos D-O ha influido fuertemente en la evolución del GrIS en el LGP.

Conclusiones generales

Todos los estudios realizados en esta tesis apuntan al océano como motor fundamental de la evolución pasada del GrIS en diferentes escalas temporales y espaciales. Por lo tanto, esta tesis sugiere que la consideración del océano como un agente de forzamiento activo debería ser un requisito esencial para los estudios de modelización que aspiran a investigar la evolución pasada del GrIS.

Chapter 1
Introduction

This chapter briefly introduces different aspects of the Greenland Ice Sheet (GrIS) related to the topic of this Thesis. First, the overall characteristics of the present-day GrIS, such as its topography, ice amount and mass balance, are described (Section 1.1). Then, the past history of the GrIS is summarised focusing on the last glacial cycle (Section 1.2). The evidence for the past evolution of the GrIS both under orbital and under millennial-scale driven climatic changes is reviewed based both on proxies and numerical models. In Section 1.3, the present-day interaction between the GrIS and the surrounding ocean is described. Finally, the main motivations and overall structure of the thesis are described in Sections 1.4 - 1.5.

1.1 The Greenland Ice Sheet (GrIS)

The GrIS is the second largest polar ice sheet in the world, after the Antarctic Ice Sheet (AIS), with an estimated total ice volume of 2.99 $\pm$ 0.02 million km^3. Excluding floating ice shelves, the volume of the grounded ice is estimated to 2.93 $\pm$ 0.02 million km^3, which would correspond to a rise in the global mean sea level by 7.42 $\pm$ 0.05 m if totally melted away (Morlighem et al., 2017). The ice sheet covers roughly 80% of the Greenland continent and it extends from north to south spanning about 20° in latitude, covering a total area of about

1.7 million km^2 (Fig. 1.1, left panel). The topography below the ice sheet is very distinctive (Fig. 1.1, right panel). It contains both mountains of 2 km height along the eastern-southeastern side and a central-northern zone which lays below sea level. This is a result of the isostatic bedrock depression induced by the massive ice-sheet load, with a maximum ice thickness of more than 3 km at the central dome (Fig. 1.1, left panel).

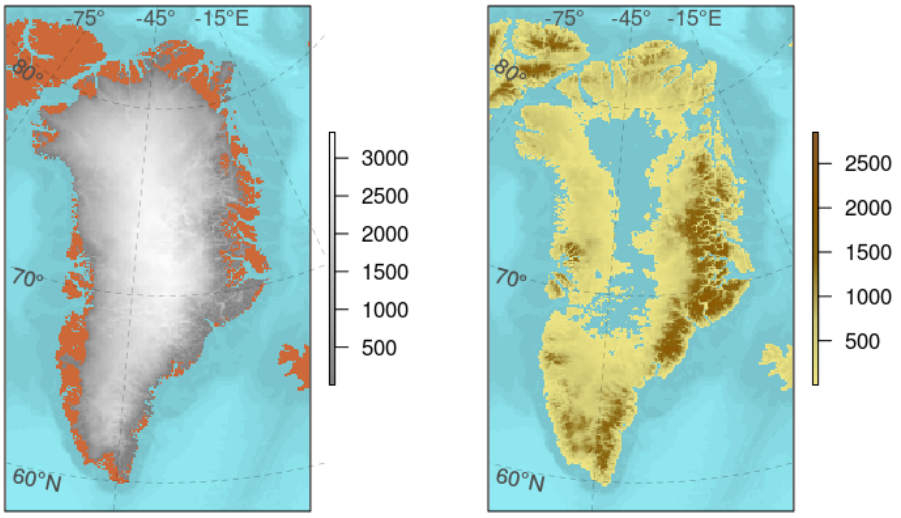

Fig. 1.1: Greenland ice thickness (m) (left) and topography elevation (m) (right).

The GrIS mass balance is the combination of surface mass balance, which is the balance between surface mass (primarily snow) accumulation and ablation, melting at the base of grounded ice, melting at the marine-terminating glaciers including sub-shelf melting below floating ice and melting at the calving fronts, and ice discharge into the ocean via iceberg calving. Ablation increases especially in the summer season, when low-elevated ice sheet regions close to the margin are subjected to atmospheric temperatures above 0°C (Cuffey and Paterson, 2010). The GrIS may end within ice-free land above-sea level or into the surrounding

ocean. The marine-terminating glaciers observed in Greenland at the present-day are of two kinds: glaciers connecting grounded ice to the ocean through floating ice shelves (e.g. Petermann Glacier, Nioghalvfjerdsbrae Glacier and Ryder Glacier, in the far North of the continent); outlet glaciers that end into the ocean through small floating tongues (e.g. Jakobshavn, Helheim, Kangerdlugssuaq glaciers) and tidewater glaciers, that flow out into narrow fjords showing a vertical calving front. In the former, ocean-induced melt is mainly of the form of submarine melt below the floating tongues and close to the grounding line; in the latter, melt mainly occurs in the form of frontal melt, a complex process that may depend on the water circulation within the fjord modulated by the formation of buoyant plums and the amount of open-ocean water entering the fjord (Straneo and Heimbach, 2013). The present-day Greenland topography does not allow for huge ice shelves, in contrast to the AIS, and only a few large floating tongues are observed, while the majority of marine outlet glaciers are today of the tidewater type. Nevetheless, both kinds of marine-terminating glaciers are subjected to strong interactions with the ocean and are responsible for ice discharge through calving (e.g. Straneo and Heimbach (2013), Hill et al. (2017)).

1.2 Paleo history of the GrIS

The onset of glacial inception in Greenland remains uncertain, but has been linked to the drop in atmospheric CO_2 concentration and temperatures that took place during the Late Pliocene, the period between ca. 5.3-2.5 million years before present (Ma BP, Lunt et al. (2008)). A first persistent large-scale Greenland glaciation likely took place around 3.3 Ma BP (Jansen et al., 2000), with a further expansion of the ice sheet at 2.7 Ma BP, as suggested by increasing ice rafted debris (IRD) contribution (Kleiven et al., 2002). However, more recent work suggests that the East GrIS existed over the past 7.5 Ma BP (Bierman et al., 2016) and that this region may have contributed to IRD deposition already before 30 Ma BP (Eldrett et al., 2007). Sediment records show that throughout the last ca. 5 Ma the Earth went through more than 150 transitions from relatively cold to

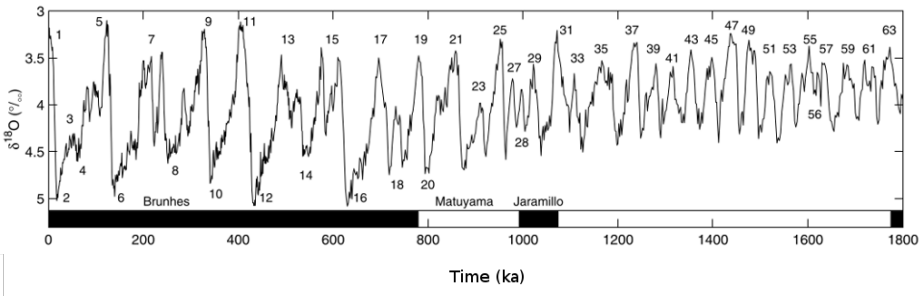

Fig. 1.2: Glacial-interglacial cycles for the last 1.8 Ma inferred from the stacked benthic δ^{18}O record built from 57 globally distributed records (from Lisiecki and Raymo (2005)).

relatively warm global climatic conditions that in the past ca. 2.5 Ma are identified with glacial-interglacial cycles (Lisiecki and Raymo, 2005). These fluctuations are ultimately driven by changes in the amount and latitudinal distribution of the incoming solar radiation as an effect of variations in the Earth's orbit (Paillard (2015) and references therein). Glacial periods are related to dry, cold climatic conditions, with low concentrations of greenhouse gases (GHGs) including CO_2 and global sea level, and high terrestrial ice volume, while interglacial periods are characterised by high global temperatures, precipitation, sea level, atmospheric GHGs concentrations and reduced ice volume (e.g. Bradley (1985); Crowley and North (1991); Paillard (2015) and many others). Glacial-interglacial cycles, especially in the last 1-1.2 Ma (since the Mid-Pleistocene transition, MPT), have been paced by a period of about 100 ka (Lisiecki and Raymo, 2005; Paillard, 2015) (Fig. 1.2). The GrIS is thought to have responded to these cycles through variations in its ice volume, with its margins likely moving back and forth across the ice-free land surface and the surrounding continental shelf (Alley et al., 2010). The paleo history of Greenland is also connected to the other Northern Hemisphere (NH) ice sheets that were present during glacial times: the Eurasian Ice Sheet (EIS), the Laurentide Ice Sheet (LIS), and the Fennoscandian Ice Sheet (FIS). Their extensive ice-sheet coverage responded to glacial-interglacial chang-

ing conditions leading to feedbacks on a global scale. However, this thesis does not aim to investigate their role for the GrIS and they are not discussed in detail.

1.2.1 Orbital-driven evolution in the last glacial cycle

Benthic-foraminifera δ^{18}O records from marine deposits allow partial reconstruction of the glacial-interglacial GrIS evolution during the last million years. However, for the last glacial cycle, Greenland ice cores provide some of the most accurate sources of paleoclimate reconstructions (e.g. Johnsen et al. (2001)), all of which extend back through the last glacial cycle. Since the last glacial inception (ca. 115 ka BP) to the present day we can reconstruct precise high-resolution climatic variations in Greenland from their δ^{18}O, methane and dust records (Andersen et al., 2004; Johnsen et al., 2001). More recently this has been possible also for the Last Interglacial period (LIG, ca. 130-116 ka BP, also called the Eemian in Europe) through the North Eemian (NEEM) ice core in northwest Greenland (NEEM, 2013). The time resolution of the data is highest within the uppers ice-core layers and decreases toward their deeper layers, as individual ice layers melt, merge, or fold, thereby increasing the uncertainty in the reconstructions (NEEM, 2013). Basal ice is thus stratigraphically disturbed. Thus, the precise age of the ice at the base of each sequence is difficult to establish, and the minimum age of the deepest ice and size of the interglacial ice sheet is a matter of debate (Yau et al., 2016a).

During the LIG, the global mean temperature is thought to have been 1.5-2°C above preindustrial values (Clark and Huybers, 2009). This anomaly was amplified in the Arctic and Greenland (e.g. Anderson et al. (2006)), where atmospheric temperature anomalies reached peaks of 8°C ± 4°C with respect to preindustrial values (NEEM, 2013; McFarlin et al., 2018). This temperature anomaly, along with surface elevation reconstructions indicating a decrease in ice thickness of 400 ± 350 m throughout the LIG, suggest that the GrIS during the Eemian was smaller than at the present day, but many uncertainties concerning its configuration remain. A comprehensive view of the GrIS at the LIG requires insight

from additional sources. To this end, sea-level reconstructions and model simulations are invaluable. It is estimated that during the LIG global sea level rose about 6-9 m above present day, 2-4 m of which have been associated to GrIS mass loss by various ice-sheet model studies (Dutton et al. (2015) and references therein). Models in the past have simulated a major disappearance of the South GrIS during the Eemian (Helsen et al., 2013; Otto-Bliesner et al., 2006; Tarasov and Peltier, 2002). However, it is now accepted that the southeast region was not completely ice free during the LIG, as older ice at the base of Dye 3 (Yau et al., 2016a) and isotopic ratios in sediments (Colville et al., 2011) suggest. These insights provide further constraints on the GrIS configuration at the LIG, and recent modelling studies suggest configurations that are likely more reliable than those implying a complete retreat in the south (Calov et al., 2015; Langebroek and Nisancioglu, 2016; Robinson et al., 2011; Stone et al., 2013; Yau et al., 2016b).

After 116 ka ago, the GrIS entered a glacial phase, with a decrease in atmospheric temperatures and culminating around the Last Glacial Maximum (LGM), ca. 21 ka BP, when it experienced temperatures lower than present day by almost 20°C (Kindler et al., 2014). Paleo reconstructions from moraines and other geomorphological records suggest that the ice sheet extended into the continental shelf (Stein et al., 1996; Winkelmann et al., 2010; Winsor et al., 2015), likely reaching the continental shelf break in some regions (Larsen et al., 2018; Dowdeswell et al., 2010). However, as for the LIG, a complete picture of the GrIS configuration during the LGM is not available. The problem has also been tackled through modelling, and one of the first studies suggested that the GrIS expanded up to the continental shelf, reaching the shelf break in some zones (Funder et al., 2011). However, those modelling results represent a minimum scenario, since at that time several proxy-derived evidence on the maximum area reached by the continental ice during the LGM were lacking. Recent work based on an ice-sheet model tested against new relative sea-level paleoreconstructions, and thus likely more reliable, show that the GrIS likely reached all-over the continental shelf break during the LGM, contributing to more than 4.5 m to the sea-level decrease

at this time compared to the present-day sea level (Lecavalier et al., 2014, 2017; Simpson et al., 2009).

1.2.2 Millennial-scale variability in the last glacial cycle

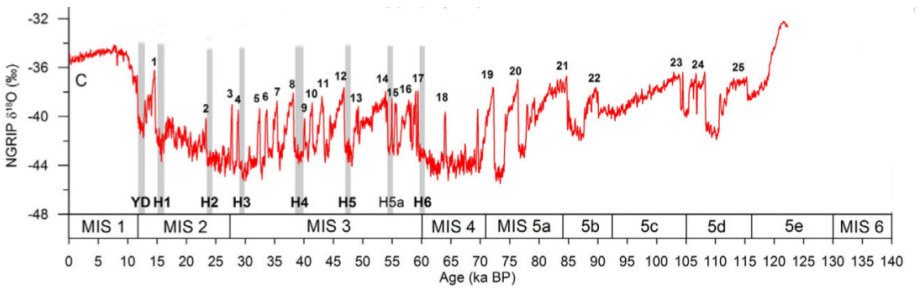

Fig. 1.3: Oxygen isotope δ^{18}O record from NGRIP ice core shown with Dansgaard-Oeschger interstadial events (numerals), Heinrich Events (in shaded grey and labeled) and Marine Isotope Stages (MIS) from Holocene (MIS-1) to MIS-6 (from Vasskog et al. (2015)).

Aside from orbital forcing driving the glacial cycles, the GrIS was also subjected to more rapid, millennial-scale climate variability during the past glacial cycle (Fig. 1.3). From the LIG to the LGM, the GrIS experienced 25 abrupt warming events, during which the temperature in Greenland increased by about 10-16°C (interstadial state) in typically less than 100 years, followed by a gradual decrease towards the background glacial (stadial) state and ending in a final, more rapid decrease (Kindler et al., 2014; Landais et al., 2004). These events represent some of the most abrupt climate changes of the Last Glacial Period (LGP). They were first discovered in the flickering of the δ^{18}O signal in the Greenland ice cores of GRIP (Dansgaard et al., 1993) and GISP2 (Grootes et al., 1993), and were dubbed Dansgaard-Oeschger (D-O) events by Wallace Broecker after the pioneering studies by Dansgaard et al. (1984) and Oeschger et al. (1983).

Each D-O cycle thus involves a transition from a stadial to an interstadial state and the subsequent return to the stadial state, and has a maximum duration of up to a few thousand years. Waiting times between events in order of decreasing probability are 1500, 3000 and 4500 years (Alley et al., 2001; Schulz, 2002).

D-O events have a global impact, as recorded by many proxies (Voelker, 2002). Apart from Greenland, strong imprints of D-O events are found in North Atlantic and Nordic Seas sediment cores (Bond et al., 1993; Kissel et al., 1999; Rasmussen et al., 1996, 2016; Shackleton et al., 2000; Sachs and Lehman, 1999; Voelker et al., 1997), but also in several tropical and subtropical speleothem proxy records from America and Eurasia (Asmerom et al., 2010; Cruz Jr et al., 2005; Kanner et al., 2012; Wagner et al., 2010), lake sediment archives (Benson et al., 1996; Stockhecke et al., 2014), and in South Atlantic marine records and AIS ice core records (Barbante et al., 2006; Brook et al., 2005; Buizert et al., 2015). The flickering between stadial and insterstadials during the LGP is also associated with changes in GHG concentrations and dust content (see the recent review by Brook and Buizert (2018)). In particular, methane (CH_4) covaries with the GrIS ice-core temperature record, indicating an origin in tropical wetlands (Loulergue et al., 2008; Rhodes et al., 2015). Although the relative phasing between some of these records might be subject to uncertainties, that between Greenland and Antarctic ice core records is extremely well constrained, thanks to synchronisation using well-mixed gases as stratigraphic markers, including methane and the isotopic composition of trapped O_2 (Barbante et al., 2006; Bender et al., 1994; Blunier and Brook, 2001; Brook et al., 2005; Buizert et al., 2015). The pattern that emerges is that of a bipolar seesaw behaviour between Greenland and Antarctica. D-O events are thus centred in the North Atlantic, and with NH and Southern Hemisphere (SH) records generally in phase with Greenland and Antarctica, respectively. Exceptions to this rule are sometimes found and suggested to reflect a global signal, generally covarying with Antarctica (e.g. Barker and Knorr (2007)). Greenland ice-core records show higher dust concentrations in stadials as compared to interstadials indicative of higher aridity and dust storm activity in East Asian deserts (Schüpbach et al., 2018). Analogously, Antarctic ice core records show higher dust loading during cold periods and lower dust

loading during warm periods, indicative aridity and storm activity variations in southern South America (Schüpbach et al., 2013). However, the opposed, global influence of Antarctica cannot be ruled out even in Greenland ice core records (Barker and Knorr, 2007).

This worldwide imprint of D-O events points to a mechanism involving a strong North-South Hemisphere connection. Almost three decades ago, Broecker et al. (1985) andBroecker (1998) proposed reorganisations of the Atlantic Meridional Overturning Circulation (AMOC) as the underlying mechanism. This paradigm, with certain nuances (Alley et al., 2001), has since robustly survived based on increasing evidence both from proxy data and models (Alley, 2007; Clark and Mix, 2002; Lynch-Stieglitz, 2017; Rahmstorf, 2002). D-O stadials are associated with relatively weak northward transport of heat in the Atlantic Ocean; interstadials instead are associated with an invigoration of this northward heat transport. Each corresponds to what has sometimes been called the weak and strong modes of the AMOC. Perturbations of the poleward, cross-equatorial heat transport have opposite temperature effects on both hemispheres, with the Antarctic counterpart damped by a large heat reservoir, commonly assumed to be the Southern Ocean (Stocker and Johnsen, 2003). Note that in addition, throughout the LGP an additional mode within this paradigm is the off mode, associated with North Atlantic Deep Water (NADW) shutdowns during so-called Heinrich Events (HEs) that took place during some of the D-O stadials (Rahmstorf, 2002) and during which massive iceberg release from the LIS took place (Hemming, 2004), but these are not within the scope of this thesis.

The direct evidence from AMOC proxy records to support this connection is less clear for D-O events than for the deglaciation and the HEs as recently reviewed by Lynch-Stieglitz (2017). This is generally because of the low resolution of the deep records as compared to the surface records from the same cores, attributed to low abundances of benthic foraminifera. For example, high δ^{13}C values in benthic records are associated with the input of northern sourced waters (NSWs) with relatively high biological productivity and sequestration of respired ^{12}C in organic matter as compared to relatively low δ^{13}C values in southern sourced waters (SSWs). Heinrich stadials are clearly registered, for example,

in benthic δ^{13}C records off the Iberian margin (Shackleton et al., 2000; Skinner and Elderfield, 2007) as excursions toward low values typical of SSWs, but similar excursions were not seen in other D-O stadials. Nd isotope ratios (143Nd/144Nd, expressed as ϵNd) is used as a proxy for changes in sources and mixing of water masses. This ratio is imprinted on waters through the exchange with terrigenous sediments (high or more radiogenic in SSW, low or less radiogenic in NSW) and recorded in precipitates on foraminifera and sediments. Thus, this tracer allows the determination of changes in the relative contributions of waters originating from the North Atlantic and the Southern Ocean. A deep marine Nd-isotope record in the South Atlantic shows excursions to lower values generally during interstadials, but not every D-O event was resolved (Piotrowski et al., 2008). Nevertheless, more recently, a sediment core from the tropical Atlantic off Brazil showed fluctuations between high and low δ^{13}C values at interstadials and stadials, respectively, for all but the shortest D-O stadials (Burckel et al., 2015). A high-resolution benthic δ^{13}C record from the Bermuda Rise also clearly shows similar variations for all D-O events except for the very shortest ones (Henry et al., 2016). In contrast, 231Pa/230Th is a measure of the overall strength of the AMOC. 231Pa and 230Th are particle reactive. The difference in the timescale of removal causes a preferential export of 231Pa to the Southern Ocean by deep currents within the AMOC. Thus low 231Pa/230Th in the deep Atlantic is an indicator of a strong, large-scale AMOC. In turn, high 231Pa/230Th approaching the production ratio (0.093) indicates a weak or collapsed AMOC. Henry et al. (2016) found changes in 231Pa/230Th over most of the D-O events, supporting D-O variability in the AMOC. Another recent sediment core from the Bermuda Rise containing both ϵNd and 231Pa/230Th shows evidence for D-O variability in both proxies as well, and continuous NADW formation with a strong contribution of NSW, with strongly disrupted NADW only during the peak glacial conditions (Böhm et al., 2015). Another related proxy is based on the concentrations of carbonate ions in the deep Atlantic, controlled by dissolution resulting from a larger influence of more corrosive SSWs as compared to NSWs or by enhanced terrigenous input. To the extent that these are not affected by enhanced dilution by terrigenous sediments, they can be interpreted as a measure of the relative

proportion of NSW and SSW. Lower values during stadials are attributed to increased dilution resulting from the replacement of NSW with SSW. Recently, Gottschalk et al. (2015) obtained records from several related proxies not affected directly by increased dilution by terrestrial material; good correspondence was found with many of the D-O events from the Greenland ice core, lending further support to the paradigm that links the origin of these abrupt warming events with reorganisations of the AMOC. Finally, changes in the magnetic mineral content in sediment cores are interpreted as changes in the efficiency of the transport of the magnetic particles by deep currents from the source to the site of deposition, because magnetic minerals mainly originate from one common source area, the Nordic basaltic region. Variations in the magnetic mineral content in several cores in the North Atlantic have been interpreted as reflecting increased deep flow from the Nordic Seas during D-O interstadials (Kissel et al., 1999).

Model studies also provide strong support to the former paradigm. Conceptual models were used to show that there may be two stable states of the North Atlantic circulation, leading to speculations that perturbations could result in transitions between them (Stommel, 1961). Climate models of a wide range of complexity, from Earth System Models of Intermediate Complexity (EMICs) to comprehensive Global circulation models (GCMs), in which the strength of the AMOC and/or the location of NADW formation is perturbed, can reproduce the bipolar seesaw pattern (e.g. Bagniewski et al. (2017); Ganopolski and Rahmstorf (2001); Menviel et al. (2014); Schmittner et al. (2003); Sévellec and Fedorov (2015); Skinner and Elderfield (2007); Stouffer et al. (2006); Vellinga and Wood (2002)). The proposed mechanisms include: variations in the freshwater budget, possibly as a result of meltwater release from NH ice sheets (Ganopolski and Rahmstorf, 2001; Menviel et al., 2014); the effect of changes in the height of the LIS on the path of the polar jet-stream (Zhang et al., 2014a), or of sea-ice variations in North Atlantic and Nordic Seas (Li et al., 2005, 2010), or of fluctuations between ice shelf and sea ice (Petersen et al., 2013); progressive CO_2 atmospheric variations (Zhang et al., 2017) due to changes in atmospheric heat transport (Wang et al., 2015) or through combined changes in wind and atmospheric CO_2 amount driven by the Southern Ocean (Banderas et al., 2015;

Zhang et al., 2017), and stochastic atmospheric forcing originating in the tropics (Kleppin et al., 2015; Steffensen et al., 2008). Recently, D-O events have been explained as the result of a non-linear internal salt oscillator in the Atlantic (as originally proposed by Broeker et al. (1990)) without the need to invoke any external forcing (Peltier and Vettoretti, 2014; Vettoretti and Peltier, 2016, 2018). It has also been suggested that AMOC variability may be a result of D-O events rather than their cause, e.g. via abrupt changes in sea-ice conditions and stratification in the Nordic and/or Labrador Seas (Kleppin et al., 2015). However, it cannot be excluded that the occurrence of D-O events is eventually due to a combination of several or all of these mechanisms. For instance, recent work has suggested that D-O events could be related to the coupled effect of freshwater flux discharge and sea-ice cover variation in the North Atlantic acting as an amplifier (Jensen et al., 2018).

Regardless of their ultimate cause, improving our understanding of the response of ice sheets to such abrupt past climate changes is important for a number of reasons (Alvarez-Solas et al., 2017). Constraining freshwater inputs into the North Atlantic is crucial for a better understanding of the driving mechanisms of glacial abrupt climate changes (Rasmussen and Thomsen, 2004), since meltwater discharge from the ice sheets surrounding the Nordic Seas is often implied as a cause of ocean instabilities. Precursor events could possibly have originated from the European and Icelandic ice sheets (Grousset et al., 2000; Scourse et al., 2000). Yet, the exact role of NH ice sheets in this mechanism is far from clear. Whether they are the cause of AMOC reorganisations through iceberg discharge, or only passively respond to oceanic changes, or form part of a more complex mechanism in the climate system as a feedback to ocean-circulation, ice-sheet and sea-ice variations, is still unclear.

In particular, very little is known about the potential effects of oceanic variations associated with D-O events on iceberg discharges from Greenland. Paleo records do not provide much information about the GrIS dynamic evolution throughout the LGP, apart from some evidence of IRD deposition toward locations not so far from the Greenland coasts (Andrews et al., 2012, 2017; Bond and Lotti, 1995; Darby et al., 2002; Jonkers et al., 2010; Stein et al., 1996; Van Krev-

eld et al., 2000; Verplanck et al., 2009). Although this evidence does not give a complete view of the role and evolution of the GrIS during the LGP, it suggests that regions of the ice sheet were responsible for iceberg discharge and that these were likely subjected to ice-mass variations and grounding-line migration during D-O events. Moreover, recent paleo reconstructions explicitly affirm that the ocean temperature increase played a fundamental role in the GrIS retreat in the last deglaciation (Jennings et al., 2017). Oceanic temperature variations associated with D-O events during the LGP and recently inferred from various sediment cores in North Atlantic suggest interstadial-stadial anomalies ranging typically from 2-6°C to a maximum of 15°C (Jensen et al., 2018). It is likely that such temperature variations in the ocean have had a non-negligible effect on the GrIS evolution during the LGP. However, investigations in that sense have not been carried out so far.

1.3 The interactions between ocean and ice in the present-day GrIS

The oceanic circulation in the surroundings of Greenland is part of the North Atlantic cyclonic subpolar gyre (Langehaug et al., 2012) and the northward warm current of the Nordic Seas (the Greenland, Iceland and Norwegian Seas). Cold and fresh polar waters flow northward along the western coast of Greenland, through Baffin Bay and southward along its eastern coast, through Denmark Strait and the Greenland Sea continental shelf; warm and saline surface waters flow southward along the Irminger Sea and northward through the Nordic Seas, although less close to the coast than the waters coming from the Arctic ocean (Fig. 1.4). The GrIS is also located close to regions of convection in the Labrador and Irminger Seas and deep water formation in the Nordic Seas where all of whih contribute to North Atlantic Deep Water (NADW) formation (Kuhlbrodt et al. (2007) and references therein).

Recent observations suggest that the ocean plays an important role for the GrIS in the present. It has been widely proved that the GrIS has lost mass at an

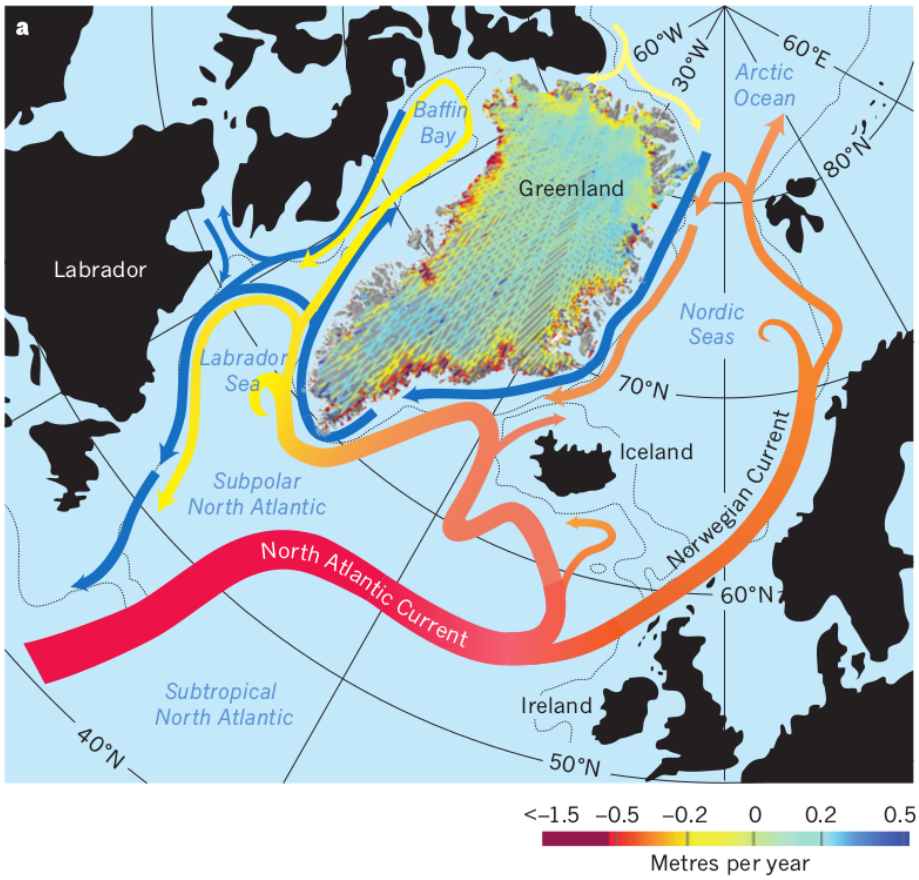

Fig. 1.4: Sketch of the ocean circulation around Greenland. Currents from the North Atlantic are from red to yellow; currents from the Arctic ocean are in blue. Rates of the recently observed dynamical thinning are superimposed on the GrIS (from Straneo and Heimbach (2013)).

accelerated rate during the past decades (e.g. Rignot et al. (2011); Sasgen et al. (2012); Shepherd et al. (2012); Velicogna et al. (2014); Zwally et al. (2011)). The GrIS mass loss increased from $0.09 \pm 0.11\ mm\,a^{-1}$ (1992-2001) to $0.59 \pm 0.16\ mm\,a^{-1}$ over 2002-2011 (Vaughan et al., 2013) and from 2010 to 2014, at a rate of $0.89 \pm 0.09\ mm\,a^{-1}$ (Yi et al., 2015). The first attempts to estimate the variations in the Greenland ice-mass balance were made more than 15 years ago (Krabill et al., 2000; Mitrovica et al., 2001), already showing at that time that the GrIS was losing mass through thinning along the coastline (Rignot and Jacobs, 2002). However, for many years it has been thought that the dominating cause of this ice-mass loss was the atmospheric temperature increase observed in Greenland (Box et al., 2009; Hall et al., 2008; Hanna et al., 2008; Tedesco et al., 2016), which enhanced surface ablation and meltwater runoff and increasing crevassing and calving at the ice front. In the last years the scientific community has started to consider the role of the ice-ocean interactions on this mass loss. Recent work suggests that from 1991 to 2015 the GrIS contributed to $0.47 \pm 0.23\ mm\,a^{-1}$ of sea level rise as a result of both enhanced surface melting and ice discharge to the ocean from marine-terminating glaciers (van den Broeke et al., 2016). This estimate is in agreement with abundant observations of acceleration and retreat of various marine-terminating glaciers all around Greenland during the last 20 years. The first evidence of rapid thinning along the GrIS coastlines was found in southeast Greenland during the 1990s (Krabill et al., 1999; Rignot et al., 2004), then at the Jakobshavn Isbrae in the west in the late 1990s (Joughin et al., 2004; Luckman and Murray, 2005) and also in the Helheim Glacier in the east at the beginning of the 2000s (Howat et al., 2005). In the following years, these and other outlet glaciers were monitored, providing an extensive amount of information about their increasing rate of acceleration and retreat (e.g. Carr et al. (2013); Howat et al. (2007); Joughin et al. (2012b); Moon and Joughin (2008); Moon et al. (2015); Murray et al. (2015); Rignot and Kanagaratnam (2006); Stearns and Hamilton (2007); Straneo et al. (2016); Sutherland and Straneo (2012)). The underlying mechanism is thought to be related to the increase of submarine melting along the grounding line and at the glacier front as a result of the intrusion of warmer Atlantic waters into the fjords (Straneo et al., 2012). The enhanced basal

melting at the outlet glaciers contributes to their acceleration, increasing ice-mass discharge into the ocean and potentially triggering their grounding-line retreat. This mechanism is thought to be the dominant driver of enhanced ice discharge in Jakobshavn Isbrae (Holland et al., 2008a; Rignot et al., 2010), where increasing basal melting rates were already observed in 1985 (Motyka et al., 2011), in Sermilik fjord in southeast Greenland (Straneo et al., 2010), in northwest Greenland glaciers (Larsen et al., 2016; Wood et al., 2018), and generally across the GrIS (Straneo and Heimbach, 2013; Morlighem et al., 2017). This melting-acceleration mechanism has been corroborated using numerical models such as that of Rignot et al. (2016) for glaciers in the west GrIS, or that of Rignot and Mouginot (2012) to explain the acceleration and retreat of GrIS glaciers during the 1990s. Other modelling studies suggest that retreat of marine terminating glaciers will continue in the future as a consequence of warmer oceanic temperatures (Fürst et al., 2015; Nowicki et al., 2013), which could especially control the ice discharge in vulnerable areas due to their bathymetry (Morlighem et al., 2017). This future ice mass loss is expected to contribute to a sea level rise relative to the 20^{st} century between 90 and 280 mm by 2100 in the worst-case scenario (RCP8.5) (Bindschadler et al., 2013; Church et al., 2013; Clark et al., 2015).

The combination of these lines of evidence with model results and future projections clearly suggests that the ice-ocean interaction is playing and will continue to play a fundamental role in the GrIS evolution in the near future. Obviously the interaction between the GrIS and the surrounding ocean depends on the GrIS configuration at a certain time: while in a warm state, such as the present day, the oceanic effect is limited to those areas whose outlet glaciers terminate onto the ocean, a glacial state associated with a fully marine-based GrIS would lead to strong ice-sheet-ocean interactions all around the ice sheet.

1.4 Motivations

Understanding the interactions between the GrIS and the other components of the climate system is fundamental to predict its future evolution under a chang-

ing climate. The unquestionable sensitivity of the GrIS to the rising atmospheric temperatures observed in the last century has been known for a long time. Countless studies concerning the interaction between the GrIS and the current changing atmosphere have been carried out for more than a decade (e.g. Box et al. (2006, 2012); Hanna et al. (2008); Peano et al. (2017); Tedesco et al. (2011)). While most scientific effort has been devoted to address this issue, the interaction between the GrIS and the ocean has not received as much attention. This changed during the late 1990s, when the first observations of accelerated retreat of some GrIS outlet glaciers led the scientific community to start looking at the ocean as a possible driver of changes in the GrIS configuration (e.g. Holland et al. (2008a); Howat et al. (2005); Joughin et al. (2004); Krabill et al. (1999); Motyka et al. (2011); Rignot et al. (2004); Rignot and Kanagaratnam (2006)). Since then, several studies, through both instrumental observations and numerical models, have been dedicated to understand the implications that a changing ocean may have on the present-day GrIS evolution (e.g. Carr et al. (2013); Cai et al. (2017); Lea et al. (2014); Millan et al. (2018); Rignot et al. (2016); Rignot and Mouginot (2012); Straneo and Heimbach (2013); Wood et al. (2018)). We now understand that the interaction between the GrIS and the surrounding ocean needs to be tackled comprehensively to assess the present and future of the GrIS.

Despite our progressively increasing understanding of the role of the ocean in the current evolution of the GrIS, we still know very little about this issue in the past. Several interrelated reasons may explain this lack of information. First, for many years it has been thought that the main factors responsible for the past GrIS evolution were changes in insolation and in the atmosphere. Thus, scientific attention has been driven in that direction. Interest in the GrIS-ocean interaction, motivated by recent observations of enhanced mass discharge in Greenland, is still incipient and the field has to be amply investigated yet. Second, paleoclimatic evidence of the interaction between the GrIS and the ocean for the past is very scarce. Useful information mainly relies on marine sediment cores of the North Atlantic, which provide sequences of past ice discharge from the GrIS during the LGP. However, the collection of available cores is limited and the precise chronology of these pulses is difficult to obtain, limiting our understanding

of the relevant ocean-related mechanisms that play a potential role in these ice discharges. Third, the necessary and complementary modelling work has for a long time underestimated the role of the ocean in the GrIS. While ice-ocean interactions in Antarctica have been widely studied from a modelling perspective, the GrIS ice-sheet modelling community has just started to force models with a transient ocean, and the majority of studies that investigated the past GrIS evolution through ice-sheet models either prescribed the oceanic conditions (Tarasov and Peltier, 2002), or completely neglected basal melting below ice shelves (eg. De Boer et al. (2013); Huybrechts (2002); Lecavalier et al. (2014); Ritz et al. (1996); Robinson et al. (2011); Stone et al. (2013)), or, still, when the ocean was considered as an active forcing in the model, the parameterisation used to solve the ice-ocean interaction was too rudimentary (Bradley et al., 2018). All these reasons have so far prevented a focused and deep understanding of the potential role of the ocean on the past GrIS evolution, and many are the scientific questions related to this topic that are still unresolved. This work particularly focuses on three of them:

Is the GrIS sensitive to oceanic temperature variations at glacial-interglacial timescales? To what extent is the GrIS affected by these during glacial periods?

Geomorphological data from moraines and model reconstructions agree in suggesting that the GrIS was fully marine based at the LGM, expanding onto the continental shelf and likely reaching the continental-shelf break, where waters of the open ocean flow at different depths. This fact suggests a potential strong role of the ocean in the GrIS evolution at glacial times. However, the evidence on the response of the GrIS due to changes in the ocean following past glacial-interglacial transition are scarce, and limited to specific areas of the GrIS. Particularly, no model has precisely investigated the impact of oceanic variations linked to orbital changes. Many of them were either absent in submarine melting parameterisations or were too simplistic, and the effect of glacial-interglacial

oceanic temperature changes on the GrIS still remains incomplete. Therefore a modelling study that aims to explore the problem is highly needed.

Can oceanic temperature variations during the LGP be responsible for fluctuations of the NEGIS marine margin and specifically trigger its retreat during MIS-3?

The NEGIS, which is the largest ice stream in the GrIS, has recently suffered enhanced ice mass loss from its terminating glaciers, which have retreated inland at an accelerated rate. This is partly due to the observed increasing temperatures of the North Atlantic waters, that promoted ice discharge, favoring the grounding line of the outlet glaciers to retreat inland. In parallel, a recent study based on proxy data suggests that the GrIS margin at the NEGIS also fluctuated during the LGP, and strongly, between a substantial inland retreat by more than 30 km in the central part of the LGP (MIS-3) to a considerable advance by ca. 200 km offshore over the continental shelf during the LGM. The proposed causes for this strong fluctuation are changes in the atmospheric conditions and insolation variations. However, the ocean was not brought into play. Assessing this problem from a modelling perspective and exploring the potential role of LGP oceanic variations in this anomalous retreat can improve our understanding of this phenomenon.

Is the GrIS sensitive to millennial-scale variability in the ocean related to D-O events?

IRD deposition records from sediment cores in the North Atlantic can help to reconstruct the history of certain GrIS regions for the LGP. Thanks to available records, we know that the GrIS has likely responded to millennial-scale variability, at least in certain coastal regions. However, assuming that the reconstruction of

time and source of IRD deposition is correct, these data are punctual and the evolution of the whole GrIS during the LGP remains poorly constrained. In parallel, very few ice-sheet models have investigated the response of the GrIS to D-O events: most focused on the whole NH ice sheet system with little to no focus on GrIS dynamics, and those that focused on the GrIS did not consider millennial-scale variability in the ocean. Therefore, so far, many uncertainties remain concerning the GrIS response to millennial-scale variability, especially in relation to potentially abrupt oceanic temperature changes during D-O events. Also, many several modelling and proxy studies suggest a link between D-O events and AMOC reorganisations, and the role of the NH ice sheets is still debated. Thus, the response of the GrIS to those oceanic temperature variations may contribute to better understanding the potential impact that the discharge of icebergs coming from the GrIS may have on these variations in oceanic currents. A modelling study tackling these problems is thus required.

1.5 Overview

The main goal of this thesis is to investigate the sensitivity of the GrIS to past changes in the oceanic conditions. Specifically, this work aims to investigate the role of past oceanic temperature variations in the paleo evolution of the GrIS at both orbital and millennial timescales from a modelling perspective, focusing on the last glacial cycle. An introduction to the past history of the GrIS, to its past and present interactions with the surrounding ocean, and the scientific questions that this thesis aims to address has been presented in this chapter. Chapter 2 describes the fundamental tool used in this thesis, a three-dimensional hybrid ice-sheet-shelf model, which has been extended in several ways during the past years in our research group with the final aim of developing a new ice-sheet-shelf model. During these years I particularly contributed to calibrate the model, test the sub-marine melting parameterisation and implement the code with small changes to facilitate simulation analysis. The model comprehensively solves the dynamics of the GrIS, from the grounded slow-moving ice to the floating ice shelves which

were likely present during cold glacial times. A submarine melting parameterisation has been implemented as a boundary condition into the model to study the impact of past changing oceanic temperatures associated with climate variations at different timescales on the evolving GrIS. The scientific results achieved in this thesis are organized in three main studies tackling the problem at various time and/or spatial scales (Chapters 3 - 5). Each work has been also summarised in a published (or near-published) scientific article. Finally, the results presented in this thesis are discussed in Chapter 6 and the main scientific conclusions are given in Chapter 7.

Scientific publications related to this thesis:

The sensitivity of the Greenland Ice Sheet to glacial-interglacial oceanic forcing (published)

Tabone, I., Blasco, J., Robinson, A., Álvarez-Solas, J. and Montoya, M., 2018: The sensitivity of the Greenland Ice Sheet to glacial-interglacial oceanic forcing. *Climate of the Past*, **14**, 455-472. DOI 10.5194/cp-14-455-2018.

This work, whose main contents are reported in Chapter 3, addressed the sensitivity of the GrIS to oceanic temperature variations driven by orbital changes during the past two glacial cycles. Paleoclimate reconstructions suggest that the GrIS has responded to climate variations at glacial-interglacial timescales with large changes in ice volume, with its margins expanding and retreating throughout the glacial cycles. It is therefore very likely that the ocean played a fundamental role in the past evolution, especially during cold periods, when the GrIS expanded onto the continental shelf and its overall margins were surrounded by the ocean. To study the response of the GrIS under these conditions, paleoclimatic simulations for the last two glacial cycles have been performed using the GRISLI-UCM ice-sheet-shelf model. The model has been forced by oceanic temperature anomalies scaled between glacial and interglacial states that evolve

following the glacial cycles. These temperatures variations are perceived by the model as changes in the submarine melting rate at the GrIS marine margin, which has been parameterised as a linear function of oceanic temperature anomalies. Transient simulations showed that the GrIS strongly reacted to the increasing oceanic forcing applied to the model. Although the sensitivity to increasing atmospheric temperatures is not investigated in this work, oceanic forcing is found to be a fundamental driver of the GrIS paleo evolution, which not only influenced the GrIS retreat during warm interglacial periods, but triggered the grounding-line advance during cold glacial times. The results of these experiments suggest that in absence of an active ocean, paleo-atmospheric forcing alone is not sufficient to reproduce the expected glacial GrIS configuration. This work therefore showed the necessity of considering the ocean as an active forcing in paleo ice-sheet modeling.

Submarine melt rate as a potential trigger of grounding-line retreat during Marine Isotope Stage 3 (submitted)

Tabone, I., Robinson, A., Álvarez-Solas, J. and Montoya, M., 2018: Submarine melt rate as a potential trigger of grounding-line retreat during Marine Isotope Stage 3. *submitted to The Cryosphere.*

This work, whose main contents are reported in Chapter 4, examined the effect of the ocean on a specific area of the GrIS, the Northeast Greenland Ice Stream (NEGIS) during Marine Isotope Stage 3 (MIS-3), ca. 60-25 ka before present(BP). The specific motivation of this work was a recent study suggesting that the NEGIS margin strongly fluctuated during the LGP. Specifically, it suggests that during MIS-3 the marine margin retreated to a position more than 200 km further inland than the maximum glacial configuration. The suggested explanations for this retreat are related to variations in the atmospheric patterns and orbital-driven changes in the insolation. However, the potential role of the ocean in this margin fluctuation had not been considered. In this work, the possibility that the ocean could have played an important role in the retreat of

the marine margin of the NEGIS region during the LGP, or in constraining its location, was investigated through a sensitivity study. High-resolution transient simulations are performed with the GRISLI-UCM model for the whole LGP, focusing the analysis on the time period corresponding to MIS-3. As in the other two papers, variations in the temperature were transmitted to the model through the submarine melting parameterisation at the marine margin. As a sensitivity study, it focused on how different orbital-driven oceanic temperature variations could affect the evolution of the NEGIS margins. It is showed that in the absence of oceanic forcing, the NEGIS grounding line was free to advance over the continental shelf for the whole LGP. Conversely, for sufficiently high oceanic forcing, the NEGIS margin was able to roughly reproduce the retreat during MIS-3, and to advance again at the glacial maximum, as suggested by proxy-derived reconstructions. This study therefore showed that changing oceanic temperatures act as drivers of the NEGIS margin evolution, suggesting that the role of the ocean in controlling the margin advance and retreat is important.

Impact of millennial-scale oceanic variability on the Greenland Ice Sheet evolution throughout the Last Glacial Period (in review)

Tabone, I., Robinson, A., Álvarez-Solas, J. and Montoya, M., 2018: Impact of millennial-scale oceanic variability on the Greenland Ice Sheet evolution throughout the Last Glacial Period. *Climate of the Past Discussion*, DOI 10.5194/cp-2018-129, in review.

This work, whose main contents are reported in Chapter 5, investigated the impact of millennial-scale oceanic variations on the GrIS evolution during the Last Glacial Period (LGP), which started about 120 ka BP and ended around 20 ka BP. These oceanic variations are associated with glacial abrupt climate events. These dramatically changed the temperatures in Greenland and had strong imprints all over the world. However, how the GrIS responded to them is far from being understood. Here, this problem was tackled by studying the effect of oceanic variations at millennial timescales on the GrIS evolution from a modelling perspective. To

do so, the GRISLI-UCM ice-sheet-shelf model was used, as in the first two papers, here forced not only by orbital but also by millennial-scale temperature variations in the ocean. Changes in oceanic temperatures are transferred to the model through the same submarine melting parameterisation used in the previous papers. To study the sensitivity of the GrIS to a broad number of possible oceanic perturbations, a large ensemble of paleoclimatic transient simulations were performed, each one representing a specific evolution of the submarine melting at the marine margin throughout the LGP. The direct comparison between the only-orbital ocean driven simulations and those expressing both orbital and millennial oceanic perturbations helped us to understand the millennial-scale oceanic variability effect on the GrIS evolution during the LGP. The results showed that the GrIS is very sensitive to the applied millennial-scale temperature changes in the ocean, potentially contributing to more than 1.5 m SLE to sea-level rise due to these abrupt warming events. In addition, the effect of these oceanic variations on the ice-sheet interior was analysed and it was found that such changes in the submarine melting rates lead to a dynamical adjustment of the ice sheet up to several tens of kilometers away from the marine margin. Moreover, these results were compared to proxy data, founding that the millennial-scale variability in the ocean alone could have been responsible for episodes of intense ice discharge into the ocean during the LGP. These results suggest that the GrIS evolution could have been deeply affected by changes in the oceanic temperatures at millennial timescales.

Chapter 2
The GRISLI-UCM ice-sheet-shelf model

The GRISLI-UCM model is a three-dimensional, hybrid thermomechanical ice-sheet-shelf model capable of resolving dynamics and thermodynamicss of continental ice sheets. Its basics follow those of the widely known ice-sheet-shelf GRISLI (GRenoble Ice-Shelf and Land Ice) model (Ritz et al., 2001), which has been used to study the past evolution of the GrIS (Ritz et al., 1996; Quiquet et al., 2013; Peano et al., 2017), the AIS (Ritz et al., 2001; Philippon et al., 2006; Alvarez-Solas et al., 2011a) and the NH ice sheets (Peyaud et al., 2007; Colleoni et al., 2014; Alvarez-Solas et al., 2011b, 2013; Banderas et al., 2018). GRISLI-UCM is an extension of GRISLI, mainly concerning parameterisations of boundary conditions such as basal dragging below the ice streams and submarine melting.

In this chapter the fundamental equations governing the dynamics of the continental ice sheets are described together with the approximations used in hybrid models, such as GRISLI and GRISLI-UCM, following Greve and Blatter (2009) and Blatter et al. (2011). Then the main novel features in the GRISLI-UCM are described, focusing on the submarine melting rate parameterisations implemented at the ice-ocean interface, particularly relevant for this thesis. The description of the model features that follow those of the GRISLI model are taken from Ritz et al. (2001) and from the user guide of the GRISLI model (Colleoni, 2015). These publications are also useful for any further detail that the reader wants on processes that are here not described, e.g. basal hydrology.

2.1 Fundamental equations and approximations

The fundamental equations that describe the dynamics of a continental ice sheet are obtained from the laws of conservation of mass, momentum and energy.

$$\frac{\partial \rho}{\partial t} + \boldsymbol{\nabla} \cdot (\rho \mathbf{v}) = 0 \tag{2.1}$$

$$\rho \frac{d\mathbf{v}}{dt} = \boldsymbol{\nabla} \cdot \boldsymbol{\sigma} + \rho \mathbf{g} \tag{2.2}$$

$$\rho c \left(\frac{\partial T}{\partial u} + \mathbf{v} \cdot \boldsymbol{\nabla} T \right) = \boldsymbol{\nabla}(\kappa_i \boldsymbol{\nabla} T) + Q_i \tag{2.3}$$

where ρ stands for the ice density, $\mathbf{v}$ for the ice velocity, $\boldsymbol{\sigma}$ for the Cauchy stress tensor, $\mathbf{g}$ for the gravitational acceleration, c for the heat capacity of ice, T for the ice temperature, κ_i for the thermal conductivity of ice, and Q_i for the deformational heat. The Cauchy stress tensor $\boldsymbol{\sigma}$, given an orthonormal basis, can be expressed as

$$\boldsymbol{\sigma} = \begin{pmatrix} \sigma_{xx} & \sigma_{xy} & \sigma_{xz} \\ \sigma_{yx} & \sigma_{yy} & \sigma_{yz} \\ \sigma_{zx} & \sigma_{zy} & \sigma_{zz} \end{pmatrix} \tag{2.4}$$

where the diagonal elements (σ_{xx}, σ_{yy}, σ_{zz}) can be interpreted as normal stresses (perpendicular to the cut plane), and the six off-diagonal elements are called shear stresses. Since ice can be considered as an incompressible fluid with a constant density, the mass conservation equation Eq. 2.1 can be rewritten as

$$\boldsymbol{\nabla} \cdot \mathbf{v} = \frac{\partial u}{\partial x} + \frac{\partial v}{\partial y} + \frac{\partial w}{\partial z} = 0 \tag{2.5}$$

where u, v, and w are the x, y and z components of the velocity vector $\mathbf{v}$, respectively. By vertically integrating Eq. 2.5 and taking into account mass balance at the ice surface as well as melting at the base leads to a prognostic equation for the ice thickness H:

$$\frac{\partial H}{\partial t} + \frac{\partial (H \cdot U_x)}{\partial x} + \frac{\partial (H \cdot U_y)}{\partial y} = M - B. \tag{2.6}$$

Here, M is the surface mass balance calculated subtracting surface ablation of ice to the ice accumulation (snow) and B is the melting (or refreezing) rate at the base of grounded or floating ice. U_x and U_y are the vertically-integrated horizontal velocities u and v, respectively, thus $H \cdot U_x$ and $H \cdot U_y$ are the x and y components of the ice volume flux. Melting of grounded ice occurs when ice is at the pressure melting point and it is related to the amount of friction and geothermal heat flux exchanged between the ice at the bed and the bedrock. Melting at the base of ice shelves mainly depends on temperature of the ocean, salinity and the heat flux exchanged between the ocean and the ice base. The evolution of the ice thickness H therefore depends on the boundary conditions at the ice surface and ice base and the ice flux (Fig. 2.1), mainly described by calving at the ice front. Therefore, an ice sheet is in equilibrium if the mass gained via accumulation or refreezing is compensated by surface or basal melting or ice discharge.

The momentum balance equation (Eq. 2.2) can be rewritten neglecting the acceleration term, which can be ignored considering the spatial and temporal scales typical of an ice sheet. The resulting steady-state (Stokes) equation is therefore:

$$\boldsymbol{\nabla} \cdot \boldsymbol{\sigma} + \rho \mathbf{g} = 0 \tag{2.7}$$

Each element of the Cauchy stress tensor $\boldsymbol{\sigma}$ can be expressed separating the deviatoric part τ from its isotropic pressure p as:

$$\sigma_{ij} = \tau_{ij} - p \tag{2.8}$$

This formulation is useful for expressing the constitutive relation for polycristalline ice that relates the deviatoric stresses to the deformation (strain) rates, as:

$$\tau_{ij} = 2\eta\dot{\epsilon}_{ij} \tag{2.9}$$

where strain rates are defined as

$$\dot{\epsilon}_{ij} = \frac{1}{2}\left(\frac{\partial u_i}{\partial x_j} + \frac{\partial u_j}{\partial x_i}\right). \tag{2.10}$$

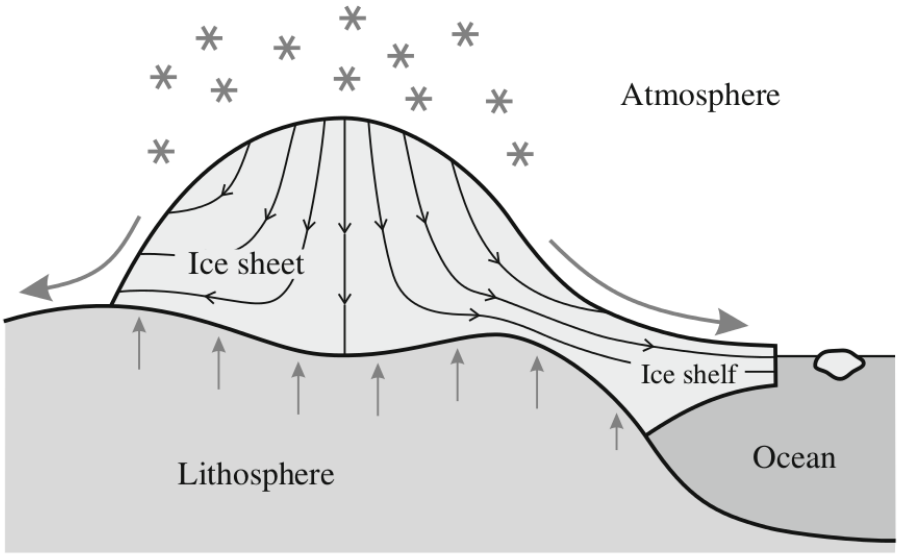

Fig. 2.1: Sketch of a continental ice sheet interacting with the climate system (Greve and Blatter, 2009). The atmosphere interacts with the ice sheet through surface ablation and accumulation. The base of grounded ice sheets interacts with the underneath lithosphere mainly via geothermal heat flux exchanged with the bedrock. Floating ice shelves interact with the ocean through calving and submarine melting.

Here, η is the viscosity. The relation that links ice rheology to ice deformation is the Glen's flow law:

$$\dot{\epsilon} = A(T,p)\tau_*^{n-1}\tau \tag{2.11}$$

where $\dot{\epsilon}$ is the effective strain rate, and $A(T,p) = A(T^*) = A_0\, exp^{Q\,/\,RT^*}$ is defined by the Arrhenius law. A_0 is a constant, Q is called activation energy, R is the universal gas constant and T^* is the temperature relative to the pressure melting point. τ_* is the effective shear stress defined as $\tau_* = \sqrt{\frac{1}{2}\sum_{ij}\tau_{ij}^2}$; n is the flow law stress exponent and is typically set to three (Cuffey and Paterson, 2010).

The full-Stokes model equation is given by combining Eq. 2.7 - 2.10. Resolving explicitly this problem has a huge computational cost. However, considering that the flow of continental ice sheets involves large spatial scales and long timescales, the complexity of the Stokes problem can be reduced by approximations depeding on the local ice flow regime. Essentially, the dynamics of an ice sheet can be described considering the ice sheet divided in regions driven by a particular flow regime (Fig. 2.2). Grounded ice sheets frozen at the bedrock are slow-moving areas driven by flow resulting from ice deformation; ice streams are grounded areas of fast-moving ice usually located in regions where the bedrock sediment is saturated by water, which promotes high velocities; floating ice shelves move under plug flow and no friction at the base, and are sustained by ice flowing from grounded ice. The location where ice starts to float is called the grounding line. The dynamics of these regions can be solved by applying specific approximations of increasing complexity that neglect different components of the stress tensor. Those used by the GRISLI-UCM model are the Shallow Ice Approximation (SIA), valid for large grounded areas moving under a slow flow and the Shallow Shelf Approximation (SSA), valid for fast floating areas moving under plug flow. Both are derived from the Hydrostatic Approximation.

2.1.1 Hydrostatic approximation

This approximation is based on the assumption for which the horizontal extent of the ice sheets (L $\approx$ 1000 km) is much larger than their vertical extent (H $\approx$ 1km). This assumption is valid for both grounded ice sheets and floating ice shelves and allows for neglecting all the shear stresses σ_{xz} and σ_{yz}, which are small compared to the vertical normal stresses σ_{zz} in Eq. 2.7. The equation of the vertical momentum is then reduced to:

$$\frac{\partial \sigma_{zz}}{\partial z} = \rho g \tag{2.12}$$

which integrated gives the hydrostatic equation:

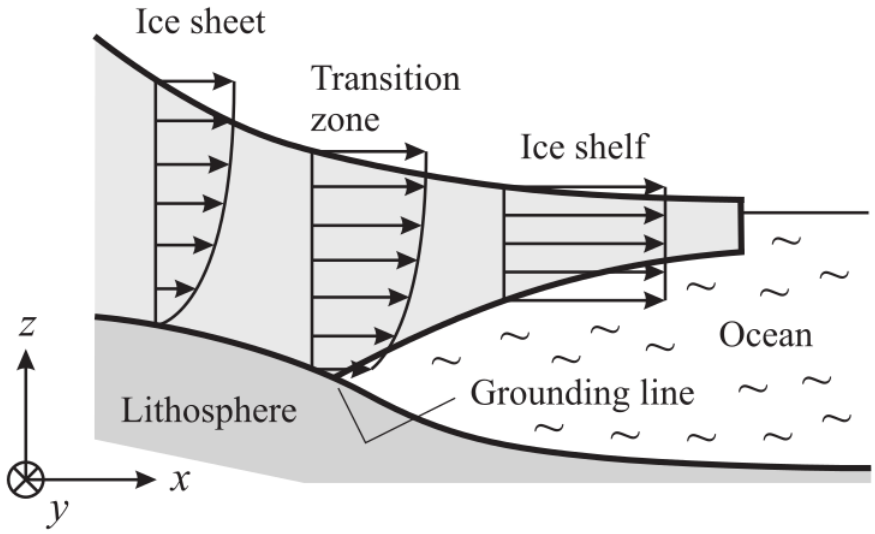

Fig. 2.2: Sketch of different flow regimes in a continental ice sheet (Greve and Blatter, 2009), where grounded ice is mainly driven by vertical shear (SIA condition), and ice shelves are in plug flow (SSA condition). Transition zones, such as ice streams, are found in proximity of the grounding line where grounded ice is connected to floating ice and the two flow regimes cohexist.

$$\sigma_{zz} = \rho g(H - z) \tag{2.13}$$

and the equations for the force balance (Eq. 2.7) reduces to:

$$\begin{aligned} 2\frac{\partial \tau_{xx}}{\partial x} + \frac{\partial \tau_{yy}}{\partial x} + \frac{\sigma_{xy}}{\partial y} + \frac{\partial \sigma_{xz}}{\partial z} &= \rho g \frac{\partial S}{\partial x} \\ 2\frac{\partial \tau_{yy}}{\partial y} + \frac{\partial \tau_{xx}}{\partial y} + \frac{\sigma_{xy}}{\partial x} + \frac{\partial \sigma_{yz}}{\partial z} &= \rho g \frac{\partial S}{\partial y} \end{aligned} \tag{2.14}$$

where τ_{xx} and τ_{yy} are the deviatoric stresses and S is the ice surface elevation. Substituting the Glen's flow law in Eq. 2.14, it returns the two-equations system of the hydrostatic approximation:

$$
\begin{aligned}
4\frac{\partial}{\partial x}\left(\eta\frac{\partial u}{\partial x}\right)+2\frac{\partial}{\partial x}\left(\eta\frac{\partial v}{\partial y}\right)+\frac{\partial}{\partial y}\left(\eta\left(\frac{\partial u}{\partial y}+\frac{\partial v}{\partial x}\right)\right)+\frac{\partial}{\partial z}\left(\eta\left(\frac{\partial u}{\partial z}+\frac{\partial w}{\partial x}\right)\right)=\rho g\frac{\partial S}{\partial x}\\
4\frac{\partial}{\partial y}\left(\eta\frac{\partial v}{\partial y}\right)+2\frac{\partial}{\partial y}\left(\eta\frac{\partial u}{\partial x}\right)+\frac{\partial}{\partial x}\left(\eta\left(\frac{\partial u}{\partial y}+\frac{\partial v}{\partial x}\right)\right)+\frac{\partial}{\partial z}\left(\eta\left(\frac{\partial v}{\partial z}+\frac{\partial w}{\partial y}\right)\right)=\rho g\frac{\partial S}{\partial y}
\end{aligned}
\tag{2.15}
$$

that solved with the continuity equation return the ice velocity components u, v and w.

2.1.2 Shallow Ice Approximation

The Shallow Ice Approximation (SIA) (Hutter, 1983; Morland, 1984), although still based on the hydrostatic approximation (H $\ll$ L), is specifically useful to describe those areas of the ice sheet that have a low curvature and their flow regime is characterised by a bed-parallel shear. Therefore if the hydrostatic approximation still considers all shear and deviatoric stresses, the SIA neglect all the normal deviatoric stresses τ_{xx} and τ_{yy} and shear stress in the vertical plane, σ_{xy}. The only SIA-relevant components of the stress tensor are the shear stresses in the horizontal plane σ_{xz} and σ_{yz} promoted by the basal drag. Thus, Eq. 2.14 becomes:

$$
\begin{aligned}
\frac{\partial \sigma_{xz}}{\partial z}&=\rho g\frac{\partial S}{\partial x}\\
\frac{\partial \sigma_{yz}}{\partial z}&=\rho g\frac{\partial S}{\partial y}
\end{aligned}
\tag{2.16}
$$

Since σ_{xz} and σ_{yz} are considered equal to zero at the ice surface (stress-free condition) and the second terms of these equations do not depend on z, Eq. 2.16 can be integrated in the vertical as

$$
\begin{aligned}
\sigma_{xz}&=-\rho g\frac{\partial S}{\partial x}(S-z)\\
\sigma_{yz}&=-\rho g\frac{\partial S}{\partial y}(S-z)
\end{aligned}
\tag{2.17}
$$

These equations evaluated at the ice base allow to define the vector

$$\tau_{\mathrm{d}} = \begin{pmatrix} \sigma_{xz}|_{z=b} \\ \sigma_{yz}|_{z=b} \end{pmatrix} = -\rho g H \begin{pmatrix} \frac{\partial S}{\partial x} \\ \frac{\partial S}{\partial y} \end{pmatrix} \tag{2.18}$$

known as the driving stress (H is the local ice thickness), that is equal to the negative of the shear stresses at the base of the ice sheet. Combining Eq. 2.17 with the flow law returns two equations for the horizontal SIA-calculated velocities:

$$\begin{aligned} u &= u_b - 2(\rho g)^n |\nabla S|^{n-1} \frac{\partial S}{\partial x} \int_b^z A(T^*)(S - z')^n dz' \\ v &= v_b - 2(\rho g)^n |\nabla S|^{n-1} \frac{\partial S}{\partial y} \int_b^z A(T^*)(S - z')^n dz' \end{aligned} \tag{2.19}$$

where $\mathbf{u_b} = (u_b, v_b)$ is the two-dimensional velocity at the base of the ice and b is the ice base. In GRISLI-UCM basal sliding is not considered for SIA-dominated areas, since they are supposed to be at the freezing point at the bedrock (no-slip condition).

2.1.3 Shallow Shelf Approximation

The Shallow Shelf Approximation (SSA) (Mac Ayeal, 1989) can be applied to those areas of the ice sheet characterised by plug flow (fast flow and low surface slope), such as ice shelves and ice streams. The hydrostatic approximation is still valid (H $\ll$ L) and under the assumption of plug flow, vertical shear of horizontal velocities is neglected, $\frac{\partial u}{\partial z} \approx 0$, $\frac{\partial v}{\partial z} \approx 0$, and the vertical shear stresses (σ_{xz}, σ_{yx}) are reduced to:

$$\sigma_{xz} = \eta \frac{\partial w}{\partial x} \ , \ \sigma_{yz} = \eta \frac{\partial w}{\partial y} \tag{2.20}$$

Under this assumption, the vertically integrated motion equations Eq. 2.14 result in a system of elliptic equations:

$$\begin{aligned} 4\frac{\partial}{\partial x}\left(\bar{\eta}\frac{\partial u}{\partial x}\right) + 2\frac{\partial}{\partial x}\left(\bar{\eta}\frac{\partial v}{\partial y}\right) + \frac{\partial}{\partial y}\left(\bar{\eta}\left(\frac{\partial u}{\partial y} + \frac{\partial v}{\partial x}\right)\right) &= \rho g H \frac{\partial S}{\partial x} \\ 4\frac{\partial}{\partial y}\left(\bar{\eta}\frac{\partial v}{\partial y}\right) + 2\frac{\partial}{\partial y}\left(\bar{\eta}\frac{\partial u}{\partial x}\right) + \frac{\partial}{\partial x}\left(\bar{\eta}\left(\frac{\partial u}{\partial y} + \frac{\partial v}{\partial x}\right)\right) &= \rho g H \frac{\partial S}{\partial y} \end{aligned} \tag{2.21}$$

where $\bar{\eta}$ is the vertically integrated viscosity of the ice and H the local ice thickness. These equations can be solved together with the mass continuity equation, applying boundary conditions at the surface and at the bed of the ice, at the grounding line and at the calving front.

2.2 Treatment of transition zones

Once the horizontal velocities have been calculated by the ice sheet model, they have to be combined or mixed together to avoid instabilities in the transition zone between areas that have been solved by the SIA and those solved by the SSA. This can be done, for example, by simply adding the non-sliding horizontal SIA velocities ($\mathbf{u}_{\mathrm{SIA}}$) to the horizontal SSA velocities ($\mathbf{u}_{\mathrm{SSA}}$) (Winkelmann et al., 2011; Pattyn, 2017) as

$$\mathbf{u} = \mathbf{u}_{\mathrm{SIA}} + \mathbf{u}_{\mathrm{SSA}} \tag{2.22}$$

Another approach combines the two velocities by mixing them through a weighting function that ensures a monotonic smooth transition between the two flow regimes (Bueler and Brown, 2009). The weighting function can have a form such as

$$f(u_{\mathrm{SSA}}) = \frac{2}{\pi} arctan\left(\frac{u_{\mathrm{SSA}}}{u_{\mathrm{ref}}}\right)^2 \tag{2.23}$$

where u_{SSA} is the module of the SSA velocity $\mathbf{u}_{\mathrm{SSA}}$. Following this definition $f(u_{\mathrm{SSA}}) \approx 0$ for small values of u_{SSA} and $f(u_{\mathrm{SSA}}) \approx 1$ for $u_{\mathrm{SSA}} \gg u_{\mathrm{ref}}$ (dominating SSA velocities), where u_{ref} is a tunable reference velocity. The horizontal velocities are then combined together as

$$\mathbf{u} = (1 - f(u_{\mathrm{SSA}}))\mathbf{u}_{\mathrm{SIA}} + f(u_{\mathrm{SSA}})\mathbf{u}_{SSA} \tag{2.24}$$

Both approaches have been used in this thesis.

An important issue in ice-sheet models is the treatment of dragging at the base of the ice. SIA internally accounts for the basal drag since it corresponds to the negative of the driving stress (Eq. 2.18), thus friction and driving forces are balanced at the base of the ice sheet. Conversely, at the base of the ice shelves,

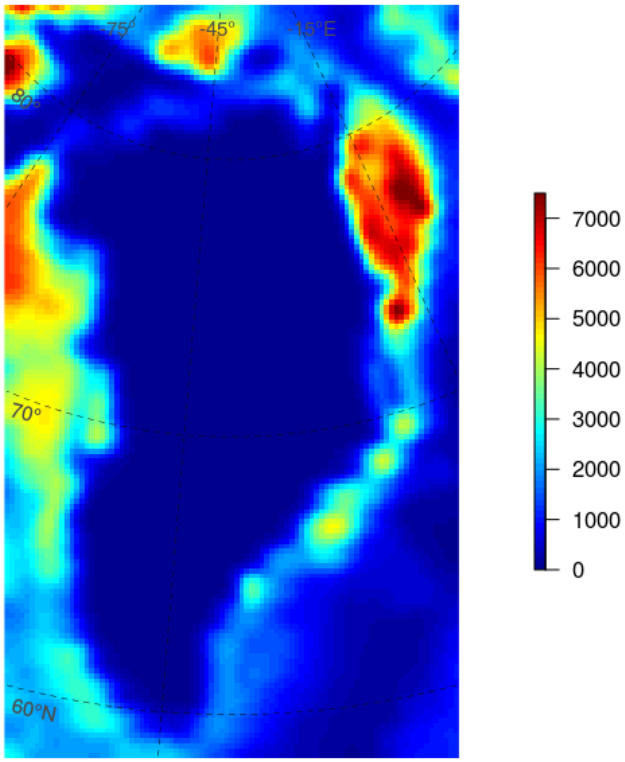

Fig. 2.3: Map of sediment thickness (m) around Greenland (data from Laske and Masters (1997)).

friction and thus basal drag is set to zero. Since transition zones are treated combining SIA and SSA solutions, basal drag at the base of the ice streams

needs to be defined. In GRISLI-UCM is determined through a linear friction law for which the basal drag term ($\tau_{\mathbf{b}}$) is defined as the negative of the basal horizontal velocity $\mathbf{u_b}$ scaled by the basal drag coefficient β, as

$$\tau_{\mathbf{b}} = -\beta \mathbf{u_b}. \tag{2.25}$$

In GRISLI-UCM β is a function of both effective pressure N_{eff} between ice and water pressure and a coefficient c_{f} that takes into account the different characteristics of the bedrock topography (e.g. presence of sediments, Fig. 2.3), as

$$\beta = c_{\text{f}}\, N_{\text{eff}}. \tag{2.26}$$

Here, N_{eff} is calculated as $N_{\text{eff}} = \rho g H - \rho_w g(SL - b)$, where ρ_w is the density of seawater, SL is the current sea level elevation, b indicates the base of the ice, ρ is the ice density and H is the ice thickness.

2.3 Thermodynamics calculation

The temperature of the ice is fundamental to describe processes involved in ice rheology, since temperature is needed to solve the Arrhenius law, to infer melting rate at the ice base and to potentially allow basal sliding if ice is at the pressure melting point. The ice temperature can be inferred solving the energy conservation equation (Eq. 2.3), after having defined some approximations in the formulation and having closed the problem with proper boundary conditions at the ice surface and base. First, it is reasonable to attribute the source of internal heat Q_i to ice deformation only. This allows to the expression of Q_i as

$$Q_i = 4\eta \dot{\epsilon_e^2} \tag{2.27}$$

where $\dot{\epsilon_e^2} = \frac{1}{2} tr(\dot{\epsilon^2})$ is the effective strain rate (Eq. 2.10). Second, the diffusion term ($\nabla(\kappa_i \nabla T)$) is given by the vertical diffusion only, since horizontal diffusion processes are small and can be neglected. Combining these approximations and

definitions, the energy equation (Eq. 2.3) can be re written as an equation for the ice temperature:

$$\frac{\partial T}{\partial t} = \frac{1}{\rho c}\left(-u\frac{\partial T}{\partial x} - v\frac{\partial T}{\partial y} - w\frac{\partial T}{\partial z}\right) + \frac{\kappa_i}{\rho c}\frac{\partial^2 T}{\partial z^2} + \frac{4\eta\dot{\epsilon}_e^2}{\rho c} \tag{2.28}$$

This equation can be solved considering the boundary conditions at the ice surface, where the ice temperature is at the surface air temperature, and at the ice base, where the ice temperature is a function of the geothermal heat flux exchanged with the bedrock. Here, in case of temperate ice, the ice temperature is defined by the pressure melting point temperature T^*.

Boundary conditions at the ice base

The temperature of ice at the base, and thus the melt rate below grounded ice, is strongly related to the geothermal heat flux exchanged between the ice base and the bedrock. Here, the distribution of heat flux below the GrIS is prescribed with the estimates inferred by Shapiro and Ritzwoller (2004) using a seismic model of the upper mantle.

Boundary conditions at the ice surface

The evolution of the ice thickness depends, between other terms, on the mass balance at the ice surface (M), that is defined as the surface accumulation minus the surface net melt (ablation). Treatment of surface processes follows that of GRISLI model. Surface accumulation is described by the amount of snow precipitation, that is exponentially proportional to atmospheric temperatures. Surface ablation is parameterised through the semi-empirical Positive-Degree Day scheme (Reeh, 1989). This simplistic method takes into account the sum of positive degree days over an year, i.e. the days in which the daily temperature is high enough to induce surface ablation, to determine the annual potential melt. The number of PDD is

defined as

$$PDD = \frac{1}{\sigma\sqrt{2\pi}} \int_{1year} \int_{0}^{\infty} exp\left(\frac{-(T - T_d)^2}{2\sigma^2}\right) dT dt \tag{2.29}$$

where T_d is the daily temperature, reconstructed from the annual cycle assumed to have a cosene evolution, and σ is its standard deviation (here set to 5 K, as done in many previous studies). The potential snow melt is then calculated from the annual PDD scaled by a melting factor that represents the typical snow melting rate in Greenland (0.003 $mm\ water\ equivalent$ $(w.e.)\ K^{-1}\ day^{-1}$). Then, a fraction of this snow melt can refreeze as superimposed ice, that in turn can be melted at a rate determined by the ice melting factor (0.008 $mm\ w.e.\ K^{-1}\ day^{-1}$, from observations in Greenland). Finally, the surface ice is melted at this ice melt rate. In paleo simulations, the PDD scheme is forced by a synthetic time-varying surface atmospheric temperature signal that expresses the temperature variation from cold (e.g. glacial) to warm (e.g. interglacial) climatic conditions. Past atmospheric temperatures are typically built following an index-anomaly method based on a combination of climate-model output and proxy records. Usually, the present-day climatology is perturbed by past temperature anomalies derived from two climate snapshots for specific times and modulated by a time-varying index, obtained from paleo data (generally, from the Greenland ice-core records). Although a method of this kind is quite simplistic, it is commonly used in paleo ice-sheet modelling studies and the results are rather satisfactory.

2.4 Processes below grounded ice

The evolution of the ice elevation depends on the vertical displacement of the bedrock below the grounded ice. Since the first ∼100 km of the Earth's mantle (litosphere) act as an elastic solid, local variations in the ice load induce vertical motions of the bedrock that correspond to an uplift when the ice load is reduced (warm periods) and to a depression when the ice load is restored (cold periods). This capacity of the bedrock to relax according to changes in the ice amount is called Glacial Isostatic Adjustment (GIA). Here, the GIA is described by the

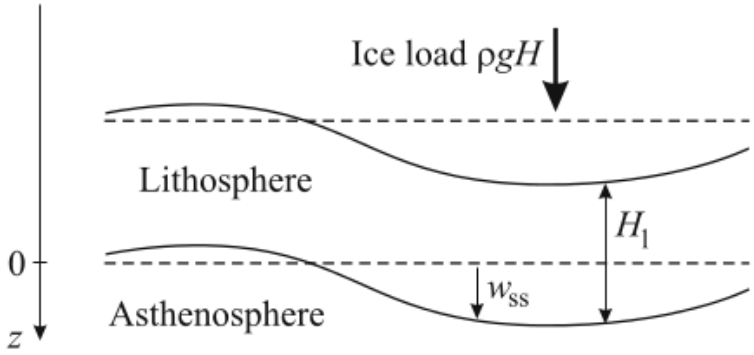

Fig. 2.4: Elastic lithosphere reacting to a locally imposed ice load (ρgH, where H as the ice thickness) in the ELRA scheme (Greve and Blatter, 2009). $\omega_{\rm ss}$ stands for the steady-state vertical movement of the litosphere and $H_{\rm l}$ for the litosphere thickness.

Elastic Lithosphere-Relaxed Asthenosphere model (Le Meur and Huybrechts, 1996), as in GRISLI model. In this simplistic scheme the lithospere is treated as a thin elastic plate that suffers the effect of an imposed ice load (ρgH) in the way that the steady-state vertical movement ω_{ss} induced by the ice load is regionally distributed (Fig. 2.4). Conversely, the underneath asthenosphere works as a viscous fluid that relaxes to its equilibrium with a characteristic relaxation time. This time is tunable and is here set to 3 ka.

2.5 Boundary conditions and treatment of processes at the ice-ocean interface

Calving

The evolution of the ice thickness H at the marine margin depends also on the ice flux (Eq. 2.6), that is mainly described by the calving process. Calving is based

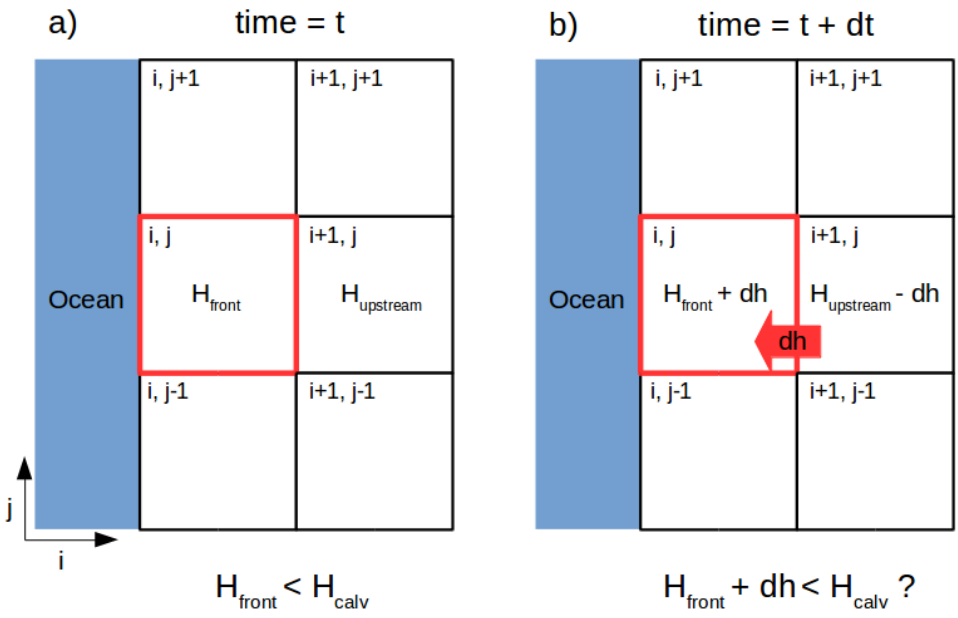

Fig. 2.5: Sketch of the calving process as treated in this thesis.

on a two-thickness criterion (Peyaud et al., 2007; Colleoni et al., 2014), as used in the GRISLI model. First, the ice thickness of the grid cell questioned for calving (point i,j of Fig. 2.5) must not exceed a user-set threshold (H_{calv}) to potentially contribute to calving. This threshold should be set to reflect the typical thickness of the ice shelves at the ice-ocean interface. Second, the ice advected from each upstream point should be insufficient to maintain the ice-front thickness higher than that threshold. The model computes this iteration solving the prognostic equation for the ice thickness Eq. 2.6 at each upstream grid point at which calving is tested. Let's consider the upstream cell i+1,j of Fig. 2.5. This upstream node has a thickness H_{upstream} which is presumabily higher than H_{calv}, while the ice thickness at the tested calving front is H_{front} (Fig. 2.5 a). The equation linking the ice thicknesses of these two points is

$$H_{\mathrm{front}} = H_{\mathrm{upstream}} + t_{\mathrm{f}} \frac{dh}{dt} \tag{2.30}$$

where t_f is the time by which ice from the upstream point flows to the front point. $H_{upstream}$ feeds the downstream point at the front of the ice shelf losing mass at a rate $\frac{dh}{dt}$ (Fig. 2.5 b). If the H_{front} has not increased for the ice mass received from the upstream point by a time t_f, and precisely, if H_{front} is still lower than H_{calv}, calving occurs at the ice shelf front.

Grounding-line treatment

The grounding-line treatment in the model is based on a simple flotation criterion, as used in the GRISLI model, by which:

$$\rho_w(SL - b) = \rho H \tag{2.31}$$

where ρ_w is the density of seawater, SL is the current sea level elevation, b is the base of the ice, ρ is the ice density and H is the ice thickness at the boundary layer. This approach is therefore based on the simplistic assumption that the grounding line lies on the last grounded coarse-grid point before ice starts to float. However, in this thesis a method that allows to diagnosis of the position of the grounding line at sub-grid scale precision, adapted from Gladstone et al. (2010), has been implemented. By interpolating the ice thickness over the grid cell including the grounding line it is possible to diagnose the grounded percentage of the grid cell, thus improving the calculation provided by the simplistic flotation criterion.

Submarine melting rate parameterisation

As introduced in Section 2.1, melting at the base of the ice shelves and in proximity of the grounding line (Fig. 2.6) is a process that needs to be accounted to solve the prognostic equation for the ice thickness (Eq. 2.6). In case that the marine terminus does not extend out into the ocean through an ice shelf, melting at the ice-ocean interface mainly occurs in form of frontal melt (Section 1.1).

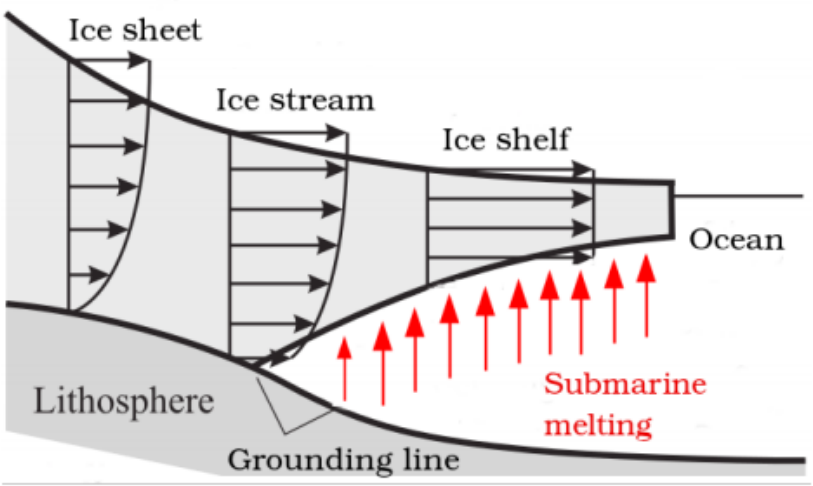

Fig. 2.6: Submarine melt at the ice-ocean interface, adapted from Greve and Blatter (2009).

Taking into account this form of melting is challenging, since it relates to a complex mechanism involving turbolent circulation of seawater within the fjord that may be enhanced by the presence of buoyant plums formed by subglacial discharge and the intrusion of warmer waters from the open ocean. For the sake of simplicity, this frontal melting is not treated in this work. The submarine melt rate production below the ice shelves and along the grounding line can be parameterised in different ways. Generally, the submarine melt rate is thought to be directly influenced by the oceanic temperature variations below the ice shelves. Accordingly, most basal melting parameterisations are built as function of the difference between the oceanic temperature at the ice-ocean boundary layer and the temperature at the ice-shelf base, generally assumed to be at the freezing point. The dependence on this temperature difference can be linear (Beckmann and Goosse, 2003) or quadratic (Holland et al., 2008b; Pollard and DeConto, 2012; DeConto and Pollard, 2016; Pattyn, 2017). Because of the increasing temperature anomaly approaching the onshore ice-shelf limit, both schemes ensure a

higher basal melting rate close to the grounding line, as suggested by observations (Dutrieux et al., 2013; Rignot and Jacobs, 2002; Wilson et al., 2017).

The submarine melting rate parameterisation implemented in the GRISLI-UCM model is assumed to be a linear function of the difference between the oceanic temperature and that at the base of the ice, that accounts separately for subaqueous regions near the grounding line and for floating ice shelves. A linear scheme is the simplest case that allows testing of the GrIS sensitivity to past oceanic temperature changes. Basal melting at the grounding line B_{gl} ($m\ a^{-1}$) is derived from a formulation valid for regions close to the grounding line and terminating in shallow ocean zones, as suggested by Beckmann and Goosse (2003):

$$B_{\mathrm{gl}}(t) = \kappa\,(T_{\mathrm{ocn}}(t) - T_{\mathrm{f}}) \tag{2.32}$$

where κ is the heat flux exchanged between ocean water and ice at the ice-ocean interface ($m\,a^{-1}\,K^{-1}$), T_{ocn} is the oceanic temperature at the grounding line (K) and T_{f} is the ice base temperature (K) assumed to be at the freezing point, which in turn depends on the depth in the water column. Since knowledge of past T_{ocn} and T_{f} is challenging for the complex heat-flux transfer between ice shelves and the surrounding water, these quantities have been substituted and the equations rearranged to make them more suitable for paleo studies. The oceanic temperature T_{ocn} can be expressed at any time as its climatological mean ($T_{\mathrm{ocn,clim}}$) corrected by its temporal deviation from that mean (ΔT_{ocn}) :

$$T_{\mathrm{ocn}}(t) = T_{\mathrm{ocn,clim}} + \Delta T_{\mathrm{ocn}}(t) \tag{2.33}$$

Under this assumption, Eq. 2.32 can be rewritten as

$$B_{\mathrm{gl}}(t) = \kappa\,(T_{\mathrm{ocn,clim}} + \Delta T_{\mathrm{ocn}}(t) - T_{\mathrm{f}}) \tag{2.34}$$

Reorganising the equation as:

$$B_{\mathrm{gl}}(t) = \kappa(T_{\mathrm{ocn,clim}} - T_{\mathrm{f}}) + \kappa\Delta T_{\mathrm{ocn}}(t) \tag{2.35}$$

leads to the expression for the basal melting rate at the grounding line B_{gl} ($m\,a^1$) as parameterised in the model:

$$B_{\mathrm{gl}}(t) = B_{\mathrm{ref}} + \kappa \Delta T_{\mathrm{ocn}}(t) \tag{2.36}$$

$B_{\mathrm{ref}} = \kappa(T_{\mathrm{clim,ocn}} - T_f)$ is assumed to represent the present-day basal melting rate around the ice sheet ($m\,a^{-1}$), κ is the sensitivity of the basal melting rate to changes in the oceanic temperature (oceanic sensitivity) ($m\,a^{-1}\,K^{-1}$), and ΔT_{ocn} (K) expresses the temporal anomaly of the temperature of the ocean at the grounding line. In this thesis ΔT_{ocn} is defined through an anomaly index approach similar to that used in other paleoclimatic studies to express the past anomaly in atmospheric temperatures (e.g. Ritz et al. (2001); Quiquet et al. (2013); Banderas et al. (2018)). This basal melting calculation is suitable for paleoclimatic simulations. The strength of this scheme is that its simplicity allows to estimation of the basal melt at the grounding line without taking into account the current temperature of the ocean at the boundary layer, or the temperature of the ice base, which is supposed to be at the freezing point and thus a function of salinity. Although convenient for paleoclimatic studies, this parameterisation might not be suitable for future predictions. The expected increase in ice retreat at the marine margins suggests that a configuration with floating tongues as that considered in this work is going to be less and less probable in Greenland, in which most of marine-terminating glaciers already show vertical calving fronts at the glacier termini. A precise understanding of the present-day and future ocean-driven retreat should be fulfilled through parameterisations that are able to appreciate the complex mechanisms that involve ablation at the calving front as a result of submarine melting and calving, potentially enhanced by increasing subglacial discharge, intrusion of warmer waters into the fjord and reduction of ice melange.

The basal melting rate for floating ice shelves (B_{sh}) is obtained by scaling the basal melt at the grounding line B_{gl} by a constant factor γ :

$$B_{\mathrm{sh}}(t) = \gamma\, B_{\mathrm{gl}}(t) \tag{2.37}$$

This correction has been introduced to account for a decrease in basal melt going away from the grounding line, which is comparable to other submarine melting parameterisations (e.g. Pollard and DeConto (2012); Beckmann and Goosse (2003); Holland et al. (2008b); Jenkins (2011); Pollard et al. (2016)). In this thesis, γ is set to 0.1. Hence, basal melting rate for ice shelves is considered to be ten times lower than that close to the grounding zone, which is qualitatively in agreement with melt rates observed in some Greenland glaciers (Münchow et al., 2014; Rignot and Steffen, 2008; Wilson et al., 2017). Conversely, the melt rate in the open ocean, that is considered as beyond the continental shelf break, is prescribed to a high value ($50\ m\ a^{-1}$) to avoid unrealistic ice growth beyond 1500 m of ocean depth.

Processes of glacial water refreezing at the ice base are implicitly taken into account by the submarine melting parameterisation as negative basal melting rates B_{gl} (or B_{sh}). However, this can be avoided by simply cutting off the resulting basal melt rate at zero after it is calculated. This approach has been applied in this thesis in the last two studies to avoid ice accretion at the ice-ocean interface which could be exaggerated by the coarse spatial resolution of the model (20km by 20km).

Chapter 3
The sensitivity of the Greenland Ice Sheet to glacial-interglacial oceanic forcing*

As introduced in Chapter 1, recent observations suggest that during the last decades the Greenland Ice Sheet (GrIS) has experienced a gradually accelerating mass loss, in part due to the observed speed-up of several of Greenland's marine-terminating glaciers. Recent studies directly attribute this to warming North Atlantic temperatures, which have triggered melting of the outlet glaciers of the GrIS, grounding-line retreat and enhanced ice discharge into the ocean, contributing to an acceleration of sea level rise. Reconstructions suggest that the influence of the ocean has been of primary importance in the past as well. This was the case not only in interglacial periods, when warmer climates led to a rapid retreat of the GrIS to land above sea level, but also in glacial periods, when the GrIS expanded as far as the continental shelf break, and was thus more directly exposed to oceanic changes. However, the GrIS response to paleo oceanic variations has yet to be investigated in detail from a mechanistic modelling perspective.

The main purpose of this chapter is to assess the impact of ice-ocean interaction on the evolution of the whole GrIS throughout the last glacial cycle. The sensitivity of the GrIS to past climatic variations, including changes in oceanic temperatures (in terms of heat-flux variations), is evaluated by using the three-

* The main contents of this chapter are published in:
Tabone, I., Blasco, J., Robinson, A., Alvarez-Solas, J. and Montoya, M., 2018: The sensitivity of the Greenland ice sheet to glacial-interglacial oceanic forcing. *Climate of the Past*, **14**, 455–472. DOI https://doi.org/10.5194/cp-14-455-2018.

dimensional hybrid ice-sheet-shelf model described in Chapter 2 provided with the submarine melting rate parameterisation defined in Section 2.5. Then, the capability of oceanic temperature variations to trigger grounding-line advance and retreat through time is investigated. The results show a very high sensitivity of the GrIS to changing oceanic conditions. Oceanic forcing is found to be a primary driver of GrIS expansion in glacial times, and, if switched off, paleo atmospheric variations alone are not able to yield a reliable glacial GrIS configuration. This study therefore suggests that considering the ocean as an active forcing should become standard practice in paleo ice sheet modelling.

This chapter is organized in this way: first, an introduction on modelling ice-ocean interactions is given focusing on the past GrIS (Section 3.1); then, the sensitivity tests performed for this study are described in Section 3.2; the results obtained in each experiment are shown in Section 3.3 and are compared with data for the Last Interglacial (LIG), the Last Glacial Maximum (LGM) and the present day (PD) found in the literature; after discussing the main model uncertainties and caveats (Section 3.4), the main conclusions of this work are summarized (Section 3.5).

3.1 Previous work on modelling ice-ocean interactions and past GrIS

Ice-ocean interactions and the complex mechanisms that lead to ice-shelf thinning, loss of buttressing and potential grounding-line instability have been studied largely for the Antarctic Ice Sheet (AIS) (DeConto and Pollard, 2016; Favier et al., 2014; Hanna et al., 2013; Joughin et al., 2014; Pritchard et al., 2012; Rignot et al., 2004; Shepherd et al., 2004; Wouters et al., 2015). The thinning of the Larsen C ice shelf (Holland et al., 2015) and its recent calving event (Hogg and Gudmundsson, 2017; Jansen et al., 2015), the collapse of Larsen B and the melting of the Antarctic Peninsula glaciers (Cook et al., 2016), the widespread retreat of Pine Island and other glaciers in West Antarctica (Alley et al., 2015; Joughin et al., 2014; Rignot et al., 2014) and the thinning of some East Antarc-

tica ice shelves (Rignot et al., 2013) are notable examples of the direct connection between changes in oceanic forcing and glacier-termini adjustment (Alley et al., 2015).

Only in the last several years has the scientific community also focused its attention on the ice-ocean interaction in Greenland, motivated by the observed acceleration and retreat of major GrIS outlet glaciers. Although marine-terminating glaciers cover only a small fraction of the entire GrIS, modifications at the ice-ocean boundaries due to oceanic changes may considerably affect the inland ice geometry. The effects induced by outlet-glacier acceleration are transferred onshore by ice-flow dynamics, causing adjustments to the entire inland ice-mass configuration (Nick et al., 2009; Fürst et al., 2013; Golledge et al., 2012). For this reason, a full understanding of the interaction between ice and ocean is crucial to assess the response of the GrIS to past and future climate changes.

Various numerical models have been used to simulate current submarine melt rates (Jenkins, 2011; Rignot et al., 2016; Sciascia et al., 2013; Xu et al., 2012, 2013) and dynamic retreat (Morlighem et al., 2016; Vieli and Nick, 2011) of the GrIS marine-terminating glaciers, as well as ice-dynamic future projections of the whole GrIS (Fürst et al., 2015; Nowicki et al., 2013), due to changes in the oceanic temperatures. However, how this thermal forcing affected the past GrIS configuration has not been explored from a modelling perspective so far. Recently, Bradley et al. (2018) simulated the GrIS evolution for the two last glacial cycles by considering a sub-shelf melt parameterisation which is a function of the water depth below the ice shelves. Under this assumption, the submarine melt rate increases when the past sea level rises. However, their approach does not take into account ocean temperature changes. Other studies have reconstructed the GrIS past evolution as driven essentially by atmospheric forcing (Langebroek and Nisancioglu, 2016; Quiquet et al., 2012, 2013; Robinson et al., 2011; Stone et al., 2013), while, the dynamic evolution of the entire GrIS including the influence of the past oceanic forcing too has only been investigated in a simplified manner. To this end, Huybrechts (2002) used a three-dimensional ice-sheet model in which marine extent is controlled by changes in water depth based on past eustatic-sea-level variations, while Tarasov and Peltier (2002), Simpson et al.

(2009) and Lecavalier et al. (2014) performed a paleo reconstruction of the entire GrIS constraining their ice-sheet models with past relative sea level (RSL) reconstructions. However, submarine melting was not taken into account as an active forcing in these studies. Therefore, the impact of the ice-ocean interaction on the past evolution of the GrIS is still unclear and a work investigating this issue is pending.

3.2 Experimental design

The oceanic sensitivity of the GrIS from the Last Interglacial to the present day is investigated using the three-dimensional, hybrid, ice-sheet-shelf model GRISLI-UCM, described in Chapter 2. Here, the entire GrIS ice dynamics and thermodynamics is solved on a computational grid of 20 km x 20 km horizontal resolution and 21 vertical layers. The hybrid scheme adopted in this work to combine non-sliding SIA with SSA horizontal velocities in the transition zones follows that of Bueler and Brown (2009) (Section 2.2). The surface mass balance (M) is calculated by the positive degree-day (PDD) scheme (Reeh, 1989) forced by surface atmospheric temperatures and precipitation. This melting scheme is admittedly too simple for paleo simulations as it omits the contribution of insolation-induced effects on surface melting, which are important in past warmer periods such as the Eemian (Robinson and Goelzer, 2014). However, since this study focuses on the melting effects induced by past ocean temperature variations, the PDD melt model is sufficient to give a first approximation of surface melt that allows the ice sheet to retreat during interglacial periods.

The atmospheric temperature forcing is a spatially and temporally variable field. It is retrieved using an index-anomaly approach in which the present-day climatological field ($T_{\mathrm{clim,atm}}$) is perturbed by past temperature anomalies derived through a spatially-uniform climatic index $\alpha(t)$ (Fig. 3.1), as follows:

$$T_{\mathrm{atm}}(t) = T_{\mathrm{clim,atm}} + \ (1 - \alpha(t))\,(T_{\mathrm{LGM,atm}} - T_{\mathrm{PD,atm}}) \tag{3.1}$$

The index $\alpha(t)$ is built through a multi-proxy approach. First, the temperature reconstruction for Greenland by Vinther et al. (2009) from 11.7 ka BP to present, the NGRIP reconstruction (Kindler et al., 2014) for 115-11.7 ka BP, and the NEEM reconstruction (NEEM, 2013) for 135-115 ka BP are combined to generate a synthetic temperature anomaly time series for 250-135 ka BP based on Antarctic isotope records, following Barker et al. (2011). Second, the composite signal undergoes a windowed low-pass frequency filter ($f_c = 1/16\ ka^{-1}$) in order to remove the spectral components associated with millennial time scales and below. Finally, the index α is obtained by normalizing the resulting signal to be in agreement with Eq. 3.1, i.e. $\alpha = 0$ at the LGM and $\alpha = 1$ at the present day. The present-day climatological field is taken from the regional climate model MAR forced by ERA-Interim (Fettweis et al., 2013). $T_{\mathrm{LGM,atm}} - T_{\mathrm{PD,atm}}$ is the 2D Surface Atmospheric Temperature (SAT) difference between the LGM and the present, as simulated by the climatic model of intermediate complexity CLIMBER-3α (Montoya and Levermann, 2008). The precipitation field is obtained following a similar approach for which the annual present-day precipitation P_{ann} is scaled by the ratio of LGM and present-day precipitation, scaled by α (Banderas et al., 2018):

$$P_{\mathrm{ann}}(t) = P_{\mathrm{clim,ann}} \cdot \left(\alpha(t) + (1 - \alpha(t)) \cdot \frac{P_{\mathrm{LGM,ann}}}{P_{\mathrm{PD,ann}}} \right). \tag{3.2}$$

The marine basal melting rate parameterisation used in this work follows the linear approach described in Section 2.5, that accounts separately for sub-ice shelf areas near the grounding line and for purely floating ice (ice shelves). As defined there, the expression for the basal melting rate at the grounding line B_{gl} ($m\,a^{-1}$) is

$$B_{\mathrm{gl}}(t) = B_{\mathrm{ref}} + \kappa\ \Delta T_{\mathrm{ocn}}(t) \tag{3.3}$$

where B_{ref} is assumed to represent the present-day basal melting rate around the ice sheet ($m\,a^{-1}$), κ represents the sensitivity of the basal melting rate to changes in the oceanic temperature, and $\Delta T_{\mathrm{ocn}}(t)$ expresses the oceanic temperature anomaly which varies through time (K). In this study, the transient oceanic temperature T_{ocn} is given by the climatological oceanic temperature $T_{\mathrm{clim,ocn}}$ cor-

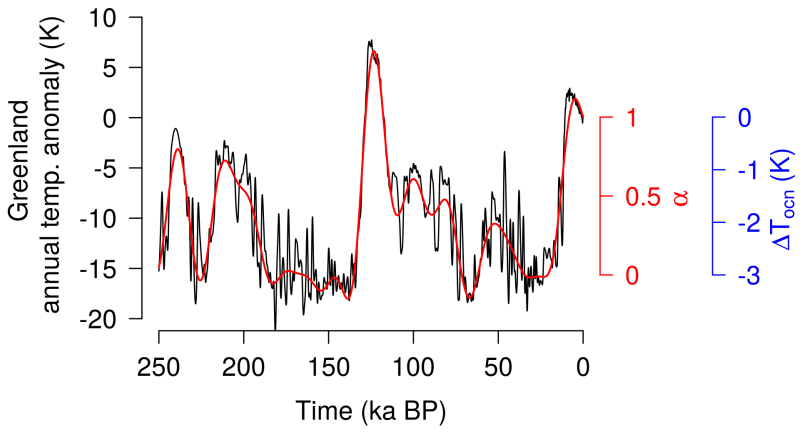

Fig. 3.1: The 250 ka Greenland annual temperature anomaly signal built through a multi-proxy approach based on the reconstruction by Vinther et al. (2009) from 11.7 ka BP to present, the NGRIP reconstruction (Kindler et al., 2014) for 115-11.7 ka BP, the NEEM reconstruction (NEEM, 2013) for 135-115 ka BP and a synthetic temperature anomaly time series for 250-135 ka BP following Barker et al. (2011) (black line). The red line shows the filtered and normalized climatic index α used to correct the present-day climatological fields when forcing the model. The same signal can be interpreted as the paleo oceanic temperature anomaly of Eq. 3.4 (in blue).

rected by the LGM-present temperature anomaly ($T_{\mathrm{LGM,ocn}} - T_{\mathrm{PD,ocn}}$) scaled by the same climatic-index $\alpha = \alpha(t)$ used to correct the atmospheric climatological fields (Fig. 3.1), such as

$$\Delta T_{\mathrm{ocn}}(t) = (1 - \alpha(t))\,(T_{\mathrm{LGM,ocn}} - T_{\mathrm{PD,ocn}}) \tag{3.4}$$

In this way, B_{gl} coincides with the present-day melt (B_{ref}) for $\alpha = 1$ and its LGM (21 ka BP) value for $\alpha = 0$. In this study, when B_{gl} is negative, the model allows for refreezing.

In a more realistic setup, all parameters in Eq. 3.3 could be described by 2D spatially variable fields. However, for the sake of simplicity, all the parameters are considered to be spatially uniform around all the GrIS marine borders. The glacial-interglacial temperature anomaly $T_{\mathrm{LGM,ocn}} - T_{\mathrm{PD,ocn}}$ (Eq. 3.4) is set constant to $-3K$, which corresponds to the mean value of the reconstructed LGM Sea Surface Temperature (SST) anomalies for the Atlantic Ocean between $60°N$ and $80°N$ of latitude (MARGO, 2009). This value slightly differs from the LGM mean SST anomaly reconstructed by Annan and Hargreaves (2013)(between $-1K$ and $-2K$). However, a variation in κ or an identical change in ΔT_{ocn} equally affect the oceanic forcing applied to the model. Therefore, considering a different value for ΔT_{ocn} would not alter the magnitude of the oceanic sensitivity applied to the GrIS. These simplifications allow here for a spatially-uniform, but time-dependent B_{gl}.

To study how oceanic changes impact the evolution of the GrIS over the last glacial cycles, a set of sensitivity tests are performed by perturbing the two key parameters of the basal melting rate equation (Eq. 3.3): the estimated present-day submarine melting B_{ref} and the heat-flux coefficient κ. For each experiment an ensemble of simulations over the GrIS domain is run throughout the last 250 ka. In this study the model is initialised with the present-day Greenland topography (Bamber et al., 2013) and past relative sea-level reconstruction of Grant et al. (2014) is prescribed in the model. The first ~ 100 ka of the simulation are considered as a spin-up and are not analyzed. A summary of all the parameter values used in the sensitivity test is shown in Table 3.1.

This work studies the sensitivity of the GrIS to the heat-flux coefficient κ. The range of tested values for κ is between 0 (expressing a temporally constant basal melting rate) and 10 $m\ a^{-1}\ K^{-1}$. The choice of this range reflects the inference made in Antarctica by Rignot and Jacobs (2002) that a variation of 1 K in the effective oceanic temperature changes the melt rate by 10 $m\ a^{-1}$. Due to the lack of data for Greenland, as a first approximation such a value can be assumed as also realistic there. This is surely a simplification of the problem, as the relation between ocean temperature and melt rate is not universal but depends on many factors, such as the water salinity, the depth, the conformation of the cavity, the

Table 3.1: Summary of all parameter values used to perturb the basal melting rate equation (Eq. 3.3).

Sensitivity to	Perturbed parameters	Units	Values
Heat-flux	B_{ref}	$m\,a^{-1}$	0, 0.2, 0.5, 1, 3, 5, 8, 10, 20, 30, 40
coefficient κ	κ	$m\,a^{-1}\,K^{-1}$	0, 0.2, 0.5, 1, 2, 3, 5, 8, 10

water velocity below the ice shelf and subglacial discharge. The sensitivity test for κ is firstly done for $B_{\text{ref}} = 1\ m\ a^{-1}$ and then for other B_{ref} values to show that the GrIS response to the melting rate sensitivity κ depends on the chosen reference basal melting rate (see Table 3.1).

3.3 Results

In this section the results of the sensitivity study aiming to assess the impact of the ocean on the evolution of the GrIS throughout the last glacial cycle are shown, especially focusing on the LIG, the LGM and the PD GrIS. The present work involved a total of 110 model simulations, although only the most representative cases are discussed.

3.3.1 Sensitivity to the heat-flux coefficient

The sensitivity to the ocean for a fix B_{ref} value of 1 $m\ a^{-1}$ (Fig. 3.2) is assessed. This B_{ref} value is within present-day submarine melting rates estimates, between those found in the largest remaining outlet glaciers in Greenland (Wilson et al., 2017) and those of smaller marine-terminating glaciers with presumably much lower ocean-induced melt. Under this assumption, the maximum ice volume simulated in both glacial periods for different κ values ranges between 4-5.4

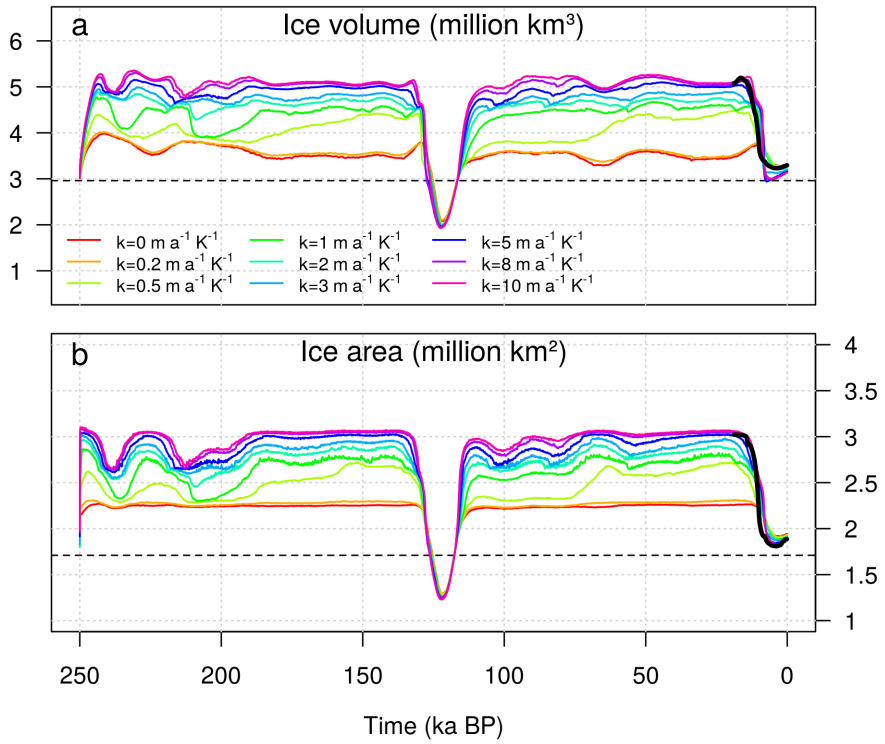

Fig. 3.2: (a) Time evolution of GrIS grounded ice volume (*million* km^3) and (b) ice area (*million* km^2) simulated for different values of the heat-flux coefficient κ, having set $B_{\text{ref}} = 1\ m\ a^{-1}$. Dashed lines shows the GrIS ice volume and area estimated for the present day (Bamber et al., 2013); solid black lines indicate the GrIS volume and area estimated by Lecavalier et al. (2014).

million km^3 . Prescribing positive or zero uniform submarine melting to the marine boundaries limits the glacial expansion of the GrIS (Fig. 3.3 a and 3.4 a) . Conversely, by intensifying the oceanic forcing applied to the margins (with increasing values of κ), the glacial ice volume increases. For $\kappa = 1\ m\ a^{-1}\ K^{-1}$ the model simulates a GrIS glacial expansion to the continental shelf break in which the grounding line has already advanced from the present-day continental

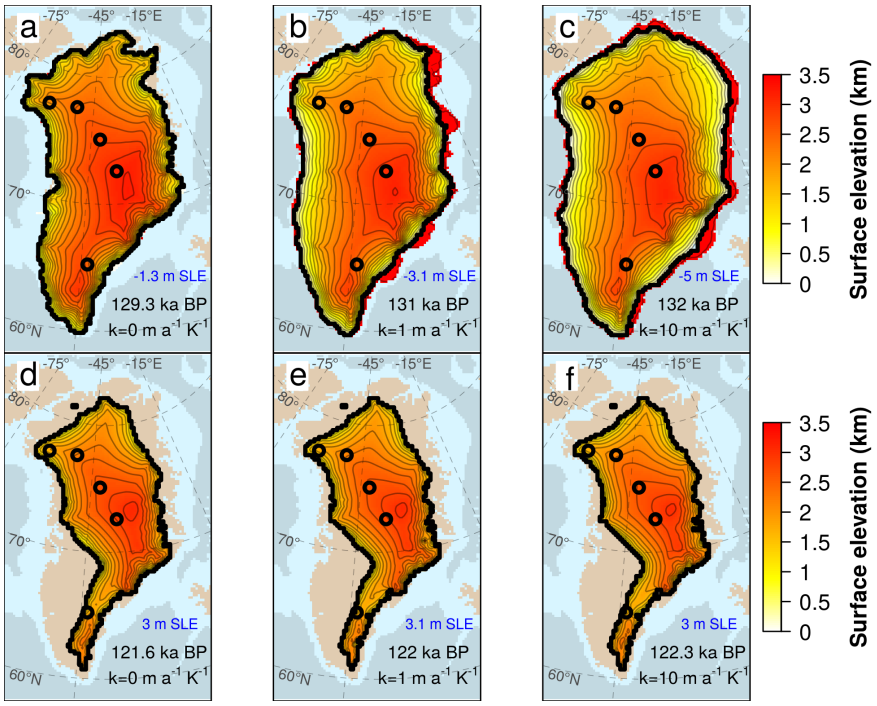

Fig. 3.3: GrIS surface elevation (km) simulated at the penultimate glacial maximum (TII) (a-c) and at the LIG minimum (Eemian) (d-f) for three values of the melting rate sensitivity κ having set $B_{\text{ref}} = 1\ m\ a^{-1}$. The timing of these snapshots depends on the experiment and is stated in black for each snapshot. Corresponding ice volume (in SLE) is shown in blue. Red zones represents the ice shelves extending beyond the glacial maximum grounding line (black line). Black circles indicate the locations of the NEEM, Camp Century, NGRIP, GRIP and Dye3 ice-cores (from North to South).

boundaries and large ice shelves are generated in the eastern GrIS, especially in the northeast (Fig. 3.3 b and 3.4 b). The maximum expansion is simulated for the last glaciation, where the grounding line has almost reached the continental shelf break and large ice shelves in the East cover the remaining shallower zones of the bathymetry. For $\kappa = 10\ m\ a^{-1}\ K^{-1}$ the GrIS extends all the way to the

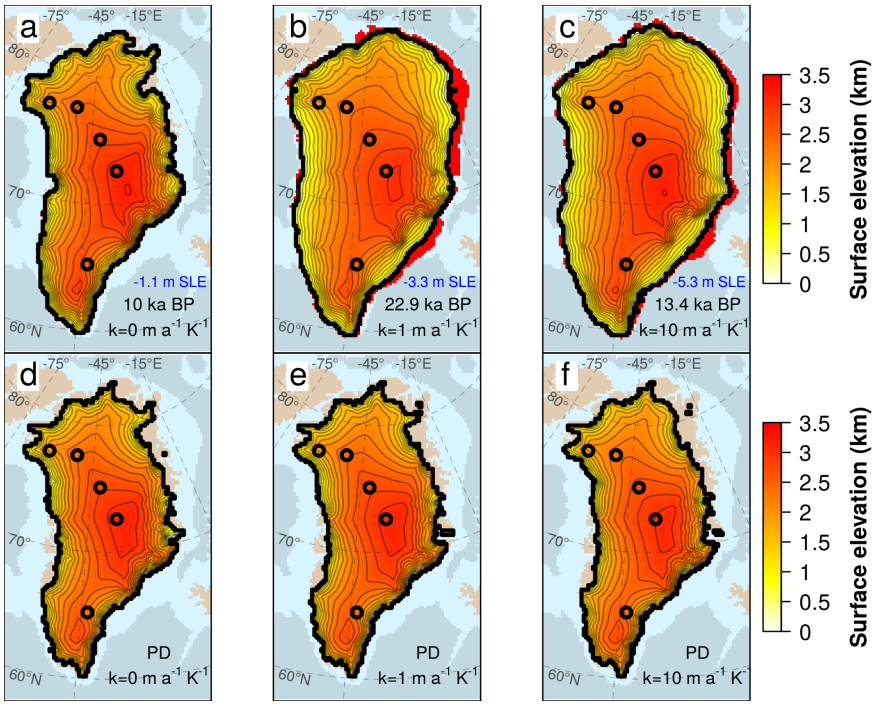

Fig. 3.4: GrIS surface elevation (km) simulated at the LGM (TI) (a-c) and present-day GrIS (d-f) for three values of the heat-flux coefficient κ having set $B_{\text{ref}} = 1\ m\ a^{-1}$. The timing of the snapshots depends on the experiment and is stated in black for each snapshot. Corresponding ice volume (in SLE) is shown in blue. Red zones represents the ice shelves extending beyond the LGM grounding line (black line). Black circles indicate the locations of the NEEM, Camp Century, NGRIP, GRIP and Dye3 ice-cores (from North to South).

continental shelf break at its glacial maximum, while only a few small floating ice shelves are present (Fig. 3.3 c and 3.4 c).

A larger ice sheet loses more ice during a deglaciation, leading to an interglacial state that is almost independent of κ (Fig. 3.2). This response is related to the saturation of the oceanic forcing in warm peaks, when the GrIS is almost totally land-based and the ice loss is hence mostly due to the increase in atmospheric

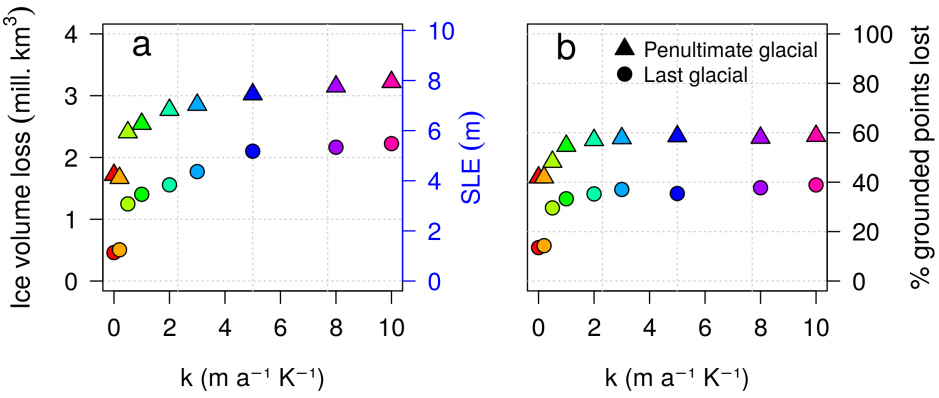

Fig. 3.5: Distribution of ice volume (a) and area (b) built during the penultimate glacial (triangles) and the last glacial as a function of κ, for $B_{\text{ref}} = 1\ m\ a^{-1}$. Grey and yellow shades show the deviation between the maximum and the minimum ice volumes (area) for LIG and Holocene, respectively (see Fig. 3.2). The loss is calculated between the time at which the ice volume reaches its maximum value simulated before deglaciation (between 140 and 128 ka BP for TII and between 19 and 10 ka BP for TI) and the subsequent ice minimum (between 122 and 121 ka BP for the Eemian and between 8 and 0 ka BP for the Holocene). The colors of the points follow the legend of Fig. 3.2 for clarity.

temperature and precipitation. Since glacial accretion affects the ice growth much more than basal melting during the retreat, the ice loss during a deglaciation monotonically increases with increasing κ (Fig. 3.5). Thus, for larger κ values, more ice grows during glacial periods and more ice is lost, and faster, during the subsequent deglaciation. Mass loss is mostly due to the large number of grounded-ice zones that are converted into ice-free areas during the deglaciation (Fig. 3.5 b). The percentage of grounded points lost until the peak of an interglacial period saturates for κ above $3\ m\ a^{-1}\ K^{-1}$ in correspondence with preceding glacial GrIS configurations which present a grounding-line expansion to the continental shelf break. The slightly increasing ice loss still observed for higher oceanic sensitivities

is mostly related to the ice lost in the GrIS interiors due to the positive elevation-melt feedback.

Due to the applied melting parameterisation (Eq. 3.3) and to the B_{ref} value chosen, water below the ice shelves is allowed to freeze for $\kappa > 0.5\ m\ a^{-1}\ K^{-1}$, favoring ice growth and GrIS expansion (Fig. 3.2). Below this threshold, the model still allows for submarine melting rates across the margins in glacial times and the GrIS expansion is almost totally driven by surface accumulation. However, the sensitivity with respect to κ strictly depends on the value of B_{ref}, as it defines the positive threshold that the glacial GrIS has to overcome to start reacting to the oceanic forcing imposed at the margins (Fig. 3.6). For $B_{\mathrm{ref}} = 10\ m\ a^{-1}$ the GrIS responds to the ocean only for $\kappa > 3\ m\ a^{-1}\ K^{-1}$, while for $B_{\mathrm{ref}} = 30\ m\ a^{-1}$ the GrIS starts to expand only for $\kappa > 8\ m\ a^{-1}\ K^{-1}$. For high B_{ref}, since a constant high submarine melting is applied overall, the glacial GrIS is almost constrained to the PD configuration and exposure to the ocean is reduced. Only a sufficiently high κ to counteract this strong melting is able to make the GrIS expand and then retreat during the interglacial. Once the reaction has started, the sensitivity of the GrIS to κ increases with increasing B_{ref}, i.e. small variations in the magnitude of κ lead to a fast and large growth of ice during glacials and consequently to a fast and large loss of ice during the deglaciation. Similar results are found for the LIG (not shown).

3.3.2 Last Interglacial

The amount of ice lost during the LIG period increases with the oceanic sensitivity κ. High κ values lead to higher glacial ice volumes and to larger ice losses during the consequent deglaciation (Fig. 3.5). The range of observed volume changes spans between 4.2 m SLE (for $\kappa = 0$) and 8 m SLE (for $\kappa = 10\ m\ a^{-1}\ K^{-1}$), above the present-day GrIS ice volume. Despite this large ice-loss range, all GrIS configurations simulated at the LIG ice minimum (Eemian) present a similar extension (Fig. 3.3 d-f). In all experiments, a large retreat is observed in the north (especially in the northeast), where melting overcomes the low accumu-

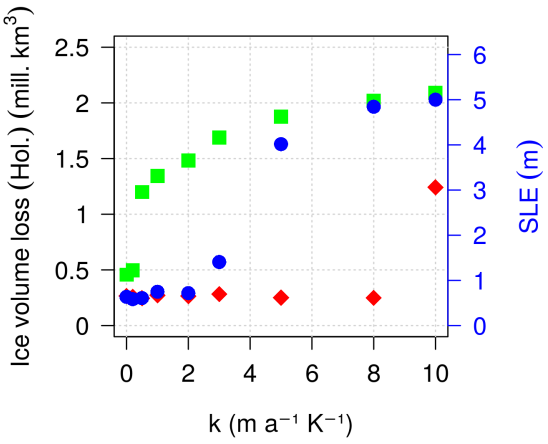

Fig. 3.6: Distribution of the ice volume lost in the Holocene as a function of the heat-flux coefficient κ, simulated for three selected reference basal melting rates ($B_{\text{ref}} = 1\ m\ a^{-1}$ in green, $B_{\text{ref}} = 10\ m\ a^{-1}$ in blue and $B_{\text{ref}} = 30\ m\ a^{-1}$ in red). The ice volume loss is calculated between the time at which the ice volume reaches its maximum value before the deglaciation and the present day. The green points are the same as the circles of Fig. 3.5 a (for the Holocene).

lation rates, and in the southwest, where the ice discharge from the interior is enhanced by the presence of fast ice streams and, in some areas, by the fact that the bedrock is below sea-level. Although the position of the land-ice borders at the Eemian is not very sensitive to κ, the corresponding surface elevation fields show some differences depending on κ. For high values of κ, a lower ice elevation is simulated over the GrIS (compare Fig. 3.3 d and f), a tendency that is reflected in a slightly lower ice volume too (Fig. 3.2). This is likely related to the isostatic response of the bedrock. A larger ice load in the previous glacial, as a result of a higher oceanic forcing, induces a larger depression of the bedrock below and, consequently, a longer isostatic rebound during the deglaciation. This slower uplift ensures the marginal regions of the ice sheet to slowly increase their surface elevation, thus, to be exposed to a prolonged ablation (Huybrechts, 2002). How-

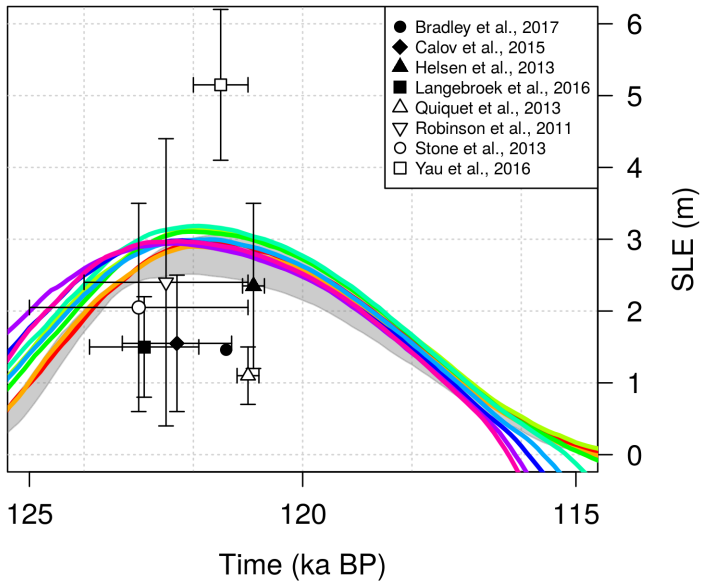

Fig. 3.7: GrIS ice volume evolution simulated for different values of the melting rate sensitivity κ during the last interglacial (see Fig. 3.2 for the line colour legend). The ice volumes have been converted to values of SLE anomaly with respect to the present-day volumes estimated in each specific simulation. Grey shading represents the reference basal melting rates B_{ref} investigated for the case of constant in time oceanic forcing ($\kappa = 0\ m\ a^{-1}\ K^{-1}$). Upper bound refers to $B_{\text{ref}} = 40\ m\ a^{-1}$, lower bound to $B_{\text{ref}} = 0\ m\ a^{-1}$. Black and white symbols indicate the LIG minimum ice volumes estimated by previous studies. The tight clustering of our estimates compared to previous work is due to the fact that the sole uncertainty is here related to the oceanic forcing through κ.

ever, a deeper investigation of the phenomenon would be needed to substantiate this hypothesis.

It is interesting to note that even when imposing a very high κ, the complete disappearance of the GrIS is not simulated. The GrIS is only partly deglaciated and all ice-core sites are still covered by ice (including the discussed ice core locations of Dye3 and NEEM). Since the oceanic-driven retreat is limited by the land-based configuration observed in the interglacials, the retreat during the LIG is mainly controlled by the atmospheric temperatures and precipitations with which the model is forced.

The amount of ice lost during the Eemian relative to the present day (Fig. 3.7), which ranges between 2.9-3.2 m SLE, is within the uncertainty range of ice volumes suggested by some previous studies (e.g., 1.2-3.5 m SLE for Helsen et al. (2013), 0.4-4.4 m SLE for Robinson et al. (2011) and 0.4-3.8 m SLE for Stone et al. (2013)). Also, the timing at which the peak of deglaciation occurs, which spans between 122.3 and 121.6 ka BP in all the simulations, agrees with the timing proposed in many previous studies (Calov et al., 2015; Langebroek and Nisancioglu, 2016; Robinson et al., 2011; Stone et al., 2013; Yau et al., 2016b). The time at which the simulated ice volume reaches its minimum value during the Eemian depends partly on the timing of the atmospheric temperature peak, and partly on the duration of the post-glacial rebound, which controls the intrusion of warm waters into the GrIS bays enhancing the ocean-driven retreat. However, the Eemian peak does not depend on the maximum insolation since the PDD scheme used does not account for past insolation changes.

3.3.3 Last Glacial Maximum

Although many uncertainties about the GrIS configuration during the last glacial period still exist, several estimates of the sea level contribution from the GrIS during the last deglaciation can be found in the literature: 2.6 m SLE (Bradley et al., 2018), 2.7 m SLE (Huybrechts, 2002), between 2 and 3 m SLE (Clark and Mix, 2002), 3.1 m SLE (Fleming and Lambeck, 2004), 4.1 m SLE (Simpson

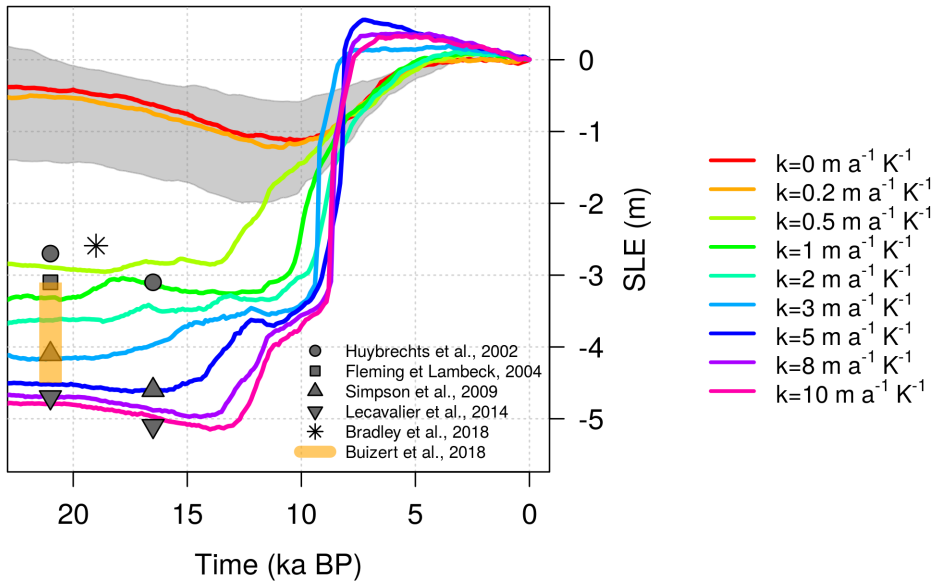

Fig. 3.8: GrIS ice volume evolution simulated for different values of the melting rate sensitivity κ during the last deglaciation. The ice volumes have been converted to values of SLE anomaly with respect to the present-day volumes estimated in each specific simulation. As in Fig. 3.7, grey shading represents the simulations for the different reference basal melting rates B_{ref} investigated for the case of constant in time oceanic forcing ($\kappa = 0$). Upper bound refers to $B_{\text{ref}} = 40$ $m\ a^{-1}$, lower bound to $B_{\text{ref}} = 0$ $m\ a^{-1}$. Grey dots and orange shading indicate estimates of the GrIS ice volume at the LGM (21 ka BP) and at the maximum ice volume reached before the last deglaciation (16.5 ka BP), as suggested by previous work.

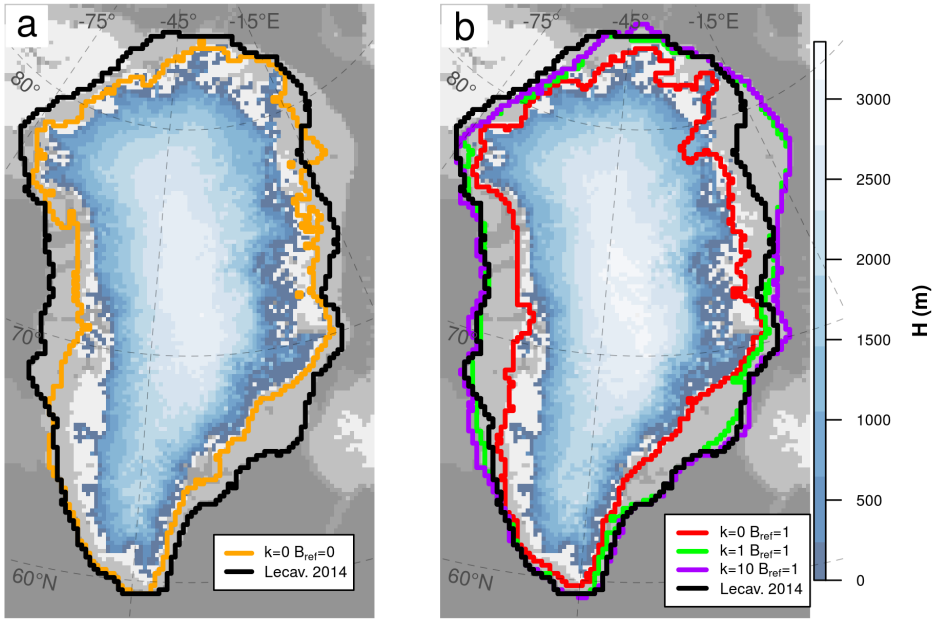

Fig. 3.9: GrIS total extent (ice shelves are included) simulated at the peak of the last glaciation for a) no melting/freezing at the grounding line (orange) and b) $\kappa = 0,\ 1$ and 10 $m\ a^{-1}\ K^{-1}$(red, green and purple lines, respectively) for $B_{\text{ref}} = 1\ m\ a^{-1}$. The timing of the glacial maximums are a) 12 ka BP and b) 10, 20, 14 ka BP for $\kappa = 0,\ 1$ and 10 $m\ a^{-1}$ respectively. LGM (21 ka BP) GrIS grounding-line position estimated by Lecavalier et al. (2014) is shown for comparison (black line). PD ice thickness H (m) is superimposed (see color scale onthe right); PD ice-free surface topography is shaded in white; grey shading represents the PD bedrock topography (0-500 m (light grey), 500-1000 m (grey) and 1000-3000 m (dark grey) depths).

et al., 2009), between 3.1 and 4.5 m SLE (Buizert et al., 2018) and 4.7 m SLE (Lecavalier et al., 2014). These estimates come from ice-sheet models of different complexity, with their own dynamics and boundary conditions. Particularly the ice-sheet model used by Simpson et al. (2009) and Lecavalier et al. (2014) is run in combination with a GIA and RSL model and then constrained by past surface elevations derived from ice-core data, observations of past changes in RSL and the present-day GrIS configuration. These models do not solve the dynamics of the ice shelves or the grounding-line migration, which is parameterised. However, their estimates of the GrIS spatial extent can be considered as the most realistic reconstructions of the recent past glacial GrIS so far.

Under constant oceanic conditions, the LGM-PD ice excess simulated by our model at 21 ka BP spans between 0 and 1.4 m SLE for B_{ref} ranging from 0 to 40 $m\ a^{-1}$, increasing with decreasing B_{ref} values (grey shaded region - Fig. 3.8). This range is well below previous LGM ice volume reconstructions found in the literature (grey points). However, slightly larger ice volumes (0.6-2 m SLE) are found at the peak simulated further in time in the glaciation ($\sim$ 13-10 ka BP). For the case with no submarine melting ($B_{\text{ref}} = 0\ m\ a^{-1}$), the maximum ice volume (lower bound of grey shadow, at $\sim$ 12 ka BP) is close to those of Huybrechts (2002) and Bradley et al. (2018). In this simulation, the GrIS increases moderately as its extension surpasses its PD borders and the grounding line approaches the continental shelf (Fig. 3.9 a). Nevertheless, the atmospheric forcing alone is not sufficient to make the GrIS expand as expected during the LGM. According to reconstructions, the GrIS extended as far as the continental shelf break in every direction, except in the northeast region where the grounding line remains closer to the coast (Lecavalier et al., 2014). In these simulations, the GrIS reaches a glacial expansion consistent with the literature only for $\kappa \geq 1\ m\ a^{-1}\ K^{-1}$(Fig. 3.9 b). However, the ice volume reached for this oceanic sensitivity is still smaller than the LGM volumes of Simpson et al. (2009) and Lecavalier et al. (2014) (Fig. 3.8), since only with $\kappa > 3\ m\ a^{-1}\ K^{-1}$ does the model simulate a maximum ice volume comparable to those ranges. The discrepancy in volumes, despite the same extension, could be related to the different dynamics and boundary conditions applied in the two models. Nevertheless, our simulated ice volumes are

in agreement with recent estimates corrected for seasonal surface air temperatures in Greenland during the LGM (Buizert et al., 2018).

The timing of the reconstructed deglaciation can also provide information for comparison. The maximum increase suggested by Simpson et al. (2009) (4.6 m SLE) and Lecavalier et al. (2014) (5.1 m SLE) occurs at 16.5 ka BP, while these simulations suggest a timing dependent on κ ranging from 20 to 10 ka BP for very low κ values (Fig. 3.8). The magnitudes of the oceanic sensitivity that best approximate the evolution of the GrIS before the Holocene are thus between 5 $m\ a^{-1}\ K^{-1}$ (4.6 m SLE at 17.4 ka BP) and 10 $m\ a^{-1}\ K^{-1}$ (5.3 m SLE at 14 ka BP). However, some discrepancies between the GrIS glacial extension suggested by this work and that of Lecavalier et al. (2014) are still present (Fig. 3.9 b).

3.3.4 Present-day GrIS

Given that the topography of the present-day GrIS is one of the trustworthy measures used to assess the reliability of an ice-sheet model,present-day GrIS ice thickness and extent simulated for $\kappa = 10\ m\ a^{-1}\ K^{-1}$ are compared to those estimated by Bamber et al. (2013) (Fig. 3.10). The choice of this particular κ value is based on the discussion above (Section 3.3.3) for the LGM and is supported by the good agreement between the simulated present-day ice volume and observations (Bamber et al., 2013) (Fig. 3.4f). The simulated extent of the GrIS matches reasonably well the observations. However, notable discrepancies are observed in some sectors. The main differences are found in the northeast, where GRISLI-UCM predicts an ice margin somewhat too far inland, and in the southwest, where the model is not able to make the GrIS retreat as expected.

The ice loss in the north is a known problem that appears in many studies when simulating the GrIS during an interglacial (Stone et al., 2010; Born and Nisancioglu, 2012). In the interior, the difference in ice thickness is relatively low. However, the GrIS simulated by the model generally shows thicker ice along the margins, a tendency that propagates inland. Other areas in which the simulated ice thickness is lower than that observed are located in the centre of the continent

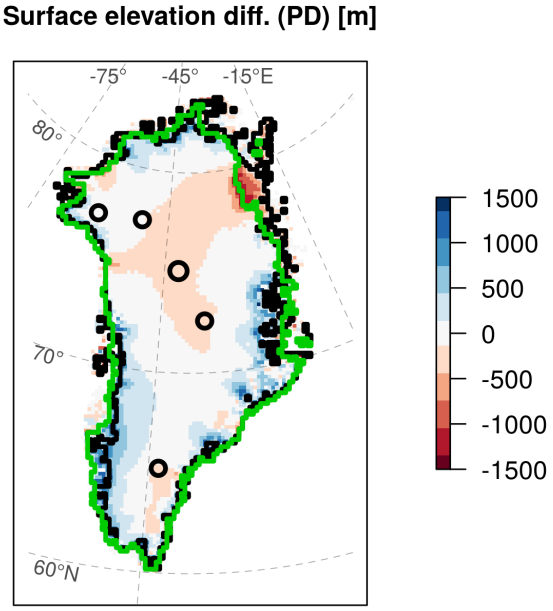

Fig. 3.10: Modelled minus observed surface elevation for the present day. Modelled data are taken from the GRISLI-UCM simulation which best estimates the presumed LGM extension ($B_{\text{ref}} = 1\ m\ a^{-1}$ and $\kappa = 10\ m\ a^{-1}\ K^{-1}$) while the observed surface elevation is taken from Bamber et al. (2013). Green and black lines represent simulated and observed GrIS extensions, respectively. Black circles indicate the locations of the NEEM, Camp Century, NGRIP, GRIP and Dye3 ice-cores (from North to South).

and in the very southeast corresponding to a mountainous region. However, the focus of this work is not to exactly reproduce the observed present-day GrIS ice volume at the end of the simulations, but rather to demonstrate the impact of the ocean on the GrIS past evolution. From this perspective, the simulations arrive at a reasonable representation of the present day and within the range of other models.

3.4 Discussion

The model simulates the advance and retreat of the GrIS for the two last glacial-interglacial cycles. Transient simulations reflect the ice-sheet response to the specific oceanic forcing applied to the model. This reaction is different for glacial and interglacial periods (Fig. 3.2). Since during the interglacial periods the GrIS is almost totally land-based and therefore less exposed to the ocean, the minimum ice volume reflects the oceanic imprint only mildly and is limited to a small range of possible values. On the other hand, the volume reached in glacial periods is much more sensitive to κ. Although the maximum ice volume loss is constrained by the imposed limited extension to the continental shelf break, the large ice loss observed for a high oceanic sensitivity is closely related to the GrIS configuration in the previous glacial, which is essentially marine-based at the margins and therefore more subjected to oceanic changes (Fig. 3.3 c). As water temperatures rise at the beginning of the deglaciation, basal melting rate increases too (Eq. 3.3), thinning ice shelves at the boundaries, enhancing outflow of ice and triggering grounding-line retreat. The effects of this ocean-driven retreat are not locally confined but are propagated inland through a dynamic response of the grounded ice sheet. The ice loss at the margins triggers ice advection from the interior which further increases the ice discharge into the ocean, and, as the thickness of the inland ice decreases, the elevation-melt feedback begins. At a given stage of the deglaciation, when the whole ice sheet starts to become land-based, this atmosphere-driven retreat, presumably still enhanced by the ongoing isostatic rebound, becomes the sole driver of ice mass loss. The simulated retreat during this phase is influenced by the choice of the surface melt scheme used in the model. At the peak of the Eemian, the melt determined by the PDD scheme can be $20 - 50\%$ lower than the melt calculated if past insolation changes are taken into account (Robinson and Goelzer, 2014). This inaccuracy of our model based on a PDD therefore influences the GrIS contributions to sea-level rise for the last interglacial (Fig. 3.7), which could be underestimated. Moreover, since the PDD scheme is known for underestimating surface ablation, ice loss related to the oceanic forcing might be emphasized in the mass balance calculation with

respect to the surface ablation. However, this work especially focuses on the effect of the oceanic forcing on the GrIS evolution during glacial times, when surface melting is presumably low due to the cool atmosphere. Thus, the usage of the PDD scheme should not jeopardise the results of this work. Nevertheless, a precise study of the impact of the ocean during an interglacial would require the usage of a more realistic atmospheric forcing to avoid any outcome that might overstate the role of the ocean in the ice retreat.

It is interesting to analyse the sensitivity of the model to different constant (in space and time) B_{ref} values applied at the base of the ice-sheet marine margins. Due to the scarcity of submarine melt observations along the GrIS coasts, and since the only available estimates have focused on few very rapid tidewater Greenland glaciers that cannot be representative of the basal melt rate for the entirety of GrIS marine areas (Rignot et al., 2010; Motyka et al., 2011; Straneo et al., 2012; Xu et al., 2013; Enderlin and Howat, 2013; Fried et al., 2015; Rignot et al., 2016; Wilson et al., 2017), present-day basal melting rates for Greenland are assumed to be comparable to those from Antarctic ice shelves (Rignot et al., 2013). The range of values of B_{ref} is set between 0 and 40 $m\,a^{-1}$, while κ is set zero to make the ocean contribution constant in time. The resulting basal melting rate is thus equal to the tested B_{ref} value and a condition of no oceanic basal melting around the GrIS is achieved only when both B_{ref} and κ are set zero. In this experiment the maximum ice volume reached in glacial times ranges between 3.4-4.3 million km^3 (Fig. 3.11), 15-45 % higher than the observed current value (Bamber et al., 2013), again suggesting that under constant oceanic forcing, the GrIS does not reach a full glacial state (Fig. 3.12). The highest glacial ice volume is reached by imposing a null basal melting to the GrIS margins ($B_{\text{ref}} = 0$), which corresponds to a simulation forced solely by paleo atmospheric variations. The varying surface mass balance throughout the cycles still results in a changing GrIS ice volume over time. However, during glacials most grounded ice remains on land above sea level, and only small ice shelves are able to grow (Fig. 3.12 a, d). For $B_{\text{ref}} > 0$, a positive basal melt rate is applied to the marine margins of the whole GrIS throughout the two glacial cycles. The submarine melting not only inhibits the grounding-line advance during the glacials, but contributes to

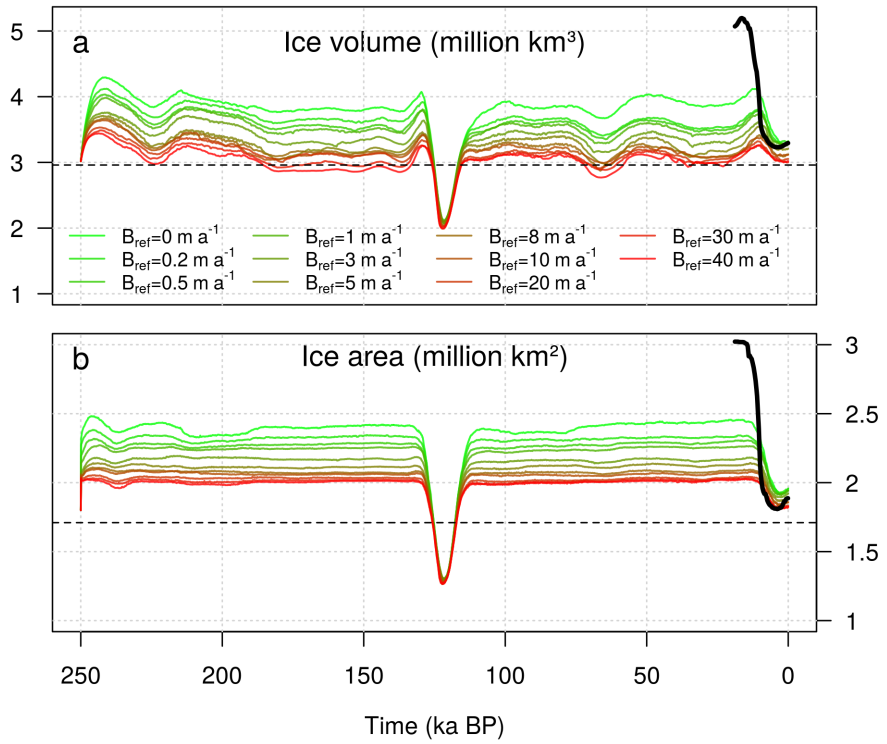

Fig. 3.11: Time evolution of (a) grounded ice volume ($million\ km^3$) and (b) ice-covered area ($million\ km^2$) simulated for different values of B_{ref} ($m\ a^{-1}$) having set $\kappa = 0$. Dashed lines show the present-day estimated volume and area of the GrIS (Bamber et al., 2013); solid black lines indicate the GrIS volume and area estimated by Lecavalier et al. (2014).

thin the few marine-terminating glaciers still present, constraining the grounding line further inland, and resulting in a GrIS extent close to the observed present-day configuration (Fig. 3.12 b, c, e, f). This mechanism can still be quite active during glacial times, such that the ice volume can be even lower than that simulated at the present (Fig. 3.11). Note that the ice volume is more sensitive to B_{ref} during the glacial periods, as during the interglacial periods the effect of the

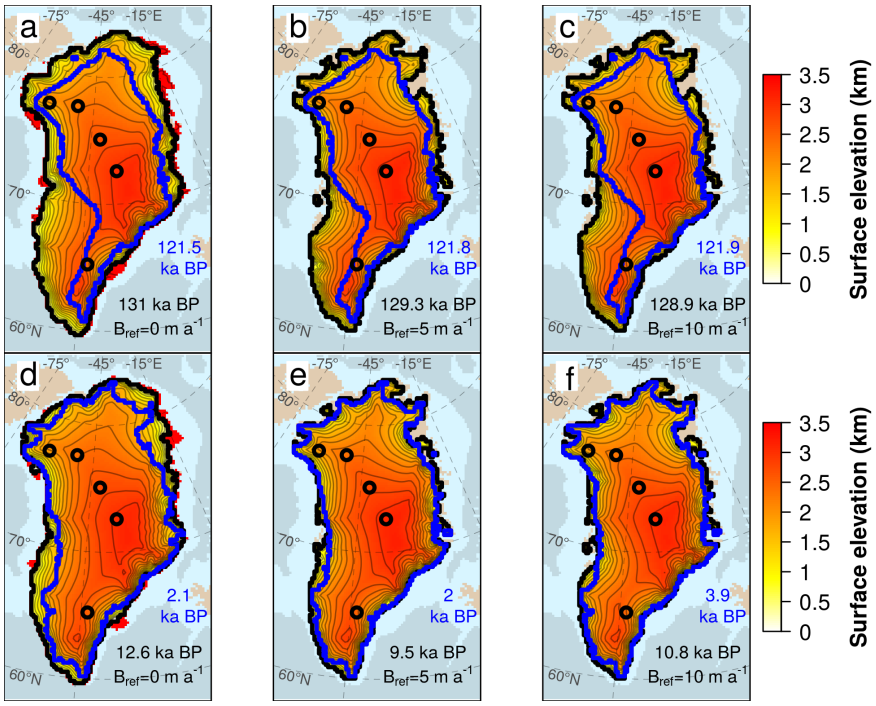

Fig. 3.12: Glacial maximum GrIS surface elevation (km) simulated at Termination II (a-c) and Termination I (d-f) for different values of the reference basal melting rate $B_{\text{ref}} = 0, 5, 10\ m\ a^{-1}$ under constant oceanic conditions ($\kappa = 0$). The timing at which the ice volume reaches its maximum value during a glacial cycle depends on the experiment and is stated in black for each snapshot. Blue lines indicate the GrIS extension at the following peak of deglaciation with its corresponding timing reported in blue. Red zones represents the ice shelves extending beyond the glacial maximum grounding line (black line). Black circles indicate the locations of the NEEM, Camp Century, NGRIP, GRIP and Dye3 ice-cores (from North to South).

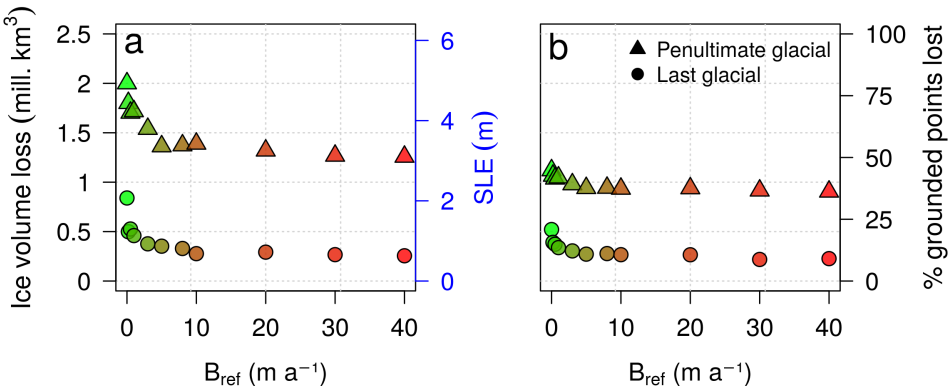

Fig. 3.13: Distribution of the ice volume (a) and area (b) built during the penultimate glacial (triangles) and the last glacial (circles) as a function of B_{ref}. Grey and yellow shades show the range between the maximum glacial and the minimum interglacial ice volumes (area) for LIG and Holocene, respectively. The loss is calculated between the time at which the ice volume reaches its maximum value simulated before the deglaciation (between 132 and 128 ka BP for TII and between 13 and 9 ka BP for TI) and its following ice minimum (between 122 and 121 ka BP for the Eemian and between 8 and 0 ka BP for the Holocene). The colors of the points follow the legend of Fig. 3.11 for clarity. Each ice volume loss has been converted to value of sea-level equivalent anomaly (m SLE) with respect to its simulated present-day volume.

ocean is limited by the topography of the Greenland itself. Thus, the retreat is almost entirely driven by the surface ablation and the elevation-melt feedback. For low B_{ref} values the ice lost in a deglaciation is to a large extent determined by the GrIS configuration in the preceding glacial. As high basal melting rates inhibit the ice growth during the cold phase, the higher the B_{ref} applied to the marine margins, the lower ice loss is simulated in the following interglacial (Fig. 3.13). However, for $B_{\text{ref}} = 5\ m\ a^{-1}$ ice loss becomes insensitive to the melting applied, since the GrIS is also totally land-based during glacial periods and any

subsequent ice mass loss is therefore uniquely driven by ablation (compare Fig. 3.12 a and b or Fig. 3.12 d and e).

As discussed in Sections 3.3.3 and 3.3.4, the oceanic forcing that seems to best reconstruct the past (LGM) and the present GrIS is achieved for a heat-flux coefficient of 10 $m\ a^{-1}\ K^{-1}$. However, the submarine melt scheme used and some simplifications made in its treatment may partly influence these results. Firstly, only a limited range of reference submarine melting rates has been investigated, since only two of the system model parameters have been explored (Table 3.1). Secondly, this melting parameterisation is highly conditioned by the B_{ref} value assumed to represent the present-day submarine melting rate around the GrIS (Fig. 3.5), as it consequently determines the minimum κ value needed to allow the GrIS to respond to the ocean (Fig. 3.12). B_{ref} stands for the present-day basal melting rate around the ice sheet, under the assumption that the present-day GrIS state is characterised by marine-terminating glaciers that end into the ocean by means of floating tongues. However, only a few ice shelves are still present in the far north today, while the rest of the marine-terminating glaciers is much of the form of tidewater glaciers that abruply end into the ocean, or show small floating tongues. The submarine melting parameterisation itself does not take into account the transition from this floating-glaciers configuration, which is likely for glacial times, to the tidewater-glacier configuration observed at the present-day. Therefore, values chosen for Bref are very uncertain, since they refer to an hypothetical present-day GrIS in which its marine margins do not precisely correspond to their actual state. Also, using a single value for Bref is a coarse approximation to reality. Melting rates observed at the present-day in Greenland should be divided into rates estimated below the remaining ice shelves and those observed at the vertical fronts of tidewater glaciers. Especially the latters are very challenging to estimate since frontal melting is related to a very complex mechanism involving a fjord-wide circulation of ocean water within the fjord (Slater et al., 2018), turbolent ice-ocean exchange enhanced by subglacial discharge (Jenkins, 2011) and connected to bedrock topography controlling open ocean waters entering the fjord (Straneo et al., 2016). A detailed distribution of those heterogeneous melting rates does not exist for Greenland and the retrieval

of a 2D field would be complex and highly uncertain. For simplicity, and because the submarine melting parameterisation applied here assumes a PD GrIS state with floating tongues at the marine termini, the order of magnitude of considered melt rates is the same as that proposed in the literature for the PD AIS, where the majority of marine outlet glaciers shows floating tongues and melt rates span from negative to above 40 $m\ a^{-1}$ in some very active regions (Rignot and Jacobs, 2002). Similar basal melting rates have been found recenty in some GrIS ice tongues (Wilson et al., 2017). Thirdly, the basal melting equation strongly depends on the oceanic temperature anomaly $T_{\mathrm{LGM,ocn}} - T_{\mathrm{PD,ocn}}$, which has been prescribed to a spatially constant value of $-3K$. Since this term impacts the oceanic sensitivity through κ (Eq. 3.3), it is clear that the same results obtained in this work would have been reached by fixing one value of κ and instead examining the influence of different levels of the ΔT_{ocn} on the GrIS past evolution. Considering a spatially constant SST anomaly represents an idealized simplification of the oceanic forcing for two reasons: the temperature of the water is clearly not uniform along the GrIS coasts and the melt at the grounding line is presumably controlled by water temperature deeper in the ocean column (between 100-1000 m in Greenland (Rignot et al., 2016)). These issues could be avoided for example by using spatially variable (horizontally and vertically) oceanic temperatures from available model outputs for Greenland. To see whether this simplification could influence the results of this study, some tests using 2D temperatures from CLIMBER-3-α snapshots (Montoya and Levermann, 2008) have been run (not shown). Despite some differences in the ice distribution and the time of the retreat, the main results obtained in this work did not change. Finally, another simplification made here is the assignation of the same climatic index α to both atmosphere and ocean. In principle, forcing the ocean with an index derived from past ocean temperatures could be more appropriate. To this end, additional simulations are run by applying the multi-proxy index α for the atmosphere, and another index for the ocean calculated from benthic-retrieved ocean temperatures (Waelbroeck et al., 2002). The results of the new simulations show very little differences from the ones reported here, while the same sensitivity

to the ocean is preserved (not shown). Thus, such a distinction in forcing does not affect the main outcomes of this work.

Results of this study may well be model-dependent, and some model limitations should be noted. As described in Section 2.4, the GRISLI-UCM ice-sheet-shelf model is provided with an internal GIA scheme which accounts for bedrock deformation due to changes in the GrIS ice load. However, since the GrIS rests on the peripheral forebulge of the North American Ice Sheets (NAIS), such as the Laurentide Ice Sheet, variations in the NAIS ice load induce consequent vertical motions of the lithosphere beneath the GrIS (Lecavalier et al., 2014). The resulting GrIS isostatic adjustment is, therefore, the combination of these local and non-local responses which make the GIA treatment rather complex. In principle, these non-local effects should be taken into account as they contribute to the sea-level variability, becoming especially relevant at the beginning of deglaciations when the ice mass loss is significantly induced by sea-level rise (Lecavalier et al., 2017). However, for the sake of simplicity, the GrIS isostatic adjustment is assumed here to be only due to local ice mass variations, as other works have done in the past (Greve and Blatter, 2009; Helsen et al., 2013; Huybrechts, 2002; Langebroek and Nisancioglu, 2016; Stone et al., 2013).

The simulated ice volume at the present day is overestimated for all investigated values of κ (Fig. 3.5). This fact suggests that the model has a tendency to overestimate the ice thickness of the GrIS, especially in the marginal zones of the domain, a well known phenomenon (Calov et al., 2015). These discrepancies are partly linked to the relatively low model resolution (20 km x 20 km), which limits the accuracy in estimating the margins especially along the fjords, and partly due to the boundary conditions applied to the ice-sheet model, such as the basal sliding. The coarse model resolution prevents the model from resolving fine-scale physical processes at the marine-terminating outlet glaciers that end in narrow fjords, although they are considered as the primary sources of ice discharge today due to oceanic changes. Such an inability of the model may be more relevant when modelling the GrIS retreat during the LIG and the Holocene. The lack of a subgrid fjord treatment does not allow for a proper analysis of the ice front processes which become relevant when the retreat has reached the continental area

above the sea level. Especially when, as here, the submarine melt goes abruptly to a high value at the grounding line, the implementation of a sub-grid scale parameterisation would allow the small processes at the fjords to be accurately resolved (Calov et al., 2015; Favier et al., 2016; Gladstone et al., 2017). However, these limitations lead to only second-order effects given the scope of this work.

The parameterisation used for the submarine melting rate at the GrIS marine margins is a simplification compared to other temperature-dependent submarine melting schemes. It is known that the melting rate depends on many regional factors such as the temperature and salinity of the ocean at the ice-shelf margin, the shape of the ice-shelf cavity and the depth of the grounding line, which our equations do not take into account. However, this simple construction allows to test the sensitivity of the GrIS to the oceanic forcing in a straightforward manner and is found to be particularly suitable for paleo studies.

Basal melting parameterisation used in this work allows for refreezing of water below the ice shelves. This mechanism may well have helped grounded-line advance during cold phases. There is no evidence that such a refreezing was present during glacial times in Greenland, since past melting/refreezing rates are quantities that cannot be inferred from paleo records. However, ice accretion due to sub-shelf refreezing is still seen today in some ice shelves of the AIS, despite the present-day interglacial conditions (Rignot et al., 2013; Joughin et al., 2012a). This mechanism is related to a local circulation of water into the ice-shelf cavities that cools seawater at the grounding line and, transported further offshore, helps supercooled water at the base of the ice shelves to freeze (Jenkins and Doake, 1991). It is likely that large ice shelves present in the GrIS during glacial periods could have been subjected to sub-shelf water freezing due to the presumably colder surrounding ocean. Still, sub-shelf freezing is not the sole mechanism required to built a glacial GrIS here, since grounding-line advance also depends on changes in relative sea-level (controlling the floating condition) and ice dynamics. It could be that another dynamics set in the model would have contributed to promote/inhibit grounding-line migration. However, here the range of uncertainty in the dynamics has not been tested, since this work focused on the impact of the oceanic forcing on the GrIS past evolution.

This basal melting scheme is implemented in such a way that the melting at the grounding line is higher than the one set below the ice shelves (Section 2.5). This approach is supported by sub-shelf melting rate estimates (Dutrieux et al., 2013; Reese et al., 2018; Rignot and Jacobs, 2002; Wilson et al., 2017). Moreover, we assume that the ratio between the two is of one-tenth, which is valid for the present day, but could be inaccurate for glacial times. However, some experiments done with ratios of one-fifth and one-fifteenth differ very little from the results presented in this work (not shown). Therefore, this parameterisation is much less sensitive to the melting rate below the ice shelves with respect to that at the grounding line. On the other hand, a recent study shows the need to make the basal melting decrease smoothly to zero when approaching the grounding line from the ice shelf to avoid resolution-dependent performances (Gladstone et al., 2017). This can be achieved for example by considering the submarine melt to be dependent on the water-column thickness beneath the ice shelf, as Bradley et al. (2018) suggested in their work. It is interesting to compare results from this work with theirs, as the same scientific problem, i.e. the impact of submarine melting on the evolution of the past GrIS, is addressed from two different points of view. The submarine melt scheme used in this work is implicitly a linear function of the water depth, as, going down through the water column, the melt rate maintains the same value until it reaches a critical zone at which the sub-shelf melt is set to 50 $m\ a^{-1}$ to avoid improbable ice expansion (Section 2.5). This work shows that without melting/freezing at the grounding line (for $B_{\mathrm{ref}} = 0$ and $\kappa = 0$), the GrIS is not able to reach the continental shelf break (Fig. 3.9 a). However, it is able to extend past the present-day coastline, similar to the simulations presented by Bradley et al. (2018). Moreover, experiments performed under the same oceanic conditions with increased basal sliding at the margins show that GRISLI-UCM model allows further expansion during the glacial periods (not shown). On the other hand, the model used by Bradley et al. (2018) has the capability of making the GrIS retreat during interglacial periods only if the submarine melt-water depth relation is exponential and if RSL variations due to both local and non-local effects are considered. On the contrary, a proper retreat during the deglaciations is always achieved in the simulations of this work (Fig. 3.12 and Fig. 3.3-3.4),

although the GIA does not account for global effects. These discrepancies are probably due not only to the different submarine melt scheme considered in each model, but also to the features of the model dynamics, such as the sliding law and the grounding-line migration scheme. Following these assumptions, a sub-grid treatment of the small-scale processes taking place at the grounding line, such as basal sliding, sub-shelf melting, hydrology and migration, will be added in the model in the future. This will provide a more realistic description of grounding-line processes such as the enhanced submarine melting as well as the basal drag at the margin of fast grounded ice.

It is finally important to remark that the GrIS evolution during the last glacial cycle has been assessed here only from an oceanic point of view, while the influence of different atmospheric forcings has not been investigated. This simplification may be especially important for the results shown for the LIG and the Holocene, in which the retreat is mostly induced by surface ablation. However, this point will be in the scope of future work.

3.5 Conclusions

In this chapter, the impact of paleo oceanic temperature variations on the evolution of the GrIS is assessed on a glacial-interglacial time scale. By using a three-dimensional hybrid ice-sheet-shelf model including a parameterisation of the basal melting rate at the GrIS marine margins, the model simulates the evolution of the whole ice sheet under temporally variable oceanic conditions. Firstly, the magnitude of the oceanic forcing applied at the ice-ocean interface triggers and drives the grounding-line advance (through water freezing) and retreat (through ice melting). Secondly, it induces a dynamic adjustment of the grounded ice sheet, determining the amount of ice grown (lost) during the cold (warm) stages. Although the GrIS evolution is a result of the atmospheric and oceanic forcings operating together, this study shows that the ocean is a primary driver of the GrIS glacial advance. Not only must the oceanic forcing be activated, but it must be strong enough to reproduce a reliable GrIS evolution

throughout the glacial cycles. It is important to remark that other factors which could affect the GrIS evolution have not yet been explored in detail. Sensitivity tests to the atmospheric forcing, glacial isostatic adjustment effects and spatially non-uniform submarine melt rates should be taken into account in the future to analyse the scientific problem from a broad range of points of view. Nevertheless, this work shows that changing oceanic conditions is a fundamental contributor to the evolution of the whole GrIS, suggesting that the oceanic component should be included as an active forcing in paleo ice sheet models.

Chapter 4

Submarine melt as a potential trigger of the North East Greenland Ice Stream margin retreat during Marine Isotope Stage 3*

As seen in Chapter 1, several coastal regions of the Greenland Ice Sheet (GrIS) have suffered a significant ice mass loss during the last decades. One of these regions, the Northeast Greenland Ice Stream (NEGIS), that is the largest ice stream in the present-day GrIS and located in the north-east, has lost mass since 2001 and has experienced huge changes in the last years. This ice mass loss is partly due to increasing oceanic temperatures in the subpolar North Atlantic, which enhance submarine basal melting and mass discharge. This demonstrates the high sensitivity of this region to oceanic changes. Alongside, a recent study suggests that the NEGIS grounding line was 20-40 km behind its present-day location for 15 ka during Marine Isotopic Stage (MIS) 3, raising an important conundrum. This retreat has been attributed to a combination of atmospheric and external forcings but a modelling approach to the problem is pending. Here, the sensitivity of the NEGIS to the oceanic forcing during the Last Glacial Period (LGP) is investigated using the three-dimensional hybrid ice-sheet-shelf model described in Chapter 2. The submarine melting at the grounding line and below the ice shelves is parameterised as defined in Section 2.5. Specifically here, it is made to evolve in such a way that is active during relatively warm time periods, such as the present, the Last Interglacial (LIG, ca. 130-115 ka BP) or MIS-

* The main contents of this chapter are included in:
Tabone, I., Robinson, A., Alvarez-Solas, J. and Montoya, M.: Submarine melt as a potential trigger of the NEGIS margin retreat during MIS-3. *submitted to The Cryosphere*

3, whereas it reaches zero at the onset of the LGM. The NEGIS marine margin response to increasing basal melting rates is here studied during the LGP to show that a sufficiently high oceanic sensitivity could have driven a considerable NEGIS grounding-line retreat during MIS-3 from its former glacial position. These results potentially explain the recently proposed NEGIS grounding-line retreat during MIS-3.

This chapter is structured as follows: first, the present-day and past NEGIS evolution is introduced (Section 4.1); the experimental design applied in this work is described in Section 4.2; the results from the transient simulations are shown in Section 4.3 and are followed by their discussion (Section 4.4. Finally, the conclusions of this work are summarised in Section 4.5.

4.1 The North East Greenland Ice Stream (NEGIS)

The Northeast Greenland Ice Stream (NEGIS) is the largest ice stream in the Greenland Ice Sheet (GrIS), extending more than 600 km inland (Joughin et al., 2001) and discharging 12 % of the whole ice sheet through three outlet glaciers: Nioghalvfjerdsfjord Gletscher (NG), Zachariae Isstrøm (ZI), and Storstrømmen Gletscher (SG) (Rignot and Mouginot, 2012). These marine-terminating glaciers have suffered huge changes in the last decades. ZI retreated and almost lost its remaining ice shelf after more than a decade of enhanced ice mass loss, increasing its speed by 50 % in less than 15 years (Mouginot et al., 2015). Although NG seems to be more stable than ZI due to its bed configuration, it has lost mass since 2001 (Mayer et al., 2018), with peaks of speedup during 2016 (Rathmann et al., 2017). Ice loss from these two marine-terminating glaciers is thought to be partly related to the increasing temperature of North Atlantic waters (Khan et al., 2014; Mouginot et al., 2015), which increases the oceanic heat flux and accelerates the submarine melting (Mayer et al., 2018). This hypothesis is supported by the three-decade-long observed warming in the subpolar North Atlantic (Straneo and Heimbach (2013) and references therein). Moreover, warmer oceanic waters in Fram Strait could directly reach the NG, further increasing its basal melting

and potentially causing the loss of its floating ice tongue (Schaffer et al., 2017). A recent study investigating the response of NG and ZI to oceanic forcing with the aim of constraining their future stability suggests a further slow retreat of NG and a complete loss of the ZI ice tongue due to increasing melt rates in the next decades (Choi et al., 2017) but these conclusions could be even too conservative (Larsen et al., 2018).

Reconstructions suggest that during the Last Glacial Maximum (LGM), ca. 21 ka BP, the northeastern region of the GrIS considerably advanced, likely reaching the continental shelf break, at 250-300 km from the present-day coastline (Arndt et al., 2015, 2017; Winkelmann et al., 2010). Although the age of these LGM reconstructions is still poorly constrained, the combination of cosmogenic exposure and radiocarbon dating has recently facilitated the reconstruction of the position of the NEGIS further back in time, over the last 45 ka (Larsen et al., 2018). This study suggests that the ice margin largely fluctuated throughout this period, even retreating by 20-40 km behind its present-day position during part of Marine Isotopic State (MIS) 3, ca. 60-25 ka BP. This retreat was attributed to a combination of atmospheric and external forcings but this conclusion was not confirmed through ice-sheet modelling. In addition, the potential role of oceanic forcing in this retreat has not been explicitly investigated. In the light of the ongoing changes in the GrIS attributed to ice-ocean interactions, this appears as a plausible mechanism that needs to be investigated.

4.2 Experimental design

The NEGIS response to past oceanic forcing is simulated using the three-dimensional, hybrid ice-sheet-shelf GRISLI-UCM model, described in Chapter 2 and already used to study the sensitivity of the GrIS to glacial-interglacial oceanic variations (Chapter 3). Here, in the transition between grounded slow-moving ice-sheet regions and floating shelves, the dynamics is solved by the simple addition of the SIA and SSA velocity solutions (Winkelmann et al., 2011) (Section 2.2). The atmospheric temperature (precipitation) forcing applied to the model follows

an anomaly method according to which the present-day climatological temperature (precipitation) is perturbed by (the ratio of) past anomalies obtained from a spatially-uniform proxy-derived index, as in Section 3.2. The climatic index is derived from the Greenland temperature reconstruction for the Holocene (Vinther et al., 2009), the North Greenland Ice Core Project (NGRIP) reconstruction for the LGP (Kindler et al., 2014) and the North Greenland Eemian Ice Drilling (NEEM) reconstruction for the LIG (NEEM, 2013) (Chapter 3). The composed signal is then smoothed so that the spectral components below orbital frequencies are removed (i.e., here, are removed periods below 16 ka). Therefore, the atmospheric forcing is assumed to be orbitally-driven only, as in the study of Chapter 3. Surface ablation is calculated by the simple positive degree (PDD) scheme (Reeh, 1989). Although this scheme does not account for past insolation changes, the primary aim of this work is to assess the sensitivity of the NEGIS to the oceanic forcing during glacial times. Therefore, it is expected that the choice of the surface melt model should not jeopardise our results.

The oceanic forcing is prescribed in the model through the parameterisation of the submarine melt rate at the grounding line and below the ice shelves defined in Section 2.5. As described there, the basal melting rate at the grounding line follows an anomaly method for which the PD submarine melt rate is perturbed by past changes in the oceanic temperature, as

$$B_{\mathrm{m}}(t) = B_{\mathrm{ref}} + \kappa \Delta T_{\mathrm{ocn}}(t). \tag{4.1}$$

$B_{\mathrm{m}}(t)$ is the melt rate at the grounding line ($m\ a^{-1}$), κ is the heat-flux exchange coefficient between water and ice at the ice-ocean front ($m\ a^{-1}\ K^{-1}$), and B_{ref} represents the reference submarine melting rate around Greenland. Past oceanic temperatures below the ice ($\Delta T_{\mathrm{ocn}}(t)$) are defined as in Section 3.2, thus evolve in phase with atmospheric temperatures as

$$\Delta T_{\mathrm{ocn}}(t) = (1 - \alpha(t))(T_{\mathrm{LGM,ocn}} - T_{\mathrm{PD,ocn}}). \tag{4.2}$$

Here, α(t) is the same climatic index filtered at orbital timescales used for the atmospheric forcing (Fig. 4.1, upper panel). $T_{\mathrm{LGM,ocn}} - T_{\mathrm{PD,ocn}}$ is the glacial mi-

nus interglacial oceanic temperature anomaly, here set to the spatially-constant value of -1 K (Annan and Hargreaves, 2013; MARGO, 2009). In this sensitivity test, B_{ref} is considered to be spatially-uniform around Greenland for the sake of simplicity, as in the experimental design of Chapter 3. Since B_{ref} is by construction proportional to the oceanic sensitivity κ (Section 2.5), B_{ref} scales with it. Here, B_{ref} is prescribed as equal to $\kappa \cdot 1K$. Investigated values of κ range from 0 to 10 $m\ a^{-1}\ K^{-1}$; thus B_{ref} ranges from 0 to 10 $m\ a^{-1}$. These κ values are consistent with the inference from the Antarctic Ice Sheet that a change of 1 K in the oceanic temperature varies the melt rate by 10 $m\ a^{-1}$ (Rignot and Jacobs, 2002). The B_{ref} values are in the range of the submarine melt observed at the grounding line of NEGIS and other Greenland glaciers (Wilson et al., 2017; Straneo and Heimbach, 2013). Note that refreezing below the grounding line is not allowed in this study and it is cut off to zero, thus there is neither melting nor refreezing during the LGM for the whole set of experiments. The spectrum of resulting submarine melt rates leads to 11 different submarine melt configurations, for which an increase in the oceanic sensitivity κ entails an increase of the melting rate during MIS-3 (Fig. 4.1). These configurations allow investigating the role of the submarine melting rate on the NEGIS margin position during the LGP. Simulations of the whole GrIS are performed for two glacial cycles with a horizontal high resolution of 10 km, with the first cycle being used as spinup. The analysis of the results focuses on the NEGIS sector.

4.3 Results

The experiment with submarine melt prescribed to zero ($\kappa = 0$, $B_{\mathrm{ref}} = 0$), which is hereafter referred to as the unperturbed experiment, shows the NEGIS margin rapidly advancing towards the continental shelf during glacial inception (Fig. 4.2). In less than 20 ka after the peak of the Eemian, the grounding line advances through the inner sector of the continental shelf, extending offshore to a distance of about 250 km from the PD NEGIS margin already at around 70 ka BP. During MIS-3, the ice-margin position remains substantially steady. The

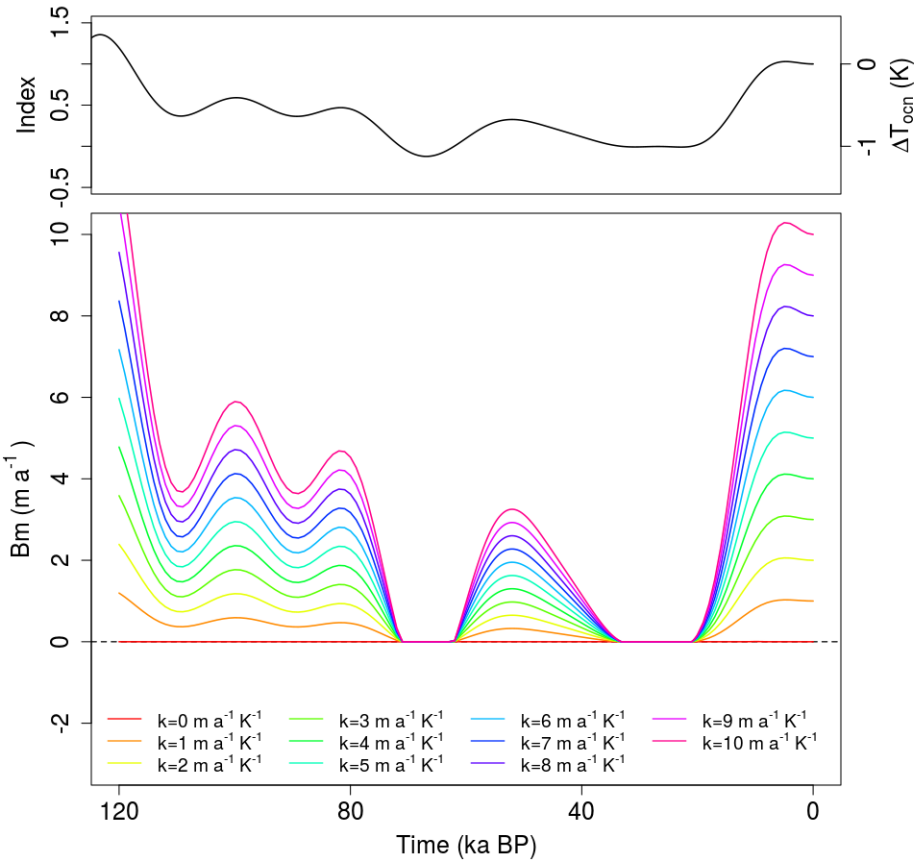

Fig. 4.1: Orbital-driven α index and its associated oceanic temperature anomaly (upper panel) and potential submarine melt-rate evolution during the LGP for increasing B_{ref} and κ values considered in the experiments (lower panel).

maximum extension of the NEGIS is reached during the LGM, when the ice sheet becomes grounded slightly further offshore (about 20 km) reducing the area of the floating ice shelf in the region (Fig 4.3 a-e).

In all other simulations, the ocean forcing is switched on ($\kappa, B_{\mathrm{ref}} > 0$) and the oceanic sensitivity gradually increases by 1 $m\ a^{-1}\ K^{-1}$ from a submarine melt configuration to another (Fig. 4.1). The location of the grounding line at

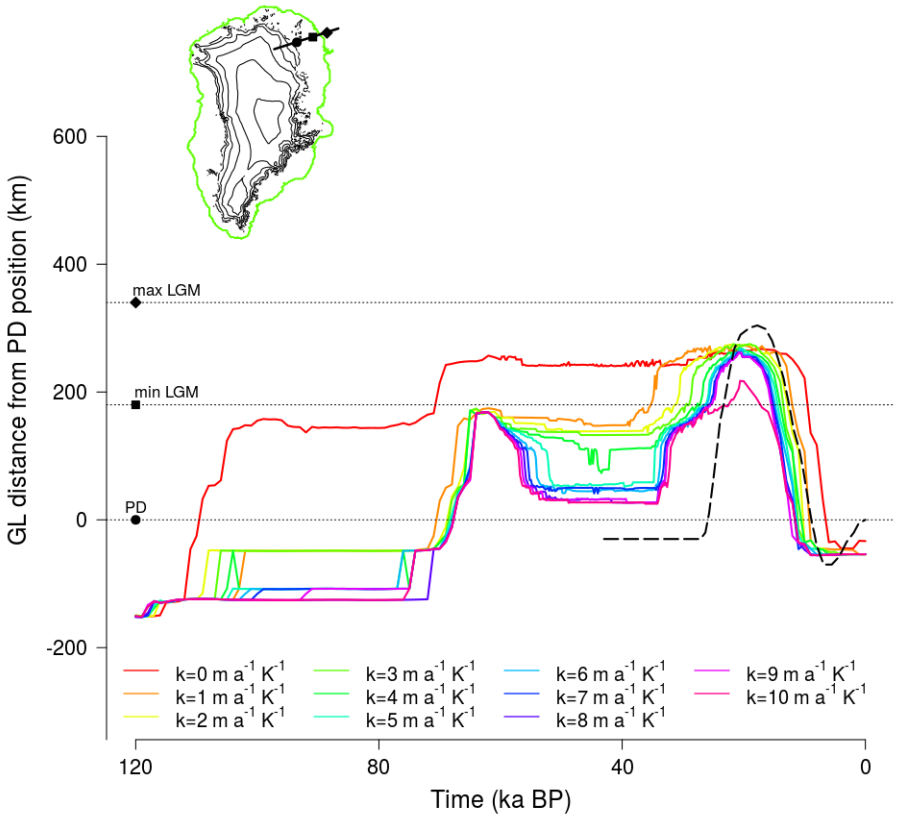

Fig. 4.2: Evolution of the NEGIS grounding line relative to its observed present-day position for the set of experiments. The grounding-line distance has been calculated along a transect which follows approximately the flow direction of NEGIS terminating-glaciers (top-left figure of the panel). Dashed black line shows the reconstruction by Larsen et al. (2018). The black points on the GrIS figure (circle, square and diamond) show the PD NEGIS grounding-line position and the minimum and maximum expected advance of the ice sheet at the LGM according to Funder et al. (2011). The maximum simulated glacial extent (grounded ice only) is also reported on the GrIS map (green line, simulated for $\kappa = 3\ m\ a^{-1}\ K^{-1}$).

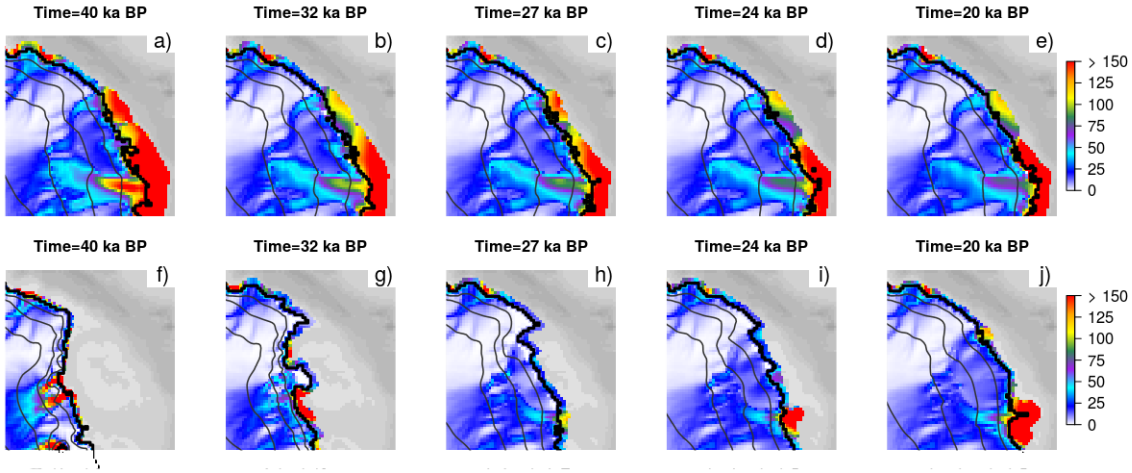

Fig. 4.3: Snapshots of the vertically-averaged velocity U ($m\ a^{-1}$) in total absence of submarine melting (a-e) and in presence of active orbital-driven oceanic forcing ($\kappa = 8\ m\ a^{-1}\ K^{-1}$, $B_{\mathrm{ref}} = 8\ m\ a^{-1}$) (f-j) at different times along MIS-3 and the LGM. U is calculated as $\sqrt{U_x^2 + U_y^2}$, where U_x and U_y are the vertically-intergrated horizontal velocities u and v, respectively (Eq. 2.6). Ice surface elevation is shown through dark grey contour lines (every 500 m). The black line represents the position of the simulated grounding line.

the LIG is the same in all simulations and thus insensitive to κ, and set mainly by the atmospheric forcing. Another common feature of these simulations is the response of the grounding-line position right after the peak of the Eemian (Fig. 4.2): the inclusion of positive melt rates before 70 ka BP somewhat constrains the NEGIS margins between 200-300 km upstream of the grounding-line position obtained for the unperturbed experiment, close to its location at the LIG. At about 70 ka BP, the ice margin starts to advance towards the continental shelf break, reaching the minimum LGM grounding-line position estimate based on reconstructions (Funder et al., 2011) in 5-10 ka.

The strongest reaction of the NEGIS grounding line to the applied submarine melting rate is found during MIS-3, when increasing the oceanic forcing not only

helps to preclude the grounding-line advance (as compared to the unperturbed case with no oceanic forcing) but furthermore triggers its retreat. By including a basal melt rate of $0 - 0.5\ m\ a^{-1}$ ($\kappa = 1\ m\ a^{-1}\ K^{-1}$), during MIS-3 the location of the NEGIS margin moves 100 km further inland with respect to the unperturbed experiment. Increasing the submarine melt up to $0 - 1.2\ m\ a^{-1}$ ($\kappa = 4\ m\ a^{-1}\ K^{-1}$) not only helps to constrain the NEGIS advance towards the continental shelf after glacial inception (ca. 115 ka BP), but subsequently triggers a slight grounding-line retreat inland by 80 km more which culminates at around 40 ka BP. A higher oceanic sensitivity ($\kappa = 5\ m\ a^{-1}\ K^{-1}$) leads to a further and earlier retreat during MIS-3. The minimum extent of grounded ice during MIS-3 is reached around 45 ka BP, when the grounding line retreats by more than 100 km inland from its position simulated at 60 ka BP. The ice margin then remains steady until the end of MIS-3 (Fig. 4.2 b). This value of κ and the resulting basal melt configuration (MIS-3 values above $1.6\ m\ a^{-1}$) act as a threshold above which the submarine melt rate forces the grounding line to retreat by several km inland during MIS-3. For higher basal melt rates the grounding line retreats further inland, stationing at only 30-40 km far from the PD position.

The effect of the submarine melt rate applied to the NEGIS marine margin during MIS-3 is also perceived far inland. The basal melt imposed at the ice-ocean interface (region B) causes the ice margin to retreat onshore and leads to ice discharge (Fig. 4.4). The reduction of buttressing previously ensured by the presence of ice on the continental shelf increases margin velocities, which propagate inland (Fig. 4.3 f), causing a decrease of ice thickness in the ice-sheet interior (region A). An initial strong peak in ice discharge is observed, following the initial increase of submarine melting and loss of buttressing, but the effect persists with further ice discharge until the end of MIS-3. At this moment, the absence of melt imposed through the LGM allows the grounding line to advance again towards the continental shelf break (Fig. 4.3 g-j). The maximum distance reached at the peak of the LGM and the time of the onset of the advance are inversely proportional to the melt rate suffered in the previous millennia (Fig.

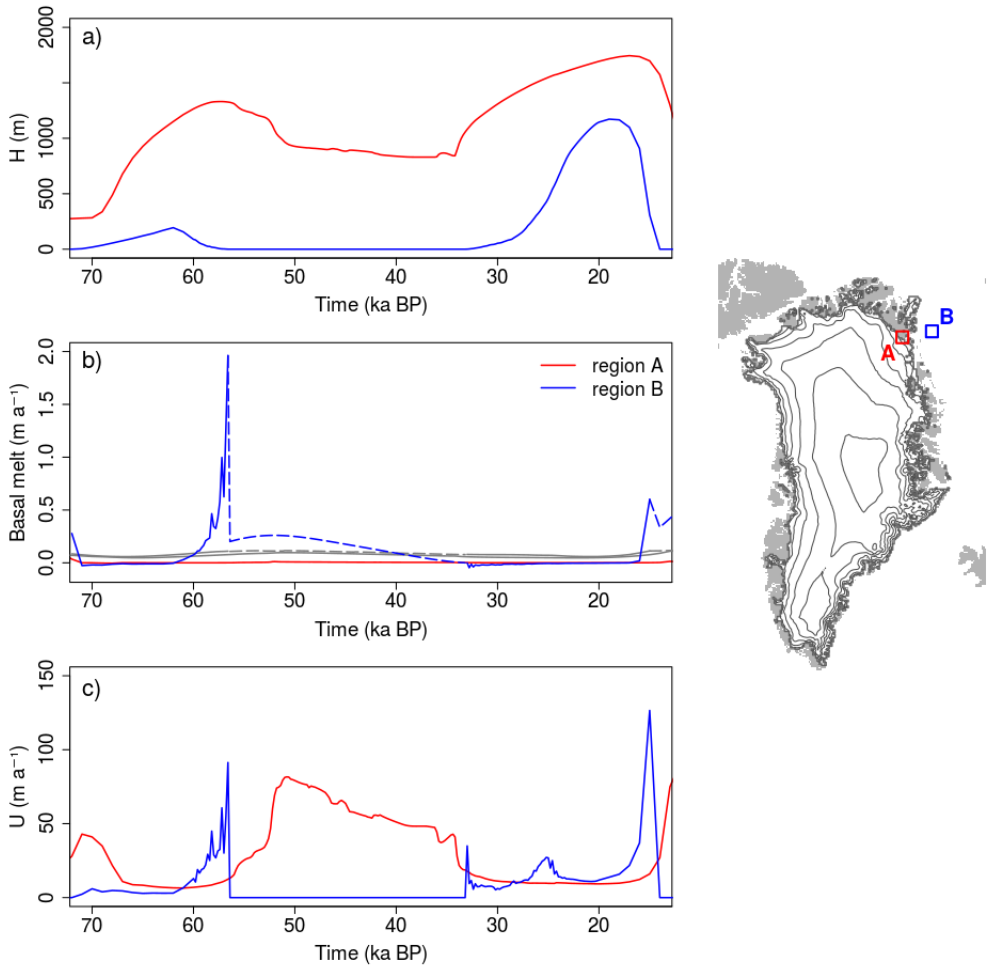

Fig. 4.4: Time series of the averaged a) H (in m), b) basal melt and c) U (both in $m\ a^{-1}$) within the area including the PD grounding line position (red lines, region A) and far offshore in the continental shelf (blue lines, region B) in presence of orbital-driven submarine melt during MIS-3 ($\kappa = 8\ m\ a^{-1}\ K^{-1}$). Grey lines in panel b) show the contribution to surface mass balance (accumulation minus ablation) for regions A and B; dashed lines in panel b) show the potential contributions that would be observed in presence of ice.

4.1). A strong melt rate imposed during MIS-3 leads to a delayed triggering and spatially-constrained grounding line advance, and vice versa.

By construction, submarine melt occurs again after 20 ka BP, when both atmospheric and oceanic temperatures increase, contributing to push the grounding line back towards the ice-sheet interior (Fig. 4.2). The fact that the unperturbed experiment simulates this retreat as well demonstrates that it is driven by both increasing atmospheric and oceanic temperatures during the Holocene. Nevertheless, the presence of submarine melt at the NEGIS marine margins enhances the retreat and triggers it slightly earlier. However, this feature saturates for high values of B_{ref}, as a further retreat inland is constrained by the bathymetry.

4.4 Discussion

The NEGIS grounding-line fluctuations simulated in response to a high oceanic forcing in this set of experiments are similar to those suggested by Larsen et al. (2018) for the last 45 ka. However, there are some major differences between the results of this work and theirs that deserve further attention.

First, this work does not simulate a grounding-line retreat farther inland than the PD position (20-40 km) during MIS-3, although these simulations do show a retreat of more than 100 km with respect to the previous millennia. The evidence of a MIS-3 retreat behind the PD NEGIS margin position has been attributed by Larsen et al. (2018) to lower accumulation rates, high incoming solar radiation and increasing summer air temperatures operating together. Since the sensitivity to these forcings has not been investigated separately and these experiments do not show such an extended retreat, it is not possible neither to confirm nor discard their hypothesis. However, this work has demonstrated that the presence of relatively high submarine melt rates at the NEGIS grounding line during MIS-3 is enough to cause a substantial retreat of its marine margins during this period.

Second, the simulated grounding-line advance during the LGM is smaller than the maximum extension suggested by reconstructions (Funder et al., 2011). This bias furthermore increases with increasing oceanic forcing. However, even in the

unperturbed experiment, which allows the largest ice-sheet expansion due to the absence of melting at the marine margins, the grounding line does not reach the continental shelf break either. This could be related to model dynamics, such as insufficient basal drag imposed at the base of the ice streams or the ice velocity mixing in transition zones, or simplified boundary conditions.

Third, the timings of the grounding-line advance/retreat for the last 35 ka of the LGP do not precisely correspond to those proposed by Larsen et al. (2018). In the experiments that show a significant retreat during MIS-3 ($\kappa > 4\ m\ a^{-1}\ K^{-1}$), both the grounding-line advance at the end of this stage and the retreat at the onset of the Holocene are simulated earlier than expected. This is due to the submarine melting signal representing oceanic temperature anomalies, which saturates at around 35 ka BP and is switched on again at 20 ka BP, assuming that the LGM starts and ends at these times. By using the same α for both atmospheric and oceanic forcing, it is assumed that the evolution of the ocean around Greenland at orbital timescales is comparable to that of the climate. Although this is a reasonable assumption, any uncertainty in the orbital forcing affects the ice-sheet retreat during the Holocene which is supposed to be a combination of atmospheric and oceanic temperatures (Larsen et al., 2018). The Holocene maximum is quite well reproduced in these submarine melting configurations (Fig. 4.1) and in the atmospheric temperature evolution. However, the slight basal melt decrease applied in the late Holocene is not sufficient to make the grounding line advance back towards the continental borders and the inaccurate position simulated at the PD is a direct consequence of this simplification.

The grounding-line retreat at the PD slightly reflects the magnitude of the submarine melt rate imposed at the NEGIS ice margins during the late Holocene, which is related to the value of B_{ref}. The simulated retreat is unrealistic (50-70 km farther inland than the observed position). Estimated PD grounding line melt rates at 79°N reach peaks of 50 $m\ a^{-1}$, which are even higher than the B_{ref} values considered in this work (Wilson et al., 2017). Imposing these would likely cause a farther retreat inland. This bias found in our experiments could be related to the low spatial resolution of the model (10 km) which does not allow for a precise treatment of the grounding line zone and may trigger nonlinear

effects, enhancing grounding-line retreat farther inland than expected. Another factor affecting this extended PD retreat is related to the design of the submarine melt signal itself during the Holocene, which shows a constant increase from 0 to the set B_{ref} value through the last 20 ka. Peaks of up to 50 $m\ a^{-1}$ occur at the NEGIS margin, however it is unlikely that this could have happened for a long period of time and in such a persistent way. This continuous and spatially-extended melt increase contributes to enhance the retreat at the PD by several km.

This work represents the first attempt to simulate the striking margin retreat reconstructed for the NEGIS during MIS-3 (Larsen et al., 2018). Here it is shown that the orbitally-driven oceanic warming during MIS-3 is sufficient to explain the retreat of the NEGIS grounding line during part of the LGP. Nevertheless, the rapid occurrence of warm oceanic pulses on millennial timescales is an important characteristic of MIS-3. Given the non-linear response of subglacial melting to temperature variations (e.g. Mikkelsen et al. (2018)), this effect could potentially modulate the orbitally-driven response on shorter timescales. A complete treatment of the problem from this perspective is difficult, however, by the absence of reconstructions of the oceanic conditions of the northeastern part of Greenland on these timescales during MIS-3.

In addition, such a retreat of the ice margin may have triggered feedbacks on the local climate that are not taken into account in this work. For example, it is possible that this large ice retreat would have caused changes in the albedo, affecting surface air temperatures and snow accumulation. Other feedbacks related to the freshwater flux into the ocean could have led to variations in sea ice and local oceanic circulation. All these processes, not included here, could have additionally contributed to variations in the ice thickness and grounding-line position, and should be investigated in the future for a complete understanding of the conundrum.

4.5 Conclusions

In this chapter, the sensitivity of the NEGIS ice margin to oceanic forcing is studied during the LGP. To this end, the three-dimensional, hybrid ice-sheet-shelf GRISLI-UCM model is used to perform simulations of the GrIS for which submarine melt follows a ice-core-proxy-derived curve assumed to represent the evolution of both atmospheric and oceanic temperatures at orbital scales. The increase in basal melt during MIS-3 reflects a relatively warm oceanic state, whereas the lack of basal melt during the LGM corresponds to the associated expected minimum in oceanic temperatures. It is shown that in the absence of submarine melting during the entire LGP, the grounding line advances towards the continental shelf just after the LIG. On the other hand, switching on the oceanic forcing helps to constrain the ice margin advance during MIS-3. Sufficiently high submarine melt rates eventually trigger its retreat by more than 100 km from its former position. The lack of basal melt during the LGM then resumes the grounding-line advance by 200 km towards the continental shelf break. These results robustly show that a prolonged presence of submarine melt at the NEGIS ice margin is enough to substantially contribute to grounding-line retreat there, which helps to explain the recently suggested NEGIS ice margin retreat during MIS-3.

Chapter 5

Impact of millennial-scale oceanic variability on the Greenland Ice Sheet evolution throughout the Last Glacial Period *

As introduced in Chapter 1, temperature reconstructions from several Greenland Ice Sheet (GrIS) ice cores indicate that the climate of Greenland experienced multiple abrupt temperature increases during the Last Glacial Period (LGP) known as Dansgaard-Oeschger (D-O) events. These millennial-scale climate fluctuations were first observed in Greenland ice cores, but strong evidence is also found in numerous marine sediments records, especially in the Nordic Seas and North Atlantic, tropical and subtropical stalagmite proxy archives, and in Antarctic Ice Sheet (AIS) ice cores, suggesting a worldwide imprint of D-O events. Although ultimate cause of D-O events is still debated, evidence from both proxy data and modelling studies robustly links these to reorganisations of the Atlantic Meridional Overturning Circulation (AMOC) and to abrupt warming events in the ocean. In parallel, during the LGP the GrIS expanded as far as the continental shelf break and was thus more directly exposed to oceanic changes than in the present, as seen in Chapter 3. Therefore oceanic temperature fluctuations on millennial timescales could have had a non-negligible impact on the GrIS. However, this aspect has not been investigated so far.

In this chapter the effect of millennial-scale oceanic variability on the GrIS evolution is assessed from the last interglacial to the present day. To do so, the

* The main contents of this chapter are included in:
Tabone, I., Robinson, A., Alvarez-Solas, J. and Montoya, M.: Impact of millennial-scale oceanic variability on the Greenland ice sheet evolution throughout the Last Glacial Period. *Climate of the Past Discussion*, DOI:https://doi.org/10.5194/cp-2018-129, in review.

three-dimensional hybrid ice-sheet-shelf model described in Chapter 2 is used and forced by millennial-scale oceanic fluctuations derived from paleo records. Variability in the ocean at millennial timescales is characterised by performing two large ensembles of simulations, one forced by both orbital and millennial components in the oceanic temperature signal and the other forced solely by the orbital frequencies. In both ensembles, the atmospheric forcing only includes orbital changes, so comparison between the two large ensembles returns the impact of millennial-driven oceanic fluctuations on the GrIS evolution. Moreover, the impact of the oceanic-induced perturbations at the marine margin is investigated onto the GrIS interior. Results show that the GrIS evolution during the LGP could have been strongly influenced by oceanic changes on millennial timescales, leading to ocean-induced ice volume contributions of more than 1.5 m SLE. Several regions across the GrIS could thus have been responsible for ice mass discharge during D-O events. This gives further insight into the potential role of the ocean in dynamic reorganisations of the ice sheet and enhanced ice discharge.

This chapter is structured as follows: first, data and model results suggesting a GrIS response to millennial-scale climate variability are introduced in Section 5.1; then, the forcing methods and the methodology used in this study are described in Section 5.2; in Section 5.3, the millennial-scale variability effect in the ocean on the GrIS evolution is first characterised and the impact of this oceanic oscillation on the GrIS transient dynamics is then described. Results and caveats of the model are then discussed (Section 5.4), and the main conclusions of this chapter are sumarised in Section 5.5.

5.1 The GrIS response to millennial-scale climate variability: proxy data and previous modelling work.

Evidence of ice-rafted debris (IRD) deposition in marine sediment cores suggests that the GrIS could have been a non-negligible source of iceberg discharge during the LGP (Jonkers et al., 2010). Cores drilled in the Irminger Sea (Van Kreveld

et al., 2000), Denmark Strait (Bond and Lotti, 1995) and close to Scoresby Sund (Stein et al., 1996) show evidence of iceberg transport sourced in East Greenland and the North-Northeast Greenland, among other sources (Andrews et al., 2017); also, sediments in Fram Strait show imprints of iceberg discharge from the Northern GrIS (Darby et al., 2002). Still, others link the IRD deposition found close to the east-southeast marine margin of the GrIS to local ice-sheet instability (Verplanck et al., 2009), and associate sediments found in the Labrador Sea to iceberg discharge coming from Baffin Bay during the Younger Dryas (Andrews et al., 2012). Also, other paleo reconstructions explicitly affirm that ocean temperature increase played a fundamental role in the GrIS retreat in the last deglaciation (Jennings et al., 2017). Recent proxy data collected by morain-derived marine shells suggest that the margin of the Northeast Greenland Ice Stream (NEGIS) region may have fluctuated throughout the LGP by more than 200 km (Larsen et al., 2018). All these examples suggest that the GrIS may have experienced substantial variability during the LGP and beyond. However, despite the evidence for millennial-scale climate variability during the Last Glacial Period (LGP) in Greenland, the specific role of the GrIS during D-O events has not been investigated in depth. Whether the GrIS contributed to oceanic reorganisations associated with D-Os via iceberg discharge is unknown and its evolution between the last interglacial and the Last Glacial Maximum (LGM) is still debated (Vasskog et al., 2015).

From a modelling perspective, only a few studies have tackled the response of the GrIS to millennial-scale climate variability throughout the LGP. Charbit et al. (2007) simulated the evolution of NH ice sheets by forcing their ice-sheet model with a glacial-interglacial climate anomaly scaled by a climatic index taken from the GRIP reconstruction, which retained millennial-scale temperature fluctuations. However, their model accounted only for grounded ice; ice shelves were not included and the effect of the ocean was thus not taken into account. Huybrechts (2002) also investigated the response of the GrIS to millennial-scale climate variability during the LGP with an ice-sheet model. However, the GrIS extent was controlled by orbital-only variations of past eustatic sea-level and millennial-scale fluctuations, both in sea level and in the ocean temperature, were omitted. Mar-

shall and Koutnik (2006) assessed the response of the NH ice sheets to climate variability at millennial timescales. They simulated the GrIS evolution using an ice-sheet model that included a calving parameterisation, and that was forced by millennial-scale temperature variations. Their results showed very little response of the GrIS to the imposed climate variability, with a weak increase in iceberg flux only during interstadials. However, this study did not explicitly investigate the effect of the millennial-scale variability in the ocean either.

A recent study has demonstrated the important role of oceanic conditions in the evolution of the GrIS throughout the past two glacial cycles (Tabone et al., 2018a). This study however focused on orbital oceanic variations. Thus, the effect of oceanic millennial-scale variations on the GrIS remains to be explored. Sea surface temperatures (SSTs) inferred from planktonic foraminifera in North Atlantic sediment cores vary typically from 7-8.5°C during interstadials to 3-3.5°C during stadials (Rasmussen et al., 2016). Recent SST estimates from a stack of sediment cores of the North Atlantic suggest a broad range of interstadial-stadial temperatures fluctuating between a maximum of 15°C and a minimum of 0°C, but typical SSTs anomalies in each location are lower (2-6°C) (Jensen et al., 2018). The oceanic temperature variation associated with D-O events may thus have an appreciable impact on the GrIS, therefore this issue needs to be investigated.

5.2 Experimental design

The response of the GrIS to millennial-scale oceanic variability during the LGP is investigated by using the ice-sheet-shelf GRISLI-UCM model (Chapter 2), already employed in Chapters 3-4 of this thesis. Here, transitional areas where deformational-flow and plug flow coexist are solved by adding the velocities of the SIA and SSA solutions (Winkelmann et al., 2011) (Section 2.2). The model is applied here to the GrIS domain with a spatial resolution of 20 km by 20 km. Atmospheric temperatures and precipitations vary through the same index approach applied in Chapters 3-4 (Banderas et al., 2018; Blasco et al., 2018;

Tabone et al., 2018a). Since the goal of this work is to investigate the sensitivity of the GrIS to past millennial-scale variability in the ocean, the atmosphere is considered as modulated only by orbital changes for simplicity, as already done in Chapters 3 and 4. This allows to study the direct effects of the millennial-scale fluctuations on the GrIS evolution due to the ocean only, being unperturbed by the millennial variability in the atmosphere too. Atmospheric temperature and precipitation are thus perturbed by orbital-only variations and their evolution is described by the same index-anomaly method of Chapter 3. Surface ablation is calculated by the positive degree day (PDD) scheme (Reeh, 1989). This scheme is known to be overly simplistic for both ice sheet models (Robinson and Goelzer, 2014) and EMICs (Bauer and Ganopolski, 2017) in the paleo context, as it does not incorporate the effect of incoming solar radiation changes. Nevertheless, since here we focus on the sensitivity of the ice sheet to millennial-scale oceanic variations during the LGP, the choice of this scheme should be sufficient for the purposes of this study.

The methodology used to force the ocean is similar to that used in the oher works of this thesis, except that the millennial-scale variability in the ocean which was omitted in the previous works is here included. This approach is analogous to that of Blasco et al. (2018) for the Antarctic domain. Basal melting at the grounding line and at the ice-shelf base is described through the parameterisation defined in Section 2.5. Once again, the basal melting rate at the grounding line B_m is parameterised as

$$B_m(t) = B_{\text{ref}} + \kappa \, \Delta T_{\text{ocn}}(t) \tag{5.1}$$

where B_{ref} is the prescribed basal melting rate for the present day ($m\ a^{-1}$), κ is the ocean-ice heat-flux exchange scaling factor ($m\ a^{-1}\ K^{-1}$) and ΔT_{ocn} is the oceanic temperature anomaly with respect to the climatological mean (K). Since the present-day basal melt rate for the whole Greenland domain is largely unconstrained, we assume it to be spatially constant, as in Chapters 3-4. The reference basal melt is then perturbed by its anomaly in time, which is here given by the sum of both orbital and millennial variability in the oceanic temperature, as

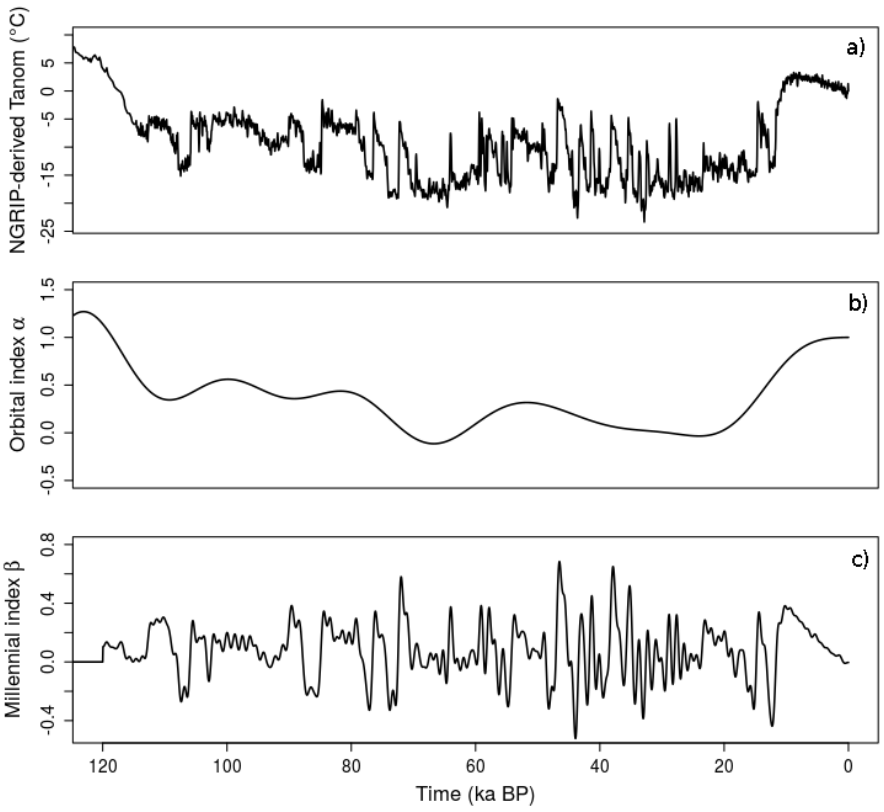

Fig. 5.1: NGRIP-Temperature anomaly reconstruction (a) used to construct the orbital-index α (b) and the millennial-index β (c) for the last glacial period. $\alpha(t)$ is built from the NGRIP-derived temperature anomalies (Tabone et al., 2018a), filtered to remove the spectral components below the orbital period ($1/f < 18\,ka$) and normalized between 0 and 1. β is derived by subtracting the orbital α index from the NGRIP-derived temperature signal, normalized between 0 ad 1, and then filtered below 1 ka to remove sub-millennial periods.

$$\Delta T_{\mathrm{ocn}}(t) = (1 - \alpha(t))\, \Delta T_{\mathrm{ocn}}^{\mathrm{orb}} + \beta(t)\, \Delta T_{\mathrm{ocn}}^{\mathrm{mil}} \tag{5.2}$$

Here, α is the same spatially-uniform climatic index used to perturb the atmosphere, built through a composite series of various proxy-derived temperature anomalies from the Last Interglacial period to the present day (Fig. 5.1a), as in Chapters 3-4. The index is then smoothed to remove the spectral components below the orbital frequencies ($1/f < 18\,ka$) and is normalized between 0 and 1 ($\alpha = 1$ at present day (PD) and $\alpha = 0$ at the LGM) (Fig. 5.1b). The β index (Fig. 5.1c) is the millennial index derived from the same normalized temperature anomaly signal as α, by subtracting the orbital α index (Fig. 5.1b) from the unfiltered multi-proxy temperature signal (Fig. 5.1a) normalized between 0 and 1, and then filtered to remove periods below 1 ka to eliminate sub-millennial components of the signal. $\Delta T_{\mathrm{ocn}}^{\mathrm{orb}}$ and $\Delta T_{\mathrm{ocn}}^{\mathrm{mil}}$ are the glacial-interglacial and interstadial-stadial oceanic temperature anomaly (K), respectively, both assumed to be in phase with the atmosphere. Here, to prevent unconstrained accretion below ice shelves and at the grounding line, negative basal melt rate (freezing) is cut off to 0 $m\ a^{-1}$. Changes in sea level at orbital timescales are prescribed following Bintanja and Van de Wal (2008).

Following the discussion above, the basal melting equation (Eq. 5.1) can be rewritten as:

$$B_m(t) = B_{\mathrm{ref}} + \kappa\, ((1 - \alpha(t))\, \Delta T_{\mathrm{ocn}}^{\mathrm{orb}} + \beta\, \Delta T_{\mathrm{ocn}}^{\mathrm{mil}}) \tag{5.3}$$

It is therefore clear that the basal melting formulation depends on the choice of four parameter values: B_{ref}, κ, $\Delta T_{\mathrm{ocn}}^{\mathrm{orb}}$ and $\Delta T_{\mathrm{ocn}}^{\mathrm{mil}}$. Here, these are all considered as spatially uniform around Greenland for the sake of simplicity. To assess the GrIS response to millennial-scale variability in the ocean we could simply consider varying the value of κ, which is the sensitivity of the oceanic forcing (Tabone et al., 2018a). However, by construction of Eq. 5.3, increasing κ does not necessarily mean increasing the millennial-scale oceanic effect alone, since this would enhance concurrently both the millennial and the orbital-scale components in the ocean. Therefore, investigating the oceanic millennial-scale variability effect on the past GrIS is not as straightforward as expected. Moreover, none of the four

parameters of Eq. 5.3 is perfectly constrained in reality, and a sensitivity study on the influence of their chosen values on the GrIS evolution would be required.

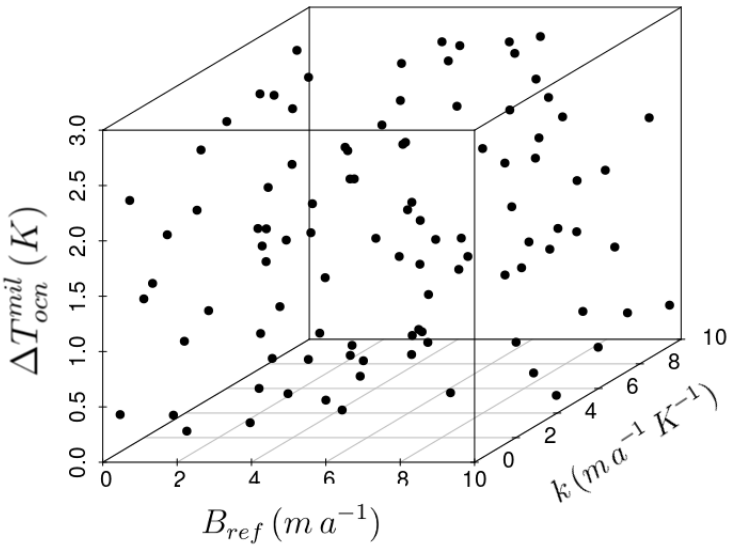

Fig. 5.2: Distribution of the simulations of the large ensemble (LE) produced by the Latin Hypercube Sampling (LHS) technique. The phase-space of parameters is built from B_{ref} ranging from 0 to 10 m a^{-1}, κ from 0 to 10 m a^{-1} K^{-1} and $\Delta T_{\mathrm{ocn}}^{\mathrm{mil}}$ from 0 to 3 K.

For these reasons, it is first useful to characterise the impact of millennial-scale variability in the ocean on the GrIS evolution testing a broad range of values of the key-parameters in Eq. 5.3. Following this approach, a large ensemble (LE) of model simulations using the near-random Latin Hypercube Sampling (LHS) technique (McKay et al., 1979) is performed. This approach allows us to efficiently explore the phase-space of the three parameters minimising the LE computational cost with respect to the full-factorial sampling technique. The LHS technique has

already been used to constrain different ice-sheet model parameters and to assess their influence on the model's behavior (Applegate et al., 2012; Robinson et al., 2017; Stone et al., 2010, 2013). By construction, the α and β indices share the same normalisation. Thus the glacial-interglacial and the interstadial-stadial oceanic temperature anomalies have the same (but opposite) amplitudes. This is also supported by estimate of both surface temperature anomalies (Annan and Hargreaves, 2013; Liu et al., 2009; MARGO, 2009; Zhang et al., 2014b). The problem is therefore reduced to only three degrees of freedom: $\Delta T_{\mathrm{ocn}}^{\mathrm{mil}}$ is set to vary between 0 and 3 K (SST around Greenland deduced from Liu et al. (2009), Zhang et al. (2014b), Vettoretti and Peltier (2015) and Bagniewski et al. (2017)), B_{ref} between 0 and 10 $m\ a^{-1}$ (chosen as a reasonable climatic mean between Rignot et al. (2010), Rignot et al. (2016), Straneo et al. (2012) and Wilson et al. (2017) for the largest tidewater glaciers around the GrIS, and Rignot et al. (2013) and Liu et al. (2015) for the Antarctic domain) and κ between 0 and 10 $m\ a^{-1}\ K^{-1}$ (following Rignot and Jacobs (2002) for the Antarctic domain). The parameter values are sampled from the specified ranges and, assuming that they are independent from each other, they are randomly combined to generate a total LE of 100 simulations (Fig. 5.2), named TOT simulations. At the same time, another set of identical simulations, except for the fact that the millennial contribution is set to 0 K for all of them, is performed. These are named ORB simulations from now on and are used for direct comparison with the TOT ones, as discussed in Section 5.3. The model is initialised using the present-day topography of Greenland from Schaffer et al. (2016). All the simulations of the LE cover the last two glacial cycles, with the first 120 ka considered as spin up and therefore not analysed.

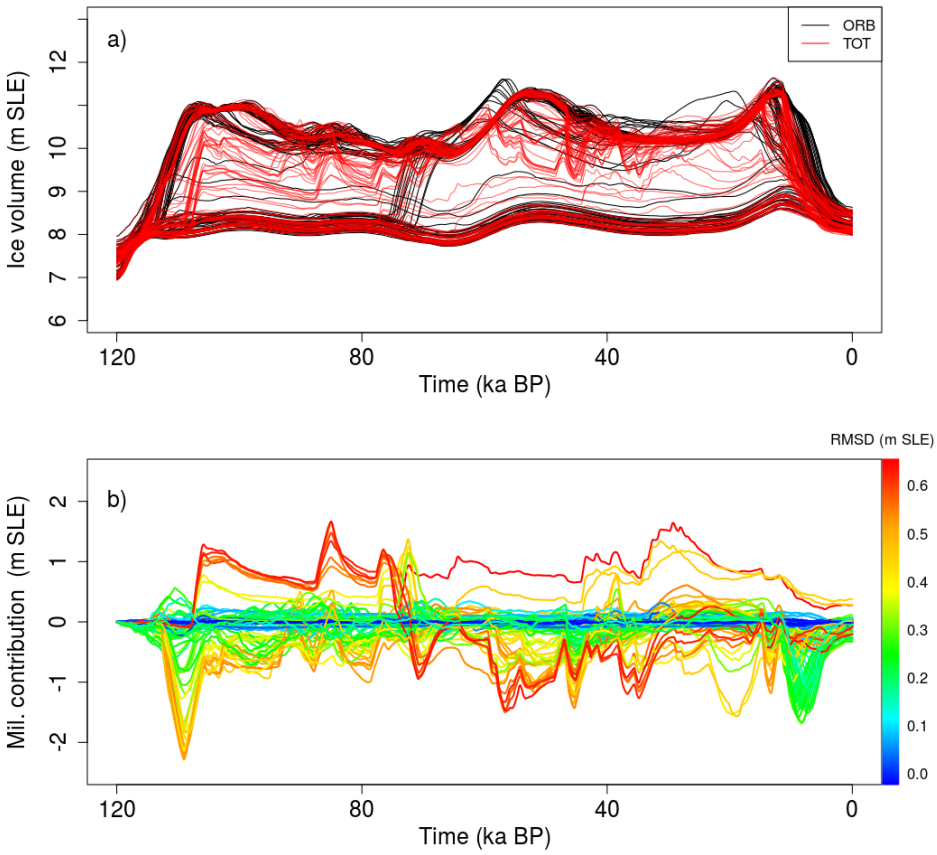

Fig. 5.3: a) Ice volume evolutions simulated by ORB (black curves) and TOT (red curves) throughout the LGP (m SLE) b) Oceanic millennial-scale variability contribution to the GrIS ice volume variation (m SLE; positive values indicate ice loss to the ocean). The color scale indicates the RMSD calculated in terms of ice volume residuals between TOT and ORB simulations (m SLE).

5.3 Results

5.3.1 Characterisation of oceanic millennial-scale variability

A first evaluation of the effect of millennial-scale oceanic variability effect on the whole GrIS can be made looking at the evolution of the simulated ice volume throughout the LGP (Fig. 5.3a). Apart for low oceanic forcing configurations for which both ORB (black curves) and TOT (red curves) present small ice volume deviations from their simulated present-day value, TOT simulations show higher ice volume fluctuations than ORB ones, especially during Marine Isotope Stage 3 (MIS-3). The impact of millennial-scale climate variability on the GrIS is better assessed through variations of the GrIS ice volume in TOT compared to the orbital-only controlled reference simulation (ORB) (Fig. 5.3b). This quantity is simply calculated as the difference between the ice volume simulated in TOT and that simulated in ORB for each pair of simulations in the LE. For a higher millennial-scale variability signal in the ocean, more millennial-scale variability in ice volume is expected. The contribution of millennial-scale climate variability to the ice-volume variations is quantified through the root mean square deviation (RMSD) of the residuals between the ice volume simulated in TOT and in ORB (m SLE), defined for the whole time series as:

$$\mathrm{RMSD_{Vol}} = \sqrt{\frac{1}{\mathrm{N_t}-1}\sum_{\mathrm{t}=1}^{\mathrm{N_t}}\left(\mathrm{Vol_{TOT}(t)}-\mathrm{Vol_{ORB}(t)}\right)^2} \tag{5.4}$$

where N_t is the total number of time steps in each simulation and $Vol_\mathrm{TOT}(t) - Vol_\mathrm{ORB}(t)$ is the ice-volume residual calculated as the difference between the two simulations at each time step. This quantity tells us how much the millennial forcing causes the volume to deviate from the background ORB simulation throughout the LGP. Fig. 5.3b associates the calculated RMSDs with the millennial-scale contribution to ice-volume variations (m SLE) for each simula-

tion of the LE. The ice-volume contribution due to millennial-scale variability can reach peaks of more than 1.5 m SLE at certain times during the LGP.

A second and complementary approach used to identify the effect of the oceanic millennial-scale variability on the GrIS evolution is to calculate the deviation of the ice velocity simulated by TOT from its background state ORB. The methodology is similar to that used for the ice volume, except for the fact that now the standard deviation is first calculated for each grid point ij as $\mathrm{RMSD}_{\mathrm{U_{ij}}} = \sqrt{\frac{1}{\mathrm{N_t}-1}\sum_{\mathrm{t}=1}^{\mathrm{N_t}}(\mathrm{U_{ij,TOT}(t)} - \mathrm{U_{ij,ORB}(t)})^2}$ and then averaged for the entire domain:

$$\mathrm{RMSD_U} = \frac{\sqrt{\sum_{\mathrm{ij}} \mathrm{RMSD_{ij}^2}}}{\mathrm{N}} \tag{5.5}$$

where N is the total number of grid points of the GrIS domain.

The resulting effect of the oceanic millennial-scale variability on the GrIS evolution during the LGP is characterised examining jointly the RMSDs calculated for ice volume and velocities. Ice-volume evolution is a good benchmark for understanding the overall effect of the oceanic variability throughout the time, but U is the direct expression of how the ice dynamics are affected by the forcing. Therefore, the largest millennial-scale variability in the ocean is associated to concomitantly high volume and velocity RMSDs. The higher the millennial-scale variability in the ocean, the more the ice volume and ice velocity in TOT are expected to deviate from the ORB simulation. Nevertheless, it is interesting understanding which combination of perturbed parameters in the basal melting equation Eq. 5.3 leads to the highest millennial variability in terms of both quantities. It is find that the effect of a high oceanic millennial-scale variability is fairly well constrained in the parameter phase-space, at least per each couple of analysed variables (Fig. 5.4). Very low oceanic-driven variability is generally associated with low values of κ and ΔT_{ocn} (weak oceanic forcing). These configurations lead to basal melting evolutions that do not deviate much from the reference-state basal melting throughout the LGP (blue curves of Fig. 5.5). Low millennial-scale variability is also found for combinations of low B_{ref} with high κ (or high $\Delta T_{\mathrm{ocn}}^{\mathrm{mil}}$), and for high κ with high $\Delta T_{\mathrm{ocn}}^{\mathrm{mil}}$. The reason is that these are associated with a basal-melt evolution that rapidly saturates at the cut-off

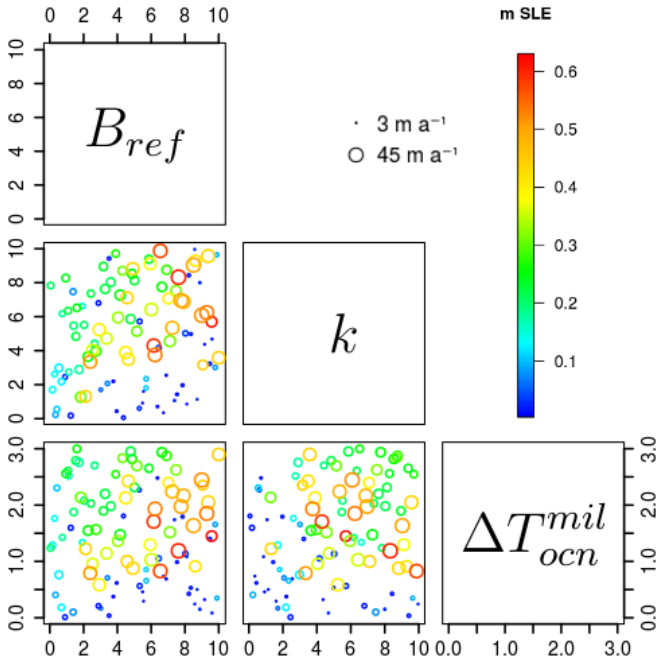

Fig. 5.4: Evaluation of the effect of the oceanic millennial-scale variability for each pair of parameters perturbed in the basal melting equation (Eq. 5.3). The range volume (m SLE, colour scale) and ice velocity ($m\ a^{-1}$, circle size) RMSDs is shown. The simulation with the highest millennial-scale variability is represented by the largest red circle; the simulation with the lowest variability is represented by the smallest blue circle.

value 0 $m\ a^{-1}$ (no melting, since freezing is not allowed) after the Eemian and maintains that state throughout the LGP (light blue curves in Fig. 5.5). It is between these two configurations, with medium-high B_{ref} and high κ, that the resulting basal melting signal allows for a high millennial-scale variability in the ocean, i.e. a signal that exhibits a sufficient number of high melting peaks at millennial time-scales that sometimes saturates at 0 $m\ a^{-1}$. A similar logic can

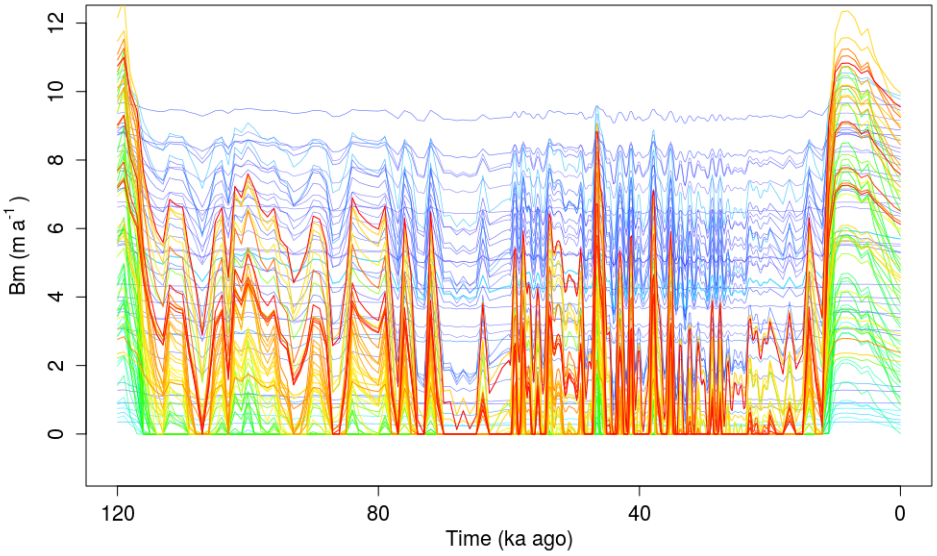

Fig. 5.5: Ensemble of basal melting rate evolutions for the 100 LE simulations throughout the last glacial period. Color scale refers to the colored legend of Fig. 5.3.

be followed considering $\Delta T_{\mathrm{ocn}}^{\mathrm{mil}}$ instead of κ. Therefore, high κ must be associated with low $\Delta T_{\mathrm{ocn}}^{\mathrm{mil}}$ and vice versa to produce high millennial-scale variability in the basal melt, as reflected in Fig. 5.4 as well.

5.3.2 Oceanic millennial-scale variability impact on transient dynamics

The aim of this section is to investigate the effect of oceanic millennial-scale variability on the transient GrIS dynamics and ice-sheet evolution during the LGP. To this end, the simulation from the LE which corresponds to the maximum millennial-scale variability response in terms of both ice volume and velocity is

chosen and compared to its corresponding background simulation. As expected from the characterisation of the millennial variability discussed above, the simulation chosen has medium-high B_{ref} (7.6 $m\ a^{-1}$), high κ (8.3 $m\ a^{-1}\ K^{-1}$) and consequently medium $\Delta T_{\mathrm{ocn}}^{\mathrm{mil}}$ (1.2 K). From now on, this simulation and its corresponding orbital-only reference simulation are referred to as $\mathrm{TOT}_{\mathrm{max}}$ and $\mathrm{ORB}_{\mathrm{max}}$, respectively.

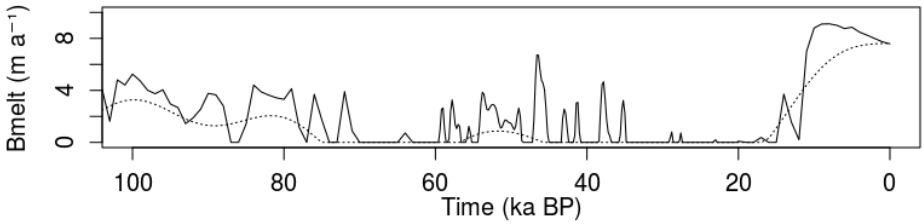

Fig. 5.6: Evolution of the submarine melting used to force the $\mathrm{TOT}_{\mathrm{max}}$ (solid black line) and $\mathrm{ORB}_{\mathrm{max}}$ (dashed black line) simulations for the last 100 ka.

Ice thickness, velocity and migration of the grounding-line position simulated by $\mathrm{TOT}_{\mathrm{max}}$ are compared with its corresponding fields simulated at the same time in the $\mathrm{ORB}_{\mathrm{max}}$ simulation throughout the whole LGP (not shown). Note that velocity is compared between two different GrIS extensions, thus a velocity difference in regions that show a mismatch in ice cover corresponds to the velocity of the simulation in which the grounding line has not retreated yet. Since the millennial-scale β index is built from the NGRIP-temperature reconstruction through filtering to retain millennial timescales, each of the submarine melting peaks is associated with a D-O event culminating in a Greenland Interstadial (GI) period. The comparison is specifically shown for the time period corresponding to GI 16 (ca. 56.8 ka BP) associated with one of the pronounced peaks in the basal melting fluctuation during the MIS-3 (Fig. 5.6). In the $\mathrm{TOT}_{\mathrm{max}}$ simulation

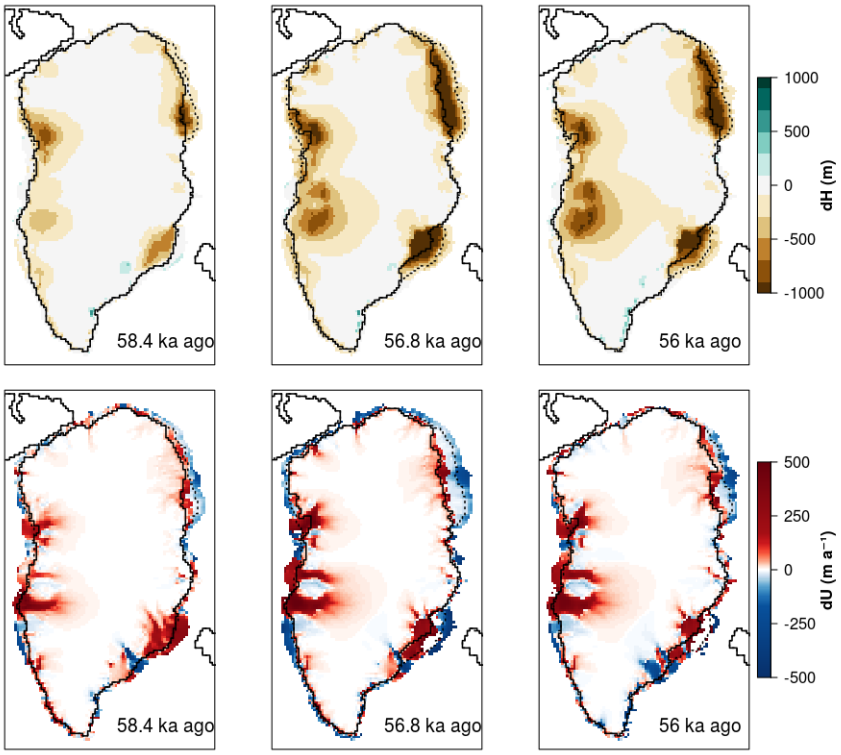

Fig. 5.7: TOT_{max} - ORB_{max} ice thickness (m, upper panels) and the corresponding TOT_{max} - ORB_{max} velocities ($m\ a^{-1}$, lower panels) for three different times during submarine melting rate peak corresponding to GI 16. The position of the grounding line in the TOT_{max} and ORB_{max} simulations are indicated by solid and dashed black contour, respectively.

a large ice thickness decrease is found in the NEGIS (NE Greenland ice stream) and the Kangerdlugssuaq fjord (SE Greenland) regions (Fig. 5.7). These ice reductions are associated with a large grounding-line retreat during GI 16. The region near Baffin Bay (NW Greenland) is also affected by inland grounding-line migration, however the retreat is limited if compared to the other regions. The ice stream related to Jakobshavn Isbrae outlet glacier in SW Greenland shows

increased velocities, leading to increased ice discharge. During the slow cooling after the peak of the GI (at ca. 56 ka BP), the grounding line advances back, but the ice recovery is limited. The ORB_{max} simulation shows very little grounding-line and ice-thickness responses for the whole analysed time period (not shown). For example, increased velocities associated with enhanced ice discharge lead to a large grounding-line retreat on the western margin of the GrIS during GI 12 (ca. 45.8 ka BP) when millennial-scale variability in ocean is included, and small ice-thickness reductions and grounding-line retreats are also simulated around NEGIS. The regions around Kangerdlugssuaq fjord and Sermilik fjord (SE Greenland) experience a large decrease in ice thickness linked to higher velocity and ice discharge throughout the peak. Appreciable grounding-line variations induced by millennial-scale variability in the ocean are also observed during the GI 8 (ca. 37.4 ka BP). Considerable grounding-line retreat and associated ice discharge are found close to Baffin Bay. The Kangerdlugssuaq region shows high velocities and an ice-thickness decrease, but this is related to only a minor grounding-line migration. The simulated NEGIS area does not show appreciable response to the submarine melting peak, since the grounding-line position reached by both simulations before the peak is maintained throughout the GI. As for GI 16, the ORB_{max} simulation does not show a substantial ice and velocity change, except for the strong velocity increase and ice-thickness reduction in Jakobshavn outlet glacier. This is related to the large ice thickness simulated in the 10 ka previous to GI 8, which increases the amount of glacial water produced at the base of the ice stream, enhancing basal sliding and ice discharge. On the other hand, the presence of millennial-scale oceanic variability allows for frequent ice discharge from the Jakobshavn glacier, limiting the basal-water amount and promoting ice growth.

Generally, ORB_{max} is much more static than TOT_{max}, showing smaller grounding-line and ice-discharge changes. Evidence from marine records suggests that stadial-interstadial temperature variations of about 3-15 K likely occurred around Greenland during DO events (Rasmussen et al., 2016; Jensen et al., 2018). Such a consistent temperature fluctuation is probably associated with large variations in submarine melting below the ice shelves likely present in Greenland

during the glacial, with grounded ice advanced onto the continental shelf. Therefore, it can be thought that a more variable submarine melt configuration as shown in $TOT_{\max}$ might better reflect the oceanic temperature variation related to DO events. However, there is no certainty as to whether more ice variability associated with this melting fluctuation is actually a better representation of reality than the $ORB_{\max}$ case. Including millennial-scale variability in the ocean leads to variations in ice-thickness of hundreds of meters with respect to the corresponding orbital-only case in locations close to the marine margin. This difference is not only exhibited at the ice-ocean front, but it also penetrates through the interior of the ice sheet by several tens of kilometers. This effect is related to the propagation of velocities, which, especially around the west GrIS, Sermilik, Kangerdlugssuaq and NEGIS regions, can penetrate far inland promoting ice discharge from the interior.

The transient effect of the oceanic millennial-scale variability throughout the ice sheet can be seen by analysing the LGP evolution of ice thickness and velocity for a single grid point of the domain, at three strategic locations: close to the glacial marine margin (A), close to the PD marine margin (B, glacial ice-sheet interior) and far inland in the ice sheet (C). The results of this analysis are shown for the Baffin Bay region (Fig. 5.8), but other two areas around the Greenland domain have been investigated (Fig. 5.9 for Jakobshavn Isbrae and Fig. 5.10 for the NEGIS). In the region close to Baffin Bay intermittent periods of high submarine melt lead to high velocity fluctuations ($600 - 800\ m\ a^{-1}$) limiting ice growth at the glacial ice margin. For more than 40 ka during the LGP, the ice thickness in the $\mathrm{TOT}_{\max}$ case (blue curve) is below that produced in the $\mathrm{ORB}_{\max}$ simulation (black curve) by 300-400 m, reaching melting peaks in which ice completely disappears for more than 4 ka. A similar ice-thickness evolution is found in the proximity of the PD marine margin, about 160 km far from the glacial ice-ocean border (point B). The effect of the millennial-scale variability in the ocean propagates inland, preserving an ice thickness increase of 500 m there and by 200 m even 300 km away from the ocean border (point C), despite minor or no observable difference in velocities. These estimates further corroborate the results found for the Baffin Bay region in the 2D plots (not shown). The

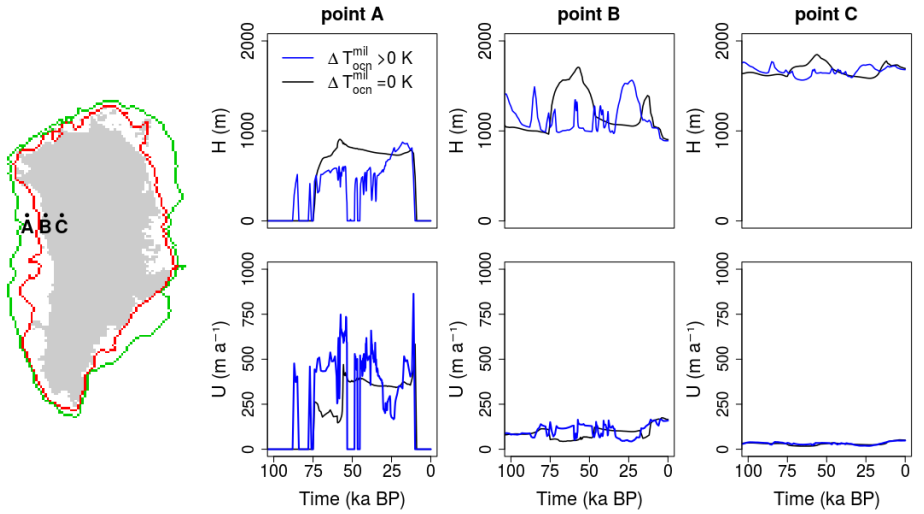

Fig. 5.8: Transient dynamics specified for three locations along Baffin Bay. Ice thickness (upper panels) and velocity (lower panels) LGP evolution is shown for the glacial marine margin (point A), present-day marine margin (point B) and far in the interior of the ice sheet (point C). Black curves indicate the dynamics of the $\mathrm{ORB}_{\mathrm{max}}$ simulation, blue curves represent the dynamics of the $\mathrm{TOT}_{\mathrm{max}}$ simulation. Green and red lines on the map on the left-hand side represent the maximum and minimum GrIS glacial extents simulated in $\mathrm{TOT}_{\mathrm{max}}$.

region including the Jakobshavn Isbrae (Fig. 5.9) seems to be less affected by the millennial fluctuation in basal melting than the region of Baffin Bay. Still, some ice-thickness variations are found close to the marine margin, especially around 50-40 ka BP, when the ice shelf repeatedly grows and disappears. Little evidence of this ice fluctuation is found in the ice interior, however, although decreased velocities with respect to the $\mathrm{ORB}_{\mathrm{max}}$ simulation around 40 ka BP lead to ice growth culminating in ice 700 m higher than that of the $\mathrm{ORB}_{\mathrm{max}}$ simulation (point B). The ocean-induced variability rapidly decays further inland (point C). However, it must be noted that this latter location is more than 600 km away from the marine margin, thus this attenuation is expected. Millennial-scale fluc-

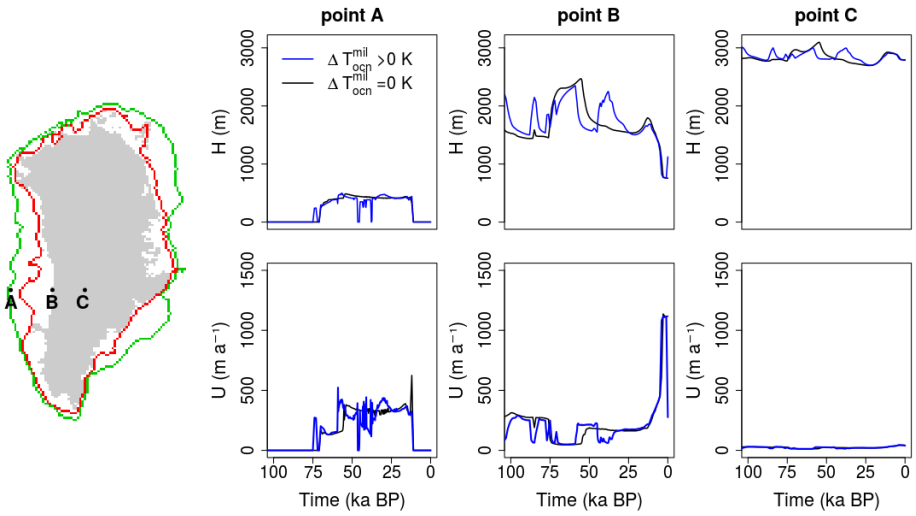

Fig. 5.9: Transient dynamics specified for three locations along Jakobshavn Isbrae outlet glacier. Ice thickness (upper panels) and velocity (lower panels) LGP evolution is shown for the glacial marine margin (point A), present-day marine margin (point B) and far in the interior of the ice sheet (point C). Black curves indicate the dynamics of the ORB_{max} simulation, blue curves represent the dynamics of the TOT_{max} simulation.Green and red lines on the map on the left-hand side represent the maximum and minimum GrIS glacial extents simulated in TOT_{max}.

tuations in submarine melting strongly impact the glacial evolution in the NEGIS region (Fig. 5.10) and very high velocity fluctuations ($1000 - 3000\ m\ a^{-1}$) between 50-30 ka BP constrain ice growth offshore (point A). The absence of ice at location A precludes the buttressing effect that limits ice discharge from the ice-sheet interior, as seen in the ORB_{max} simulation. On the contrary, the presence of millennial-scale fluctuations in the ocean helps to maintain ice advection from the interior toward the ice-ocean margin, favouring ice discharge from the interior and limiting the ice increase by 1000 m (point B) and 500 m far inland (point C).

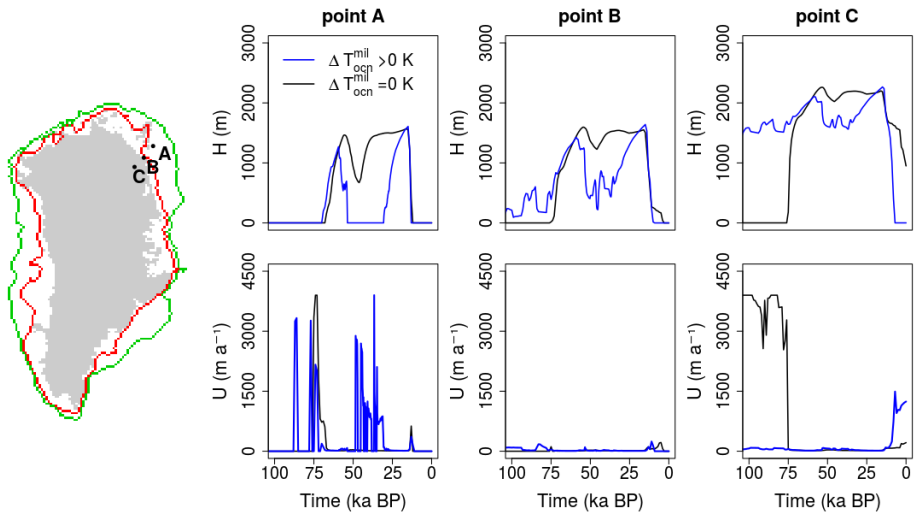

Fig. 5.10: Transient dynamics specified for three locations along the NEGIS area. Ice thickness (upper panels) and velocity (lower panels) LGP evolution is shown for the glacial marine margin (point A), present-day marine margin (point B) and far in the interior of the ice sheet (point C). Black curves indicate the dynamics of the $\mathrm{ORB}_{\mathrm{max}}$ simulation, blue curves represent the dynamics of the $\mathrm{TOT}_{\mathrm{max}}$ simulation. Green and red lines on the map on the left-hand side represent the maximum and minimum GrIS glacial extents simulated in $\mathrm{TOT}_{\mathrm{max}}$.

The effect of millennial-scale variability in the ocean throughout the LGP is summarised in Fig. 5.11 at large spatial scales. Ice thickness and velocity RMSDs both calculated following Eq. 5.5 for the whole time period show that regions that exhibit a strong response to the ocean in terms of ice thickness variations are also subjected to strong changes in velocity. This is highlighted in regions such as Baffin Bay, Jakobshavn Isbrae, Kangerdlugssuaq and Sermilik fjords and NEGIS, confirming the results discussed in this Section for specific times and locations.

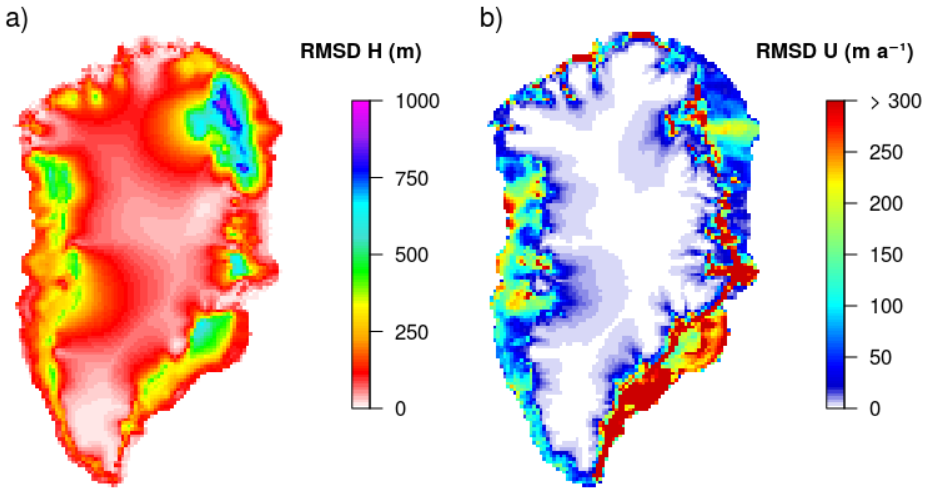

Fig. 5.11: RMSD for a) ice thickness H (m) and b) velocity U ($\mathrm{m\,a^{-1}}$) calculated between $\mathrm{TOT_{max}}$ and $\mathrm{ORB_{max}}$, following Eq. 5.5.

5.4 Discussion

5.4.1 Comparison of model results to proxy data

Our simulations show that small temperature changes can result in significant ice-volume fluctuations from the background glacial GrIS configuration. Also, the GrIS may have contributed to IRD discharge during the LGP, as suggested by proxy records (Andrews et al., 2012) and it is therefore interesting to outline its possible imprint associated with millennial-scale variability in the ocean.

These model results are compared to proxy data taken from sediment cores drilled in locations that could have been partly affected by recurrent ice discharge from the GrIS throughout the LGP. The locations are situated in the Labrador Sea (MD95-2024, Weber et al. (2001)), in the northwestern margin of Iceland (PS2644-5, Voelker and Haflidason (2015)) and in the North Atlantic along the

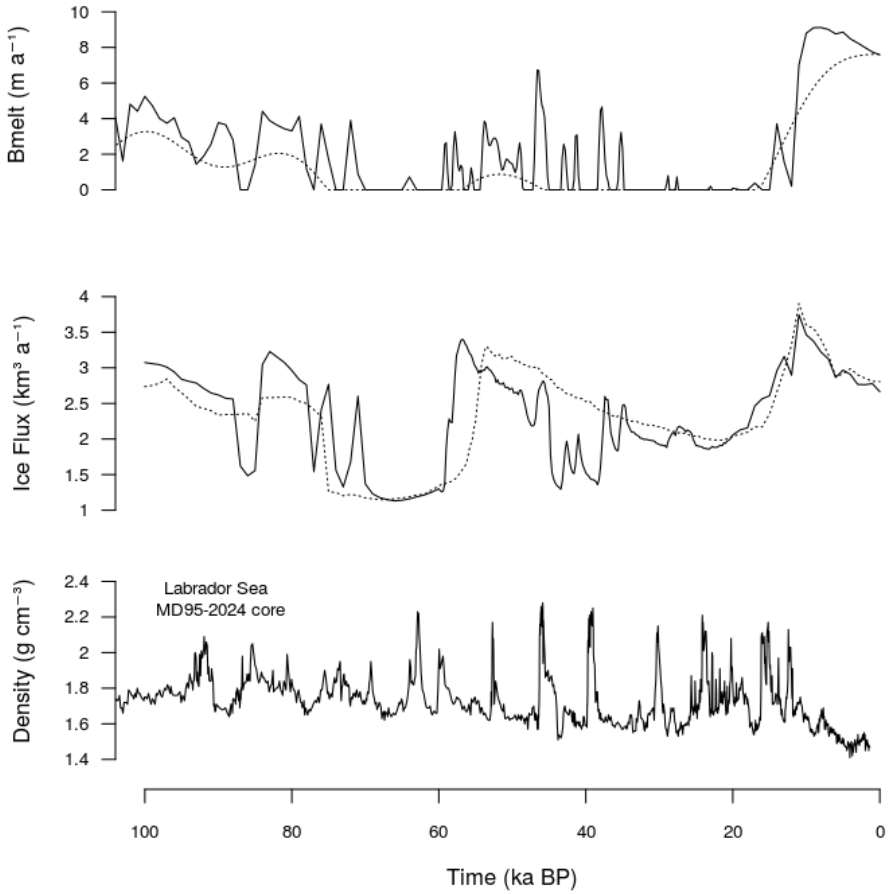

Fig. 5.12: Simulated submarine melt (upper panel) and simulated ice flux averaged over the Baffin Bay region (middle panel) in $\mathrm{ORB}_{\mathrm{max}}$ (dashed) and $\mathrm{TOT}_{\mathrm{max}}$ (solid) are compared to proxy-derived gamma ray density from the sediment core MD95-2024 in the Labrador Sea (lower panel).

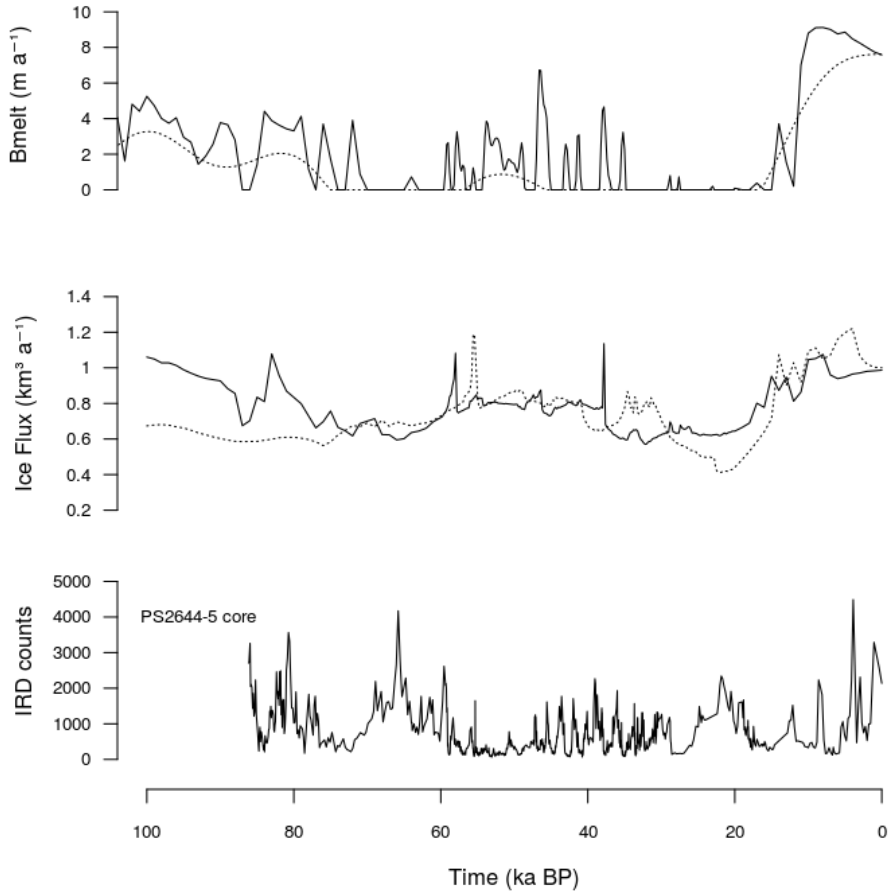

Fig. 5.13: Simulated submarine melt (upper panel) and simulated ice flux averaged over the Northern part of Denmark Strait (middle panel) in $\mathrm{ORB}_{\mathrm{max}}$ (dashed) and $\mathrm{TOT}_{\mathrm{max}}$ (solid) are compared to the total lithic fragments extracted from the sediment core PS2644-5 close to the North West Iceland (lower panel).

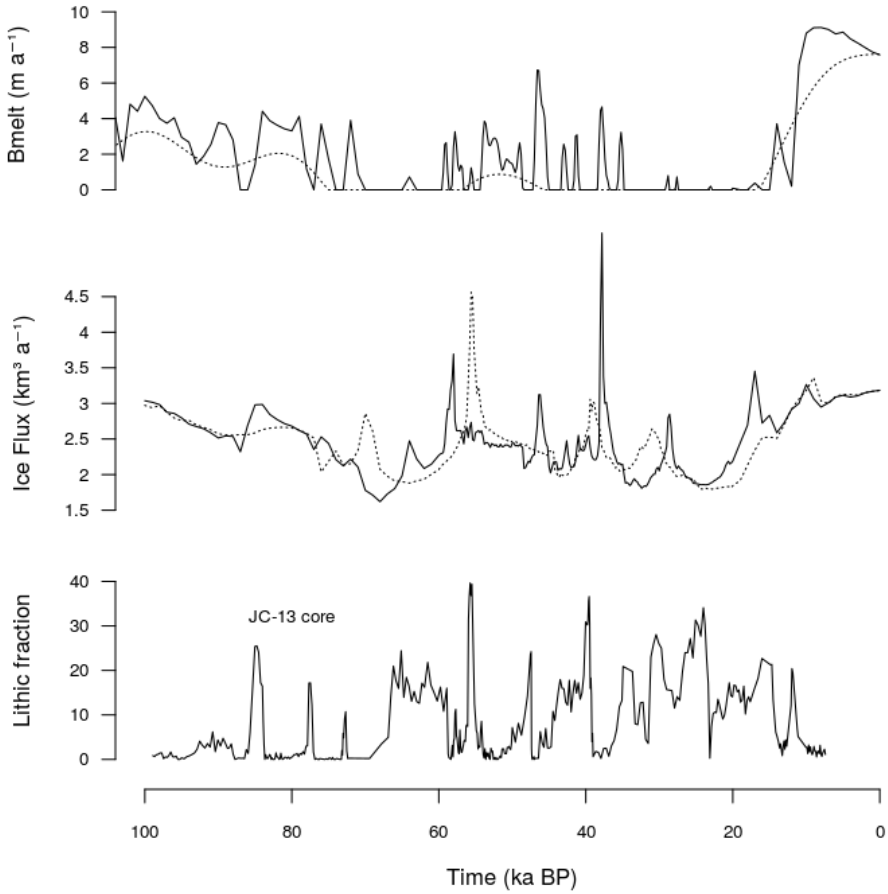

Fig. 5.14: Simulated submarine melt (upper panel) and simulated ice flux averaged over the South East GrIS region (middle panel) in $\mathrm{ORB}_{\mathrm{max}}$ (dashed) and $\mathrm{TOT}_{\mathrm{max}}$ (solid) are compared to the percentage of total lithic fraction induced by the JPC-13 sediment core in southern Gandar Drift in the North Atlantic (lower panel).

eastern side of the Reykjanes Ridge (JPC-13, Hodell et al. (2010)), close to the so-called IRD belt (Ruddiman, 1977). For each analysis, the ice flux averaged over the closest coastal zone in Greenland, and simulated by $\mathrm{TOT}_{\mathrm{max}}$ (solid line) and by $\mathrm{ORB}_{\mathrm{max}}$ (dashed line), is shown and compared to a specific proxy data for the LGP (Fig. 5.12 - 5.14). Gamma ray density ($g\ m^{-3}$) reconstructed from sediment core MD95-2024 (Labrador Sea, Fig. 5.12) is compared to the simulated ice flux averaged over the Baffin Bay region. All main Heinrich Events (HE) and some of the GI of the LGP can be recognised in the gamma ray density signal (Weber et al., 2001), which follows the IRD data extracted from the same sediment core. A weak correlation between model and data is found, especially for GI 16, GI 12 and GI 1. The most important source of IRD found in the Labrador Sea is thought to be Hudson Bay, which is likely responsible for the majority of iceberg discharge during HEs. However, some of the D-O events found in that region have been attributed to ice discharge from Baffin Bay (Andrews et al., 2012) and our results seem to partly follow this hypothesis. The total lithic fragment (IRD and thepra grains) extracted from sediment core PS2644-5 (NW Iceland, Fig. 5.13) is compared to the simulated ice flux averaged over the ice-covered Denmark Strait area close to Scoresby Sund. Peaks GI-21, GI-18, GI-12, GI-8 and GI-1 are visible in the modeled ice flux, showing a good correspondence between ice flux from the East GrIS and IRD deposition. Thus millennial-scale variability in the ocean could be partly responsible for enhanced iceberg production from East-Southeast GrIS bringing IRD to the PS2644-5 site by the East Greenland Current (Voelker and Haflidason, 2015). IRD data (% of lithic fraction) from sediment core JPC-13 in southern Gandar Drift in the North Atlantic (Fig. 5.14) are compared to the simulated ice flux averaged over the glacial marine-based GrIS area between Kangerdlugssuaq and Sermilik Fjords. Some agreement between modeled ice flux and lithic fraction is found for HE-1, HE-3, HE-4, HE-5, HE-6. However, the model seems to lag each HE by 2-3 ka, suggesting that these ice flux peaks are likely a response to D-O events as simulated in the submarine melting rather than to the observed HEs. The lack of temporal correspondence between model results and proxy data can be explained considering that the IRD found in JPC-13 may have come from other NH ice sheets and transported by icebergs via

the stronger Iceland-Scotland current during MIS-3 (Hodell et al., 2010). On the contrary, icebergs discharged from SE Greenland may likely be transported far from the IRD belt region towards the Labrador Sea. Another possible explanation for this low model-data correspondence is related to the usage of SSTs to force the ocean, which results in ice discharge peaking in phase with the NGRIP-derived atmospheric temperatures. On the contrary, ice discharge during HEs is thought to be related to subsurface waters, which are supposed to be in antiphase with respect to the atmosphere, thus leading to warmer ocean temperatures during stadials (Alvarez-Solas et al., 2013; Marcott et al., 2011). It is therefore possible that considering oceanic temperatures at other depths in the water column could improve the synchronization between modelled and reconstructed IRD discharge during HEs.

Despite individual disagreements, all these comparisons show that a more responsive GrIS, as obtained when the model is forced with millennial-scale oceanic variability ($\mathrm{TOT}_{\mathrm{max}}$), seems to better emulate the variability in ice discharge suggested by proxy records, when compared to the orbital-only simulation ($\mathrm{ORB}_{\mathrm{max}}$). Rapid (millennial-scale) basal melting fluctuations allow for ice-flux increases that to some extent match the timing of some of the peaks of the proxy data. This results suggest that under a highly-variable oceanic temperature variation during the LGP, the GrIS could have partly contributed to the ice discharge at those times. However, these results would be significant if the GrIS had been the sole source of IRD deposition into these sediment cores, which is not the case, or at least if the percentage of IRD contribution from each NH ice sheet to each of these cores had been known. This analysis does not aim to precisely reconstruct the timing and spatial distribution of the iceberg discharge during D-O events. Instead, it aims to explore the implications of considering the oceanic millennial-scale variability on the GrIS ice fluctuation during the LGP. It is surprising how much the sole presence of millennial-scale variability in the ocean can influence the GrIS evolution and ice discharge during the LGP interstadials, notwithstanding that millennial-scale variability is neglected in the atmosphere. However, tracing the origin of IRD deposition is a complex and open problem that needs a deeper understanding of changes in the ocean column during D-O

events, as well as a better knowledge of the oceanic and glaciological processes that ultimately determine the deposition of IRD on the ocean floor due to iceberg discharge.

5.4.2 Model limitations and caveats in basal melting parameterisation

Some of the GRISLI-UCM model limitations already discussed by Tabone et al. (2018a), such as the coarse model resolution (20 km by 20 km), which impedes the correct solution of small and steep fjords, the relatively simple GIA scheme, which takes into account only local changes in the ice load, and the PDD ablation scheme, which does not consider changes in past insolation, are also present in this work.

In the basal melting rate parameterisation is introduced a cutoff value to prevent freezing at the ice-shelf base and thus limit ice accretion during the glacial period. This assumption is reasonable for the low spatial resolution of the model, however, it ignores an existing process, since freezing is observed at the base of many marine glaciers, even for the present day (Rignot et al., 2013).

The parameters B_{ref}, $\Delta T_{\mathrm{ocn}}^{\mathrm{mil}}$ and $\Delta T_{\mathrm{ocn}}^{\mathrm{orb}}$ in the basal melting equation are assumed to be spatially uniform. It is recognised that spatially-variable fields should be taken into account for an exhaustive investigation of the problem. Both stadial-interstadial and glacial-interglacial temperature anomalies could be taken from existing transient model outputs, for instance. However, a complete map of the observed PD basal melting rates for the whole Greenland domain does not exist yet, in contrast to Antarctica (Rignot et al., 2013), thus limiting the effectiveness of including additional complexity at this time.

The indices α and β used to create the past orbital and millennial forcings, in particular for the submarine melting, are built based on the NGRIP-derived temperature signal. As far as it is known, no high-resolution ocean temperature reconstructions covering the entire LGP exist for the North Atlantic. However, our assumption that the first layers of the ocean vary in phase with the atmo-

sphere is reasonable and using the same climatic indices for the ocean is thus a fair approximation to assess the problem. By allowing the glacial-interglacial and stadial-interstadial anomaly temperatures to range between 0 and 3 K, basal melting rates at the grounding line and below the ice shelves are considered as driven by SST variations (Annan and Hargreaves, 2013; Bagniewski et al., 2017; Jensen et al., 2018; Liu et al., 2009; MARGO, 2009). However, grounding lines of many outlet glaciers in Greenland are estimated to be located deeper in the water column (Wilson et al., 2017). Therefore subsurface temperature anomalies should be considered in these cases, which may lead to slightly different results, since they are probably in antiphase with the atmosphere (Vettoretti and Peltier, 2015; Zhang et al., 2014b). However, as a sensitivity study it does not aim to perfectly reproduce reality but rather analyse the possible effects of an ocean driven by millennial-variability on the ice-sheet evolution in Greenland. This assumption, combined with the use of a linear basal melting parameterisation based only on temperature variations without refreezing, lead us to ignore more complex mechanisms that occur at the ice-ocean bed interface, such as meltwater buoyancy and water convection in the ice-shelf cavity (Jenkins, 2011). However, in the framework of a sensitivity study these limitations should not influence the main objective of this work.

The basal melting evolution produced in the $\mathrm{TOT}_{\mathrm{max}}$ simulation (solid line in Fig. 5.6) is strongly related to a specific combination of the perturbed parameters in the basal melting equation (Eq. 5.3). This combination is chosen from the range of possible values as it produces the maximum oceanic millennial variability in the LE. Comparing the most millennial-driven variable simulation to its corresponding only-orbital case is useful to have an idea of the possible range of impact of the millennial-scale variability in the ocean on the evolution of the GrIS throughout the LGP. However, the same analysis could be performed for other basal melting configurations. A different magnitude of the melting peaks during MIS-3 (Fig. 5.5) or a different distribution of the melting peaks (resulting from the use of a different temperature reconstruction to create the α and β indices) may vary the timing of grounding-line advance and retreat or ice growth and loss. This is also true for the orbital-driven basal melting forcing applied to

the $\mathrm{ORB}_{\mathrm{max}}$ simulation (dashed line in Fig. 5.6), which shows submarine melting rates higher than 0 $m\ a^{-1}$ for only 10 ka during MIS3 (between 55 and 45 ka BP). A different melt configuration could vary the timing and spatial distribution of grounding-line migration and ice cover. A similar analysis to that presented here has been performed considering sub-surface oceanic temperatures instead of SST (ΔT_{ocn}^{mil} in Eq. 5.3 has reversed sign with respect to the SST case, not shown). The maximum oceanic millennial variability found for this ensemble shows peaks of melting that occur in antiphase with respect to the atmosphere and the magnitude of the peaks itself is lower than that of the melt configurations analysed in this chapter (being Dtocn mil negative now, Eq. 5.3 leads to less melt than in the SST case, by construction). In these experiments sea-level contribution due to oceanic millennial variability has been reduced of about 0.1-0.2 m, grounding-line fluctuations tipically occur lagged by 2-3 ka, as they follow the timing of the melting peaks, and variations in ice volume may change locally (e.g. the melting peaks are now not sufficiently high to induce the full ice loss over the near-NEGIS continental shelf for a large part of the LGP, as seen in Fig. 5.11). However, the overall pattern of ice thickness and velocity variabilities observed for the whole LGP is very close to that of Fig 5.11 and the most responding regions to millennial-scale variability in the sub-surface are found to be the same as those reported here (not shown).

Finally, millennial-scale variability in the atmosphere is not considered here. This simplified experimental design is chosen following previous results demonstrating the important role of the ocean in the GrIS evolution over the last glacial periods at orbital timescales (Tabone et al., 2018a). The experiments here allow us to directly investigate how millennial-scale variability in the ocean can impact the evolution of the GrIS. However, an important component of the climate system has been omitted and to comprehensively understand the effect of millennial-scale fluctuations on Greenland, further experiments should be done by including this variability in air temperature and precipitation.

5.5 Conclusions

In this chapter, the effect of millennial-scale oceanic variability on the evolution of the GrIS is assessed during the LGP. To do so, the same ice-sheet-shelf model already used in Chapter 3-4 is used. Here, the millennial-scale variability in the ocean is imposed as a fluctuation in the basal melting rate at the grounding line and below the ice shelves. First, the millennial variability is characterised through a sensitivity test for a broad range of values of the perturbed parameters in the submarine melting equation. It is shown that the millennial-scale contribution to ice-volume variations during the LGP could have reached peaks of more than 1.5 m SLE. The southeastern area around Kangerdlugssuaq fjord, Baffin Bay and the NEGIS regions were found to be very sensitive to millennial-scale variability in the ocean. Ice thicknesses simulated at the marine margin differed by 500-1000 m from that simulated by orbital-only driven oceanic variations. Moreover, imprints of these differences are still found for several tens (hundreds - in certain regions) of kilometers far from the ice-ocean interface due to the velocity-driven upstream propagation of the ice-flow perturbation. Although the aim of this work was far from assessing the true timing and spatial distribution of any GrIS ice discharge that occurred during the D-O events, it is shown that considering the millennial-scale variability in the ocean is necessary to reproduce some of the IRD peaks observed in North Atlantic proxy data. Our work thus suggests that millennial-scale induced changes in ocean circulation and temperature may be important drivers of the GrIS evolution during the LGP, advancing the hypothesis of a potential role of the GrIS in oceanic reorganisations at millennial timescales.

Chapter 6
Discussion

Using a three-dimensional hybrid ice-sheet-shelf model the impact of past orbital and millennial-scale climate variations on the GrIS paleo evolution has been evaluated. Although these include variations both in the atmosphere and in the ocean, the focus of this work has been the role of the ocean. Specifically in this scope, the ice-sheet-shelf model was expanded by implementing a parameterisation of basal melting at the grounding line and at the base of the ice shelves which takes into account the temporal variation of oceanic temperatures. Transient simulations of the last glacial cycles have facilitated investigation into the potential implication of the ocean on the past GrIS evolution at various timescales and spatial extents. The results obtained through running and analysing these paleoclimatic simulations address the three scientific questions posed in Section 1.4.

Is the GrIS sensitive to oceanic temperature variations at glacial-interglacial timescales? To what extent is the GrIS affected by these during glacial periods?

To answer this question, transient simulations of the ice-sheet-shelf model GRISLI-UCM forced by paleo glacial-interglacial oceanic temperature variations have been performed for the last two glacial cycles. These temperature anomalies are

expressed in the submarine melt parameterisation in terms of variations in the heat-flux exchange between the ocean and the ice at the marine margin. Increasing the oceanic sensitivity corresponded to increasing the exchange coefficient that converts temperature anomalies into heat-flux exchange, and thus the oceanic forcing at glacial timescales. Launching a set of paleoclimatic experiments with increasing oceanic sensitivities allowed assessment of the extent to which oceanic changes could have impacted the evolution of the GrIS over the last glacial cycles. These transient simulations suggested that the GrIS strongly responded to glacial-interglacial temperature variations in the ocean. Increasing the oceanic forcing led to large advance and retreat of the GrIS margins, across the continental shelf, following the time evolution of the imposed oceanic forcing. Strong advance during glacial times and retreat at the onset of interglacial times was obtained with a high oceanic forcing. Moreover, the amount of ice lost in a glacial-interglacial transition reflected the ice growth reached at the end of the glacial, which was higher for higher oceanic forcing.

As a first test of realism, it is important that the model is able to adequately simulate the present-day GrIS configuration. This is an important requirement to define the quality of an ice-sheet model in reproducing paleo conditions. The GrIS simulated at the end of the transient runs of the sensitivity experiment reasonably reproduces the observed GrIS configuration in terms of ice thickness and extent (Bamber et al., 2013) and shows that the simulated present-day does not strongly depend on the oceanic forcing. Therefore, this agreement does not further corroborate the results shown for the oceanic forcing, but suggests that model dynamics and atmospheric forcing are reliable, at least for the present day.

This GrIS expansion and retreat associated with ice growth and loss throughout the glacial cycles has allowed assessment of the GrIS configuration and the GrIS contribution to the sea-level variations simulated for the two main discussed reference periods of the last glacial cycles: the Eemian (ca. 120 ka BP), which corresponds to the warming peak of the LIG or Eemian, and the LGM (ca. 21 ka BP). An interesting result is that a complete disappearance of the GrIS during the Eemian is not simulated, even when the model is forced by a high oceanic forcing. The major retreat is simulated in the interior of the Jakobshavn Isbrae.

These results are consistent with all ice core sites suggesting the presence of ice during the LIG (Andersen et al., 2004; NEEM, 2013; Yau et al., 2016a,b). This is in good agreement with the recent estimates from other ice-sheet model studies (Langebroek and Nisancioglu, 2016; Robinson et al., 2011; Stone et al., 2013). This result is actually more dependent on the atmospheric forcing than on the oceanic one, since the ocean plays a role only in the first millennia of the interglacial period, due to the rapid retreat of the ice beyond the current coasts. Another interesting result concerns the GrIS configuration simulated at the LGM. These results suggest a glacial GrIS that is able to expand offshore over the continental shelf, and to reach the continental shelf break for a sufficiently high oceanic forcing. Although many uncertainties remain from paleo data concerning the precise reconstruction of the GrIS marine margins during the last glacial cycle, we can consider these results as in good agreement with recent ice-sheet model reconstructions constrained by past relative sea-level changes and other proxy-derived data (Lecavalier et al., 2014, 2017; Simpson et al., 2009).

However, it is important to note that in this set of experiments freezing below the ice shelves and along the grounding line was allowed. It is not known if this process is present at the bed of outlet glaciers of Greenland, although it has been observed in some of the AIS ice shelves, even at the present day (Rignot et al., 2013). Accounting for refreezing could have led to an overestimate of the grounding-line advance during glacial periods through ice accretion and a further expansion of the GrIS over the continental shelf. We cannot discard that this factor slightly influenced the estimations of the contribution in sea-level rise during the last interglacial (4.2 - 8.0 m SLE) and for the last deglaciation (4.6 - 5.3 m SLE), given a high oceanic forcing, although further sensitivity tests performed under both approaches showed that refreezing at the grounding line was not the main responsible for the glacial ice accretion. However, to avoid possible incongruities due to this process, in the following studies refreezing was prevented by imposing a minimum value of basal melt equal to zero.

A proper representation of the surface mass balance (M) and, in particular, of surface ablation is an important issue for precisely modelling the GrIS, especially during interglacial periods in which the ice sheet is strongly affected by warmer

atmospheric temperatures, such as the Holocene and the Eemian. The scheme used in the ice-sheet-shelf model to account for changes in the surface ablation is the widely-used Positive-Degree Day (PDD) scheme (Reeh, 1989). This is an efficient but admittedly simple approach. The reason is the surface melt is parameterised from atmospheric temperatures at the ice surface, while the effect of the albedo is implicitly implemented through empirical coefficients for snow and ice. However, this approach does not account for past changes in insolation and therefore is not be the most suitable approach for modelling interglacial periods. Indeed, it has been estimated that the surface melt calculated at the Eemian could be 20-50 % lower than that produced by a more realistic ablation schemes that takes insolation changes into consideration (Robinson and Goelzer, 2014). Therefore, the GrIS contribution to sea-level rise suggested for the Eemian could be underestimated by these studies, although it was not the focus here. A related issue is the fact that the effect of increasing atmospheric forcing has not being investigated. Such a sensitivity study would help not only to better understand the GrIS evolution during the last two glacial cycles, especially during interglacial periods, but also to constrain its future behavior under a changing climate.

It is important to remark that the sensitivity of the GrIS to glacial-interglacial oceanic temperature variations has been investigated for only a limited set of parameters of the submarine melting scheme. Also, for the sake of simplicity, the present-day reference basal melting and the glacial-interglacial oceanic temperature anomaly in that parameterisation have been considered as spatially uniform around Greenland. These simplifications allow for only a simplified representation of reality. Grounding-line melting is likely related to the temperature of waters that vary regionally, both in the horizontal as in the vertical, and in time as ice shelves expand or shrink. These issues should be taken into account for a more profound investigation.

Can oceanic temperature variations during the LGP be responsible for fluctuations of the NEGIS marine margin and specifically trigger its retreat during MIS-3?

To answer this question, transient simulations throughout the whole LGP were performed by forcing the ice-sheet-shelf model with varying oceanic temperatures. As in the previous study, the oceanic temperature anomalies were translated into ocean-ice heat fluxes through the submarine melting parameterisation at the ice-ocean interface. To explore the sensitivity of the NEGIS to the oceanic forcing a set of experiments considering orbital-scale variability only (both in the atmosphere and ocean) were carried out. This experimental design allows assessment of the sensitivity of the NEGIS to changes in the submarine melting rate at the marine margin exploring the effect of the ocean as a potential driving forcing. The orbitally-driven oceanic temperature variations are explicitly designed to follow the orbital component of the NGRIP-derived temperature anomaly, thus the resulting submarine melting rate is higher during relatively warm phases such as MIS-3, and cutoff at zero basal melting at the LGM. This set of experiments allows assessment of the impact of a persistent orbital-driven submarine melting rate on the NEGIS margin, with a simple experimental design. The results suggest that a persistent, sufficiently high submarine melt signal applied at the NEGIS marine margin at MIS-3 is capable of inducing a retreat of the grounding line by more than 100 km from the former glacial position. The margin then remains more or less steady as long as the submarine melting is active. During the LGM, colder climatic conditions translating both in a drop in atmospheric temperatures and in the absence of submarine melting trigger the grounding-line advance by 200 km over the continental shelf. However, in none of these experiments was the model able to simulate a grounding-line MIS-3 retreat behind the PD position, in contrast to the the 20-40 km retreat relative to today suggested by reconstructions (Larsen et al., 2018).

An important result that comes out from this work is the fact that adequate and prolonged oceanic forcing is sufficient to trigger the retreat of the NEGIS margin during MIS-3. Another important, more general, result is that in absence

of submarine melting, no substantial fluctuation of the NEGIS margin is simulated. This therefore suggests that the atmospheric forcing alone, is not capable of triggering the NEGIS grounding-line to fluctuate over the continental shelf, unless the oceanic forcing is present.

These results are significant as they bring new insight in understanding the mechanisms responsible for the large grounding-line migration of the NEGIS found during MIS-3 (Larsen et al., 2018). The explanations suggested for this recent evidence involve lower accumulation rates, high incoming solar radiation, and increasing of summer air temperatures operating together; however, the potential effect of the ocean was not taken into consideration. This suggestion is novel and further modelling studies should be performed to investigate the effect of all other changing factors not considered herein. Thus, sensitivity studies of the NEGIS margin to e.g. changes in the atmospheric temperatures, changes in precipitations, variation in external forcings (insolation changes), changes in greenhouse gases, with each forcing investigated alone, should be performed in the future to comprehensively study the problem. Particularly, a sensitivity study including variations in the atmospheric temperatures with a prescribed ocean could help to constrain the role of the atmosphere in this phenomenon and provide further insight on the driving role of the ocean in the NEGIS margin retreat at orbital timescales.

This work was the first attempt to understand the possible implications of the oceanic forcing in the NEGIS margin retreat and the experimental design was specifically chosen to be as simplest as possible. Considering temperatures of the ocean as spatially uniform around Greenland and assuming that these vary in phase with the atmosphere is not a precise representation of the reality, although it is a justifiable choice for a sensitivity study. However, since this work focuses on a specific limited portion of the GrIS, precise informations on the oceanic conditions during MIS-3 would have been required to investigate this issue from a more realistic point of view. Nevertheless, oceanic- temperature reconstractions close to the NEGIS marine margins are not available, since almost no proxy records from which such information could be retrieved exist in the northeastern side of Greenland.

Another point that should be investigated in more detail is the position reached by the grounding line at the LGM and the forcings that control its advance. In this work, the NEGIS margin is able to readvance towards the continental shelf break by about 200 km from the MIS-3 configuration. Despite this, even in this experiment the position reached by the NEGIS margin is behind the GrIS maximum extent suggested by reconstructions for the LGM (Arndt et al., 2015, 2017; Funder et al., 2011; Winkelmann et al., 2010). The fact that the margin does not reach the continental shelf break at the LGM, conversely to what has been observed in the first work of this thesis, is likely due to the current prevention of glacial water refreezing at the ice-ocean interface. However, the forcing responsible for this reduced advance at the LGM cannot be directly inferred from this experiment only and further sensitivity tests need to be performed.

Is the GrIS sensitive to millennial-scale variability in the ocean related to D-O events?

This question has been tackled by investigating the effect of past millennial-scale oceanic temperature variations on the GrIS evolution during the LGP. To this end, transient simulations of the ice-sheet-shelf model forced with stadial-interstadial oceanic temperature variations were performed for this period. Here, the effect of the millennial-scale variability in the ocean on the GrIS evolution has been investigated through a broad range of possible submarine melting configurations and a large ensemble of transient simulations has been analysed to assess the sensitivity of the GrIS to oceanic temperature changes at millennial timescales.

A first important result of this work is that ice-volume variations induced by millennial-scale variability in the ocean could have contributed to more than 1.5 m SLE during the LGP. This result suggests that the GrIS likely underwent significant changes associated with abrupt warmings observed throughout the LGP (D-O events). A deeper investigation of the results helped to characterise the spatial distribution of these ice-volume variations and pointed out at Kangerd-

lugssuaq fjord in southwest Greenland, Baffin Bay and the NEGIS as the regions that most responded to the millennial-scale variability in the ocean. Such variability was able not only to trigger large ice-thickness differences (500-1000 m) at the ice-sheet oceanic margins, but also to induce profound changes in thickness and velocity at several tens of kilometers inland away from the coast. All these findings strongly indicate a very sensitive GrIS to variations in the oceanic temperatures on millennial timescales.

An interesting analysis corroborating this result was given by the comparison between IRD deposition evidence from North Atlantic marine sediment data (Hodell et al., 2010; Voelker and Haflidason, 2015; Weber et al., 2001) and the simulated ice flux averaged over the GrIS coastal region close to each sediment core site. Surprisingly, some of the IRD peaks reconstructed from proxy data were also found in terms of ice flux in the simulations that had been forced by the millennial-scale variability in the ocean, suggesting that the model was simulating a strong ice discharge in those regions. The goal of this experiment was not to precisely define the timing and source of iceberg discharges. Nevertheless, the observed agreement with sediment cores supports the hypothesis that the GrIS responded strongly to oceanic temperature variations associated with D-O events leading to non-negligible ice discharge. This conclusion is very powerful since it opens the possibility of a significant role of the GrIS in the oceanic reorganisation during D-O events.

Some of the IRD peaks from sediment cores, however, did not compare well with the ice flux signal calculated from the millennial-scale forced simulation. This was found particularly for the piston core JPC-13 (Hodell et al., 2010) of the North Atlantic, close to the IRD belt (Ruddiman, 1977). The pronounced IRD peaks of JPC-13 corresponding to the recognised HEs of the LGP were found to lead the simulated ice flux peaks by 2-3 ka. A possible explanation for this could be the use of SST anomalies to construct the submarine melting rate in the model. In this work, stadial-interstadial oceanic temperature variations used to force the ocean were scaled to peak in phase with the atmospheric temperatures anomalies derived by the NGRIP ice core. Conversely, ice discharge during HEs could have been triggered by subsurface waters (Alvarez-Solas et al., 2011b, 2013;

Marcott et al., 2011), which are expected to be warmer during stadials. Models suggest that, in response to a ceased NADW formation, subsurface warming occurs in antiphase to atmospheric (and ocean surface) changes, (Mignot et al., 2007; Shaffer et al., 2004; Vettoretti and Peltier, 2015; Zhang et al., 2014b). The halt of convection in the North Atlantic induces a slow warming of mid-depth oceanic waters at low latitudes by heat diffusion from the surface. This heat can be partly transported northward reaching subsurface waters at high latitudes in the North Atlantic (Shaffer et al., 2004). It is therefore possible that using temperatures from deeper oceanic layers to build the submarine melt signal could lead to a better agreement between model and data. An even more realistic parameterisation would take into account the exact (time-varying) depth of the ice shelves involved, whether they were present, and the ablation occurring in front of marine-terminating glaciers with small floating tongues or abrupt vertical terminus, very likely to be present in a GrIS warm configuration such as it is observed at the present day.

As mentioned above, these results were obtained with a specific submarine melting configuration that was generated by using spatially homogeneous basal melting rates for the present-day and spatially homogeneous oceanic surface temperature anomalies, which followed the millennial-scale variability of the NGRIP-derived atmospheric temperature anomaly. These simplifications, combined with a high oceanic sensitivity chosen to represent a high millennial-scale variability in the ocean, allow for one precise submarine melting signal that follows the warming peaks of NGRIP. Choosing another submarine melting configuration would likely result in simulating ice discharge from the GrIS at other times and with slightly different intensity.

Finally, some general interrelated model limitations shared by all these studies need to be discussed. The GRISLI-UCM model is a hybrid model that resolves grounded ice dynamics via SIA and dynamics of fast moving areas, such as the ice shelf, via SSA. The numerical transition between these two approximations is challenging (Bueler and Brown, 2009) and, if the dynamics of fast-flowing areas and at the grounding line is not accurately solved, it cannot completely capture the processes related to ice flux at the boundary layer (Pattyn et al., 2012). Also,

hybrid models are generally sensitive to the spatial model resolution, especially at the grounding-line areas if they are described by only one grid cell at coarse resolution (Bernales et al., 2017), as in this work. The low spatial resolution of this model (20 by 20 km), therefore, does not allow for an accurate treatment of the dynamics at the marine boundary layer, especially if the outlet glaciers lay on steep fjords, mostly present in the east Greenland. Although the spatial resolution was increased to 10 km for investigating the NEGIS margin response to the oceanic forcing, the capability to resolve fine-scale physical processes at the ice-ocean interface is limited. One of the direct consequences of this limitation is the overestimation of the ice thickness at the margins and the grounded ice volume at the PD. A refinement of the mesh along the ice-ocean boundary, such as parameterising at sub-grid resolution the grounding-line position, could help to overcome this issue (Gladstone et al., 2010). Alternative empirical solutions could be e.g. parameterising the boundary layer with grounding-line ice flux as a function of ice thickness (Schoof, 2007), or refining the mesh in an adaptive way to have a very high resolution at the grounding line (Cornford et al., 2013), but this latter could have high computational costs and thus may not currently be suitable for paleoclimatic modelling studies.

Another caveat of the model is related to the submarine melt parameterisation adopted, which is solely a function of the temperature of the ocean at the depth of the grounding line. Its simplicity allows for a direct investigation of the effect of past oceanic temperatures, however it may disregard complex processes occurring at the ice-ocean interface. A parameterisation accounting for variations in salinity too (Holland et al., 2008b), or the geometry of the ice-shelf cavity (Gladstone et al., 2012), or the slope of the base of the ice shelf (Little et al., 2012), or more complex schemes describing the evolution of meltwater plumes forming at the ice-shelf base (Jenkins, 2011) could help to describe in detail the processes below the ice-shelves and along the grounding line. Recently, a parameterisation applied for the ice shelves in the AIS resolving the ice-shelf cavities and using a boundary-layer theory for the melt, has been capable of capturing the effect of ocean circulation below the ice shelves through a fairly simple parameterisation (Reese et al., 2018). Basal melting at the grounding line is applied to the last

grounded grid point in the model. The way of applying a high melting rate at the last grounded point which stands for the grounding line is highly debated in the modelling community, since it is probably unphysical but at the same time it is very useful to make the grounding line to respond. Since this process is dominant with respect to the sub-shelf melting by construction, it may well be the primary factor in controlling the advance (through freezing) and retreat (through melting) of the GrIS marine margins.

In this work, refreezing of glacial water has been first reduced and then cutoff to avoid unrealistically high ice accretion rates. Although we did so to improve the realism of the results, sensitivity tests with both methods showed that ice accretion through this mechanism was not the main driver of ice growth. However, this is not a definitive solution for solving the problem, since refreezing is an important process observed in many glaciers, even today, at least below the AIS ice-shelves (Rignot et al., 2013). Probably, a subgrid treatment of the grounding line could be suitable for allowing refreezing below floating ice without considering the process for the entire grid cell. Moreover, although it is well-known mechanism, whether freezing below ice shelves should be included or not in an ice sheet model is debated by the community, since this decision may depend on the capability of the model in resolving sub-shelf cavities, presence or not of ice shelves in the analysed domain, model spatial resolution and the used melting parameterisation. Due to the coarse resolution of our model and to the submarine parameterisation used, the amount of refreezing simulated by our model in Chapter 3 risked to be unphysical, since, for a high oceanic sensitivity, it would have involved a very high amount of heat-flux exchanged between the ocean and the ice during cold periods (despite the likely proximity of glacial oceanic temperatures to the freezing point). To avoid this problem, refreezing was prevented in the subsequent work and a different dynamics was chosen to make grounding-line advance easier. Therefore, two main model modifications have been carried out between the version used in the first work and the others: presence of sub-shelf refreezing (first allowed and then prevented) and velocity mixing calculation (first, by following the scheme from Bueler and Brown (2009) and then by simply adding up SIA and SSA velocities). A one-to-one comparison between the

first work and the others is thus improper. This is well seen when in absence of melting/refreezing (κ=0, B_{ref}=0), the glacial GrIS expands up more in the second work than in the first one (compare orange line in Fig. 3.12 a) and green curve in GrIS map of Fig. 4.2). Since the oceanic forcing is off, that discrepancy in growth may be due to the solely change in the dynamics. Despite the apparent inconsistency between results from the first and the following work that might put in danger the conclusions reached in the first study, main results of Chapter 3 still hold. In that work, the presence of an active ocean was sufficient to ensure a glacial GrIS configuration with its grounding line expanding up to the continental shelf break (Fig. 3.12 b). On the contrary, a full glacial state is never completely achieved in the study of Chapter 4, neither when the model is forced by an active ocean ($\kappa > 0$) and despite the employment of a likely less conservative dynamics (Fig. 4.2). This reduced glacial advance suggests that sub-shelf refreezing should be probably taken into account to properly reproduce a full GrIS glacial growth that covers up the entire continental shelf, as shown in Chapter 3. Moreover, this fact suggests that the oceanic forcing is likely the factor triggering and driving the grounding-line advance during glacials through accretion, as concluded in Chapter 3. However, as already mentioned in Chapter 3, the impact of different dynamics on the glacial advance has not been investigated in this thesis and uncertainties about how that aspect have influenced glacial-interglacial growth-retreat still remain.

It is important to remark that the submarine melt parameterisation applied here does not account for frontal melt, that is the typical form of melting observed at the ice-ocean interface of tidewater glaciers. This type of glaciers is widely observed in Greenland at the present day and it is very likely that a similar tidewater-based GrIS configuration also resulted in other interglacial periods. Therefore, despite this parameterisation can be a suitable representation of melting processes during glacial times, when marine-terminating glaciers likely extended out into the ocean via large floating tongues, it is considered less adequate for representing ocean-induced melt occurring in an interglacial period, such as the present day or the Eemian, since it is not capable of resolving melting at the calving fronts.

Finally, some limitations are related to the GIA scheme used in this model, the elastic lithosphere-relaxed asthenosphere (ELRA) method (Le Meur and Huybrechts, 1996), for which the viscous asthenosphere responds to variations in the GrIS local ice load by a characteristic relaxation time. This relatively simple scheme does not take into account the resulting effect of the GIA in Greenland due to changes in the ice load of the neighboring North Atlantic ice sheets, such as the LIS, which is known to induce vertical movements in the GrIS bedrock. Moreover, all of these ice sheets, which existed only during the glacial periods, contributed to sea-level variations and, since the grounding-line calculation in the model is based on a flotation criterion, this issue could have been especially relevant at the onset of the interglacial periods when the GrIS ice mass loss was primarily controlled by sea-level rise (Lecavalier et al., 2017) and the depth of the GrIS bedrock (Huybrechts, 2002).

Chapter 7
Conclusions

In this thesis, the sensitivity of the GrIS to past variations in the oceanic state has been investigated from a modelling perspective. Such a study was needed to address the lack of knowledge concerning the GrIS evolution throughout the past glacial cycles, which was a consequence of the scarcity of proxy-derived evidence and limited modelling efforts. Specifically, the role of the ocean has been overlooked so far and this work provides new insight into this issue. Three sensitivity studies have been carried out to specifically assess the role of the ocean on the GrIS paleo evolution focusing on various time periods over the last glacial cycle and exploring different spatial scales.

The first study (Tabone et al., 2018a) was used to assess the effect of orbital-scale (glacial-interglacial) temperature variations in the atmosphere and in the ocean on the GrIS evolution of the last two glacial cycles. This work showed the potential of oceanic forcing to drive the grounding-line migration of the GrIS on orbital timescales. Particularly, this study showed that a sufficiently high oceanic forcing could be responsible for triggering the grounding-line advance during cold glacial periods and contribute to its retreat during warm interglacial periods, at least in the first stages of the interglacial onset. These changes at the marine margin were propagated inland into the ice-sheet interior. Together with glacial-interglacial changes in the atmosphere, this was found to lead to an overall reorganisation of the GrIS. Moreover, the GrIS configuration at various time

periods was investigated. A new possible configuration of the GrIS at the LIG (ca. 120 ka BP) was suggested, with 2.9-3.2 m SLE of ice-mass loss relative to present, as well as the likely contribution of the GrIS in sea-level rise throughout Termination II of 4.2 - 8.0 m SLE. A similar analysis for the LGM (ca. 21 ka BP) suggested that a GrIS likely contributed 4.6 - 5.3 m SLE during the last deglaciation (Termination I). These estimates are in agreement with the literature and helped to constrain the model parameters. The introduction of the ocean as an active forcing mechanism in the model allowed for changes in the ice-sheet configuration that would not have been achievable with atmospheric forcing alone, such as the grounding-line advance up to the continental shelf break during the LGM. This work therefore has given a first insight into the potential role of the ocean on the past GrIS evolution.

The second study (Tabone et al. (2018c), submitted) aimed to investigate the potential role of past oceanic changes in the evolution of a specific region of the GrIS, the NEGIS, in northeast Greenland, during the LGP. This work builds on the results of the previous study that suggested that orbital changes in the ocean could have had a fundamental role in the expansion and retreat of the GrIS in the past glacial cycles. This work was designed to specifically investigate the suggestion by a recent study that the grounding line of the NEGIS had retreated behind its present-day position for several kilometers during MIS-3 (60 - 25 ka BP), in spite of the glacial climatic conditions. Therefore, the response of the NEGIS to oceanic variabilities was investigated by means of a sensitivity study. The results showed that considering the ocean as an active forcing component in the ice-sheet-shelf model is necessary to trigger grounding-line movement during the LGP. By applying orbital-scale oceanic variations in submarine melting, the model was able to reproduce an inland grounding-line retreat of more than 100 km during MIS-3, followed by a large advance over the continental shelf at the LGM, as suggested by the recent reconstruction. This work showed that the presence of strong submarine melting at the NEGIS ice margins could have been responsible for triggering its grounding-line retreat and, more generally, that a changing oceanic state through the LGP could have been necessary to trigger

the NEGIS margin fluctuations. These results therefore helped to build a further understanding of the possible causes behind the NEGIS margin retreat during the LGP.

The third study (Tabone et al. (2018b), in review) was useful to study the impact of millennial-scale variability in the ocean, associated with D-O events, on the GrIS evolution during the LGP (ca. 120 - 21 ka BP). This work was pursued as a consequence of the outcome of the other two studies, which showed an important role of the ocean in the glacial GrIS configuration. In this work it was shown that high peaks of submarine melting at the grounding line, caused by abrupt warming events in the ocean, can cause large changes in the margin position of the GrIS during the LGP. Contributions to sea level of more than 1.5 m SLE are produced in simulations with strong oceanic-forcing fluctuations, which is around one third of the expected difference in ice volume between the LGM and present day. A deeper investigation showed that the regions of Kangerdlugssuaq fjord in southwest Greenland, Baffin Bay and the NEGIS strongly reacted to these oceanic changes, exhibiting large variations in ice thickness (500-1000 m) and velocity not only at the marine margins, but also up to hundreds of kilometers inland from the coast, suggesting an intense ice discharge during warming events. The latter results are supported by comparison with IRD-deposition data derived from North Atlantic sediment cores. This work therefore suggests that the GrIS could have responded strongly to millennial-scale oceanic temperature variations.

To conclude, this thesis is one of the first works that has investigated the impact of the oceanic forcing on the GrIS past evolution at different timescales and its results have provided new insights into this issue. The overall conclusion that results from all of these studies is that changes in the paleo oceanic conditions have very likely played a fundamental role in shaping the GrIS configuration throughout the past. Variations in oceanic temperatures may have triggered and driven the retreat and advance of the GrIS marine margins in response to orbital and millennial-scale variability. Particularly, in glacial times, when the GrIS was fully marine based over the continental shelf, variations in temperatures of the

surrounding oceans likely triggered large grounding-line migrations, leading to important dynamic ice adjustments in the interior of the ice sheet and profound changes in the overall GrIS configuration. A direct consequence of this conclusion is the need to comprehensively involve the ocean in ice-sheet models that aim to study the paleo evolution of the GrIS. The past interaction between the ocean and the GrIS is an aspect that has been overlooked until now, leading to potentially ignored mechanisms that could help to explain open questions related to the past GrIS evolution. Therefore, this thesis strongly suggests that all ice-sheet models used for paleoclimatic studies should at least include a parameterisation apt to solve the processes at the GrIS ice-ocean interface, even if it is a relatively simple one as that used in this work, to properly evaluate its past expansion and retreat. The coupling of ice-sheet models with climate models will undoubtedly lead to a comprehensive view of the mutual interactions between ice and ocean, and thereby to further advances in the process of understanding the paleo history of the GrIS.

List of publications and conference contributions related to this thesis

Scientific publications as first author

- Tabone, I., Blasco, J., Robinson, A., Álvarez-Solas, J. and Montoya, M., 2018: The sensitivity of the Greenland Ice Sheet to glacial-interglacial oceanic forcing. *Climate of the Past*, **14**, 455-472. DOI 10.5194/cp-14-455-2018.

- Tabone, I., Robinson, A., Álvarez-Solas, J. and Montoya, M., 2018: Submarine melt rate as a potential trigger of grounding-line retreat during Marine Isotope Stage 3. *submitted to The Cryosphere.*

- Tabone, I., Robinson, A., Álvarez-Solas, J. and Montoya, M., 2018: Impact of millennial-scale oceanic variability on the Greenland Ice Sheet evolution throughout the Last Glacial Period. *Climate of the Past Discussion*, DOI 10.5194/cp-2018-129, in review.

Contribution in other scientific publications

- Blasco, J., Tabone, I., Robinson, A., Álvarez-Solas, J. and Montoya, M., 2018: The Antarctic Ice Sheet response to glacial millennial scale variability. *Climate of the Past Discussion*, DOI 10.5194/cp-2018-95, in review.

- Anzalone, A., Bertaina, M. E., Briz, S., Cassardo, C., Cremonini, R., de Castro, A. J., Ferrarese, S., Isgró, F., Lopez F. and Tabone, I., 2018: Methods to Retrieve the Cloud-Top Height in the Frame of the JEM-EUSO Mission. *IEEE Transactions on Geoscience and Remote Sensing*, **99**, 1-15, DOI 10.1109/TGRS.2018.2854296.

Oral contributions - Conferences

- Tabone, I., Robinson, A., Álvarez-Solas, J. and Montoya, M., 2016: The ocean sensitivity of the Greenland Ice Sheet. XI congress TOPCART 2016, Toledo (Spain), 27 september 2016. This contribution has been published in: Especial TOPCART 2016, XI Congreso de Geomática y Ciencias de la Tierra - Criosfera y Cambio Climático, Vol. XXXII, num. 170, 2016, ISSN: 1212-9280.

- Tabone, I., Robinson, A., Álvarez-Solas, J. and Montoya, M., 2017: The Greenland Ice Sheet-ocean interaction in the past two glacial cycles. *Geophysical Research Abstracts*, **19**, EGU2017-823, 2017. Contribution presented at EGU General Assembly, Vienna (Austria), 23-28 April 2017.

- Tabone, I., Robinson, A., Álvarez-Solas, J. and Montoya, M., 2017: Sensitivity of the Greenland Ice Sheet to oceanic changes in the last 150 kyrs., *PAGES Abstract Book*, PAGES17-01675, 2017. Contribution presented at PAGES - 5^{th} Open Science Meeting on Global Challenges for our Common Future: a

paleoscience perspective, Zaragoza (Spain), 9-13 May 2017.

Poster contributions - Conferences and Schools

- Tabone, I., Blasco, J., Robinson, A., Álvarez-Solas, J. and Montoya, M., 2018: Optimizing ice-sheet-shelf model performance through a skill-score study. *Geophysical Research Abstracts*, **20**, EGU2018-14145, 2018. Contribution presented at EGU General Assembly, Vienna (Austria), 8-13 April 2018.

- Tabone, I., Blasco, J., Robinson, A., Álvarez-Solas, J. and Montoya, M., 2018: The Greenland Ice Sheet sensitivity to oceanic forcing on a glacial-interglacial timescale. *Geophysical Research Abstracts*, **20**, EGU2018-13648, 2018. Contribution presented at EGU General Assembly, Vienna (Austria), 8-13 April 2018.

- Tabone, I., Robinson, A., Álvarez-Solas, J. and Montoya, M., 2018: The ocean as a trigger of Greenland Ice Sheet evolution at millennial timescale, presented at the 17^{th} International Swiss Climate Summer School - Earth system variability through time, Grindelwald (Switzerland), 26-31 August 2018.

Other oral and poster contributions

- Tabone, I., Blasco, J., Robinson, A., Álvarez-Solas, J. and Montoya, M., 2017: The sensitivity of the Greenland Ice Sheet to glacial-interglacial oceanic forcing. *Poster contribution*, PhDay Físicas 2017, Madrid (Spain), 15-20 December 2017.

- Tabone, I., 2018: The sensitivity of the Greenland Ice Sheet to glacial-interglacial oceanic forcing. *Oral contribution*, I Jornada Jóvenes Investi-

gadores en Ciencias de la Tierra, IGEO, Madrid (Spain), 10 May 2018.

- Tabone, I., 2016: Modeling the evolution of the Greenland Ice Sheet using a hybrid ice-sheet model. *Oral contribution*, Jornadas de doctorandos de la UCM, Madrid (Spain), 14-16 December 2016.

References

Alley, R., S. Anandakrishnan, and P. Jung, 2001: Stochastic resonance in the North Atlantic. *Paleoceanography and Paleoclimatology*, **16**, 190–198.

Alley, R. B., 2007: Wally was right: Predictive ability of the North Atlantic conveyor belt hypothesis for abrupt climate change. *Annual Review of Earth Planetary Sciences*, **35**, 241–272.

Alley, R. B., S. Anandakrishnan, K. Christianson, H. J. Horgan, A. Muto, B. R. Parizek, D. Pollard, and R. T. Walker, 2015: Oceanic forcing of Ice-Sheet retreat: West Antarctica and more. *Annual Review of Earth Planetary Sciences*, **43**, 207–231, doi:10.1146/annurev-earth-060614-105344.

Alley, R. B., J. T. Andrews, J. Brigham-Grette, G. Clarke, K. M. Cuffey, J. Fitzpatrick, S. Funder, S. Marshall, G. Miller, J. Mitrovica, et al., 2010: History of the Greenland Ice Sheet: paleoclimatic insights. *Quaternary Science Reviews*, **29**, 1728–1756.

Alvarez-Solas, J., R. Banderas, A. Robinson, , and M. Montoya, 2017: Oceanic forcing of the Eurasian Ice Sheet on millennial time scales during the Last Glacial Period. *Climate of the Past Discussions*.

Alvarez-Solas, J., S. Charbit, G. Ramstein, D. Paillard, C. Dumas, C. Ritz, and D. M. Roche, 2011a: Millennial-scale oscillations in the Southern Ocean in response to atmospheric CO_2 increase. *Global and Planetary Change*, **76**, 128–136.

Alvarez-Solas, J., M. Montoya, C. Ritz, G. Ramstein, S. Charbit, C. Dumas, K. Nisancioglu, T. Dokken, and A. Ganopolski, 2011b: Heinrich event 1: an example of dynamical ice-sheet reaction to oceanic changes. *Climate of the Past*, **7**, 1297–1306, doi:10.5194/cp-7-1297-2011.

Alvarez-Solas, J., A. Robinson, M. Montoya, and C. Ritz, 2013: Iceberg discharges of the last glacial period driven by oceanic circulation changes. *Proceedings of the National Academy of Sciences*, **110, 41**, 16350–16354, doi:10.1073/pnas.1306622110.

Andersen, K. K., N. Azuma, J.-M. Barnola, M. Bigler, P. Biscaye, N. Caillon, J. Chappellaz, H. B. Clausen, D. Dahl-Jensen, H. Fischer, et al., 2004: High-resolution record of Northern Hemisphere climate extending into the last interglacial period. *Nature*, **431**, 147.

Anderson, P., O. Bennike, N. Bigelow, J. Brigham-Grette, M. Duvall, M. Edwards, B. Fréchette, S. Funder, S. Johnsen, J. Knies, et al., 2006: Last Interglacial Arctic warmth confirms polar amplification of climate change. *Quaternary Science Reviews*, **25**, 1383–1400.

Andrews, J., G. Dunhill, C. Vogt, and A. Voelker, 2017: Denmark Strait during the Late Glacial Maximum and Marine Isotope Stage 3: Sediment sources and transport processes. *Marine Geology*, **390**, 181–198.

Andrews, J. T., D. Barber, A. Jennings, D. Eberl, B. Maclean, M. Kirby, and J. Stoner, 2012: Varying sediment sources (Hudson Strait, Cumberland Sound, Baffin Bay) to the NW Labrador Sea slope between and during Heinrich events 0 to 4. *Journal of Quaternary Science*, **27**, 475–484.

Annan, J. D. and J. C. Hargreaves, 2013: A new global reconstruction of temperature changes at the Last Glacial Maximum. *Climate of the Past*, **9**, 367–376, doi:10.5194/cp-9-367-2013.

Applegate, P. J., N. Kirchner, E. J. Stone, K. Keller, and R. Greve, 2012: An assessment of key model parametric uncertainties in projections of Greenland Ice Sheet behavior. *The Cryosphere*, **6**, 589–606.

Arndt, J. E., W. Jokat, and B. Dorschel, 2017: The last glaciation and deglaciation of the Northeast Greenland continental shelf revealed by hydro-acoustic data. *Quaternary Science Reviews*, **160**, 45–56.

Arndt, J. E., W. Jokat, B. Dorschel, R. Myklebust, J. A. Dowdeswell, and J. Evans, 2015: A new bathymetry of the Northeast Greenland continental shelf: Constraints on glacial and other processes. *Geochemistry, Geophysics, Geosystems*, **16**, 3733–3753.

Asmerom, Y., V. J. Polyak, and S. J. Burns, 2010: Variable winter moisture in the southwestern United States linked to rapid glacial climate shifts. *Nature Geoscience*, **3**, 114.

Bagniewski, W., K. J. Meissner, and L. Menviel, 2017: Exploring the oxygen isotope fingerprint of Dansgaard-Oeschger variability and Heinrich events. *Quaternary Science Reviews*, **159**, 1–14.

Bamber, J. L., J. A. Griggs, R. T. W. L. Hurkmans, J. A. Dowdeswell, S. P. Gogineni, I. Howat, J. Mouginot, J. Paden, S. Palmer, E. Rignot, and D. Steinhage, 2013: A new bed elevation dataset for Greenland. *The Cryosphere*, **7**, 499–510, doi:10.5194/tc-7-499-2013.

Banderas, R., J. Alvarez-Solas, A. Robinson, and M. Montoya, 2015: An interhemispheric mechanism for glacial abrupt climate change. *Climate Dynamics*, **44**, 2897–2908.

Banderas, R., J. Alvarez-Solas, A. Robinson, and M. Montoya, 2018: A new approach for simulating the paleo-evolution of the Northern Hemisphere ice sheets. *Geoscientific Model Development*, **11**, 2299–2314.

Barbante, C., J.-M. Barnola, S. Becagli, J. Beer, M. Bigler, C. Boutron, T. Blunier, E. Castellano, O. Cattani, J. Chappellaz, et al., 2006: One-to-one coupling of glacial climate variability in Greenland and Antarctica. *Nature*, **444**, 195–198.

Barker, S. and G. Knorr, 2007: Antarctic climate signature in the Greenland ice core record. *Proceedings of the National Academy of Sciences*, **104**, 17278–17282.

Barker, S., G. Knorr, R. L. Edwards, F. Parrenin, A. E. Putnam, L. C. Skinner, E. Wolff, and M. Ziegler, 2011: 800000 years of abrupt climate variability. *Science*, **334**, 347–351, doi:10.1126/science.1203580.

Bauer, E. and A. Ganopolski, 2017: Comparison of surface mass balance of ice sheets simulated by positive-degree-day method and energy balance approach.

Climate of the Past, **13**, 819–832.

Beckmann, A. and H. Goosse, 2003: A parameterization of ice shelf-ocean interaction for climate models. *Ocean Modelling*, **5**, 157–170, doi:10.1016/S1463-5003(02)00019-7.

Bender, M., T. Sowers, M.-L. Dickson, J. Orchardo, P. Grootes, P. A. Mayewski, and D. A. Meese, 1994: Climate correlations between Greenland and Antarctica during the past 100,000 years. *Nature*, **372**, 663.

Benson, L. V., J. W. Burdett, M. Kashgarian, S. P. Lund, F. M. Phillips, and R. O. Rye, 1996: Climatic and hydrologic oscillations in the Owens Lake Basin and adjacent Sierra Nevada, California. *Science*, **274**, 746–749.

Bernales, J., I. Rogozhina, R. Greve, and M. Thomas, 2017: Comparison of hybrid schemes for the combination of shallow approximations in numerical simulations of the Antarctic Ice Sheet. *The Cryosphere*, **11**, 247–265.

Bierman, P. R., J. D. Shakun, L. B. Corbett, S. R. Zimmerman, and D. H. Rood, 2016: A persistent and dynamic East Greenland Ice Sheet over the past 7.5 million years. *Nature*, **540**, 256.

Bindschadler, R. A., S. Nowicki, A. Abe-Ouchi, A. Aschwanden, H. Choi, J. Fastook, G. Granzow, R. Greve, G. Gutowski, U. Herzfeld, C. Jackson, J. Johnson, C. Khroulev, A. Levermann, W. H. Lipscomb, M. A. Martin, M. Morlighem, B. R. Parizek, D. Pollard, S. F. Price, D. Ren, F. Saito, T. Sato, H. Seddik, H. Seroussi, K. Takahashi, R. Walker, and W. L. Wang, 2013: Ice sheet model sensitivity to environmental forcing and their use in projecting future sea level. *Journal of Glaciology*, **59**, 195–224, doi:10.3189/2013JoG12J125.

Bintanja, R. and R. Van de Wal, 2008: North American ice-sheet dynamics and the onset of 100,000-year glacial cycles. *Nature*, **454**, 869.

Blasco, J., I. Tabone, J. Alvarez-Solas, A. Robinson, and M. Montoya, 2018: The Antarctic Ice Sheet response to glacial millennial scale variability. *Climate of the Past Discussion*, doi:10.5194/cp-2018-95.

Blatter, H., R. Greve, and A. Abe-Ouchi, 2011: Present state and prospects of ice sheet and glacier modelling. *Surveys in geophysics*, **32**, 555–583.

Blunier, T. and E. J. Brook, 2001: Timing of millennial-scale climate change in Antarctica and Greenland during the last glacial period. *Science*, **291**, 109–

112.

Böhm, E., J. Lippold, M. Gutjahr, M. Frank, P. Blaser, B. Antz, J. Fohlmeister, N. Frank, M. Andersen, and M. Deininger, 2015: Strong and deep Atlantic meridional overturning circulation during the last glacial cycle. *Nature*, **517**, 73.

Bond, G., W. Broecker, S. Johnsen, J. McManus, L. Labeyrie, J. Jouzel, and G. Bonani, 1993: Correlations between climate records from North Atlantic sediments and Greenland ice. *Nature*, **365**, 143.

Bond, G. C. and R. Lotti, 1995: Iceberg discharges into the North Atlantic on millennial time scales during the last glaciation. *Science*, **267**, 1005–1010.

Born, A. and K. H. Nisancioglu, 2012: Melting of Northern Greenland during the last interglaciation. *The Cryosphere*, **6**, 1239–1250, doi:10.5194/tc-6-1239-2012.

Box, J., X. Fettweis, J. Stroeve, M. Tedesco, D. Hall, and K. Steffen, 2012: Greenland ice sheet albedo feedback: thermodynamics and atmospheric drivers. *The Cryosphere*, **6**, 821–839.

Box, J. E., D. H. Bromwich, B. A. Veenhuis, L.-S. Bai, J. C. Stroeve, J. C. Rogers, K. Steffen, T. Haran, and S.-H. Wang, 2006: Greenland ice sheet surface mass balance variability (1988–2004) from calibrated polar MM5 output. *Journal of Climate*, **19**, 2783–2800.

Box, J. E., L. Yang, D. H. Bromwich, and L.-S. Bai, 2009: Greenland ice sheet surface air temperature variability: 1840-2007. *Journal of Climate*, **22 (14)**, 4029–4049, doi:10.1175/2009JCLI2816.1.

Bradley, R. S., 1985: Quaternary paleoclimatology.

Bradley, S. L., T. J. Reerink, R. S. van de Wal, and M. M. Helsen, 2018: Simulation of the Greenland Ice Sheet over two glacial-interglacial cycles: investigating a sub-iceshelf melt parameterization and relative sea level forcing in an ice-sheet-ice-shelf model. *Climate of the Past*, **14**.

Broecker, W. S., 1998: Paleocean circulation during the last deglaciation: a bipolar seesaw? *Paleoceanography*, **13**, 119–121.

Broecker, W. S., D. M. Peteet, and D. Rind, 1985: Does the ocean–atmosphere system have more than one stable mode of operation? *Nature*, **315**, 21.

Broeker, W., G. Bond, M. Klaus, G. Bonani, and W. Wolffli, 1990: A salt oscillator in the glacial Atlantic. *Paleoceanography*, **5**, 469–477.

Brook, E. J. and C. Buizert, 2018: Antarctic and global climate history viewed from ice cores. *Nature*, **558**, 200.

Brook, E. J., J. W. White, A. S. Schilla, M. L. Bender, B. Barnett, J. P. Severinghaus, K. C. Taylor, R. B. Alley, and E. J. Steig, 2005: Timing of millennial-scale climate change at Siple Dome, West Antarctica, during the last glacial period. *Quaternary Science Reviews*, **24**, 1333–1343.

Bueler, E. and J. Brown, 2009: Shallow shelf approximation as a sliding law in a thermomechanically coupled ice sheet model. *Journal of Geophysical Research*, **114**, F03008, doi:10.1029/2008JF001179.

Buizert, C., B. Adrian, J. Ahn, M. Albert, R. B. Alley, D. Baggenstos, T. K. Bauska, R. C. Bay, B. B. Bencivengo, C. R. Bentley, et al., 2015: Precise interpolar phasing of abrupt climate change during the last ice age. *Nature*, **520**, 661.

Buizert, C., B. A. Keisling, J. E. Box, F. He, A. E. Carlson, G. Sinclair, and R. M. DeConto, 2018: Greenland-wide seasonal temperatures during the last deglaciation. *Geophysical Research Letters*, **1944-8007**, doi:10.1002/2017GL075601.

Burckel, P., C. Waelbroeck, J. M. Gherardi, S. Pichat, H. Arz, J. Lippold, T. Dokken, and F. Thil, 2015: Atlantic Ocean circulation changes preceded millennial tropical South America rainfall events during the last glacial. *Geophysical Research Letters*, **42**, 411–418.

Cai, C., E. Rignot, D. Menemenlis, and Y. Nakayama, 2017: Observations and modeling of ocean-induced melt beneath Petermann Glacier Ice Shelf in northwestern Greenland. *Geophysical Research Letters*, **44**, 8396–8403.

Calov, R., A. Robinson, M. Perrette, and A. Ganopolski, 2015: Simulating the Greenland ice sheet under present-day and palaeo constraints including a new discharge parameterization. *The Cryosphere*, **9**, 179–196, doi:10.5194/tc-9-179-2015.

Carr, J. R., C. R. Stokes, and A. Vieli, 2013: Recent progress in understanding marine-terminating Arctic outlet glacier response to climatic and oceanic

forcing: Twenty years of rapid change. *Progress in Physical Geography*, **37**, 436–467.

Charbit, S., C. Ritz, G. Philippon, V. Peyaud, and M. Kageyama, 2007: Numerical reconstructions of the Northern Hemisphere ice sheets through the last glacial-interglacial cycle. *Climate of the Past*, **3**, 15–37.

Choi, Y., M. Morlighem, E. Rignot, J. Mouginot, and M. Wood, 2017: Modeling the response of Nioghalvfjerdsfjorden and Zachariae Isstrøm Glaciers, Greenland, to ocean forcing over the next century. *Geophysical Research Letters*, **44**.

Church, J., P. Clark, A. Cazenave, J. Gregory, S. Jevrejeva, A. Levermann, M. Merrifield, G. Milne, R. Nerem, P. Nunn, A. Payne, W. Pfeffer, S. D., and A. Unnikrishnan, 2013: Sea Level Change. *Climate Change 2013: The Physical Science Basis. Contribution of Working Group I to the Fifth Assessment Report of the Intergovernmental Panel on Climate Change*.

Clark, P. U., J. A. Church, J. M. Gregory, and A. J. Payne, 2015: Recent progress in understanding and projecting regional and global mean sea level change. *Current Climate Change Reports*, **1**, 224–246.

Clark, P. U. and P. Huybers, 2009: Global change: Interglacial and future sea level. *Nature*, **462**, 856.

Clark, P. U. and A. C. Mix, 2002: Ice sheets and sea level of the Last Glacial Maximum. *Quaternary Science Reviews*, **21(1)**, 1–7.

Colleoni, F., 2015: *GRenoble Ice-Shelf and Land-Ice model: a practical user guide*, volume RP0249. Centro Euro-Mediterraneo sui Cambiamenti Climatici, Bologna (Italy).

Colleoni, F., S. Masina, A. Cherchi, A. Navarra, C. Ritz, V. Peyaud, and B. Otto-Bliesner, 2014: Modeling Northern Hemisphere ice-sheet distribution during MIS 5 and MIS 7 glacial inceptions. *Climate of the Past*, **10**, 269–291, doi:10.5194/cp-10-269-2014.

Colville, E. J., A. E. Carlson, B. L. Beard, R. G. Hatfield, J. S. Stoner, A. V. Reyes, and D. J. Ullman, 2011: Sr-Nd-Pb isotope evidence for ice-sheet presence on southern Greenland during the Last Interglacial. *Science*, **333**, 620–623.

Cook, A. J., P. R. Holland, M. P. Meredith, T. Murray, A. Luckman, and D. G. Vaughan, 2016: Ocean forcing of glacier retreat in the western Antarctic Peninsula. *Science*, **353(6296)**, 283–286, doi:10.1126/science.aae0017.

Cornford, S. L., D. F. Martin, D. T. Graves, D. F. Ranken, A. M. Le Brocq, R. M. Gladstone, A. J. Payne, E. G. Ng, and W. H. Lipscomb, 2013: Adaptive mesh, finite volume modeling of marine ice sheets. *Journal of Computational Physics*, **232**, 529–549.

Crowley, T. J. and G. R. North, 1991: Paleoclimatology.

Cruz Jr, F. W., I. Karmann, O. Viana Jr, S. J. Burns, J. A. Ferrari, M. Vuille, A. N. Sial, and M. Z. Moreira, 2005: Stable isotope study of cave percolation waters in subtropical Brazil: implications for paleoclimate inferences from speleothem.s. *Chemical Geology*, **220**, 245–262.

Cuffey, K. M. and W. S. B. Paterson, 2010: *The physics of glaciers.*. Academic Press.

Dansgaard, W., S. Johnsen, H. Clausen, D. Dahl-Jensen, N. Gundestrup, C. Hammer, C. Hvidberg, J. Steffensen, A. Sveinbjörnsdottir, J. Jouzel, et al., 1993: Evidence for general instability of past climate from a 250-kyr ice-core record. *Nature*, **364**, 218.

Dansgaard, W., S. Johnsen, H. Clausen, D. Dahl-Jensen, N. Gundestrup, C. Hammer, and H. Oeschger, 1984: North Atlantic climatic oscillations revealed by deep Greenland ice cores. *Climate processes and climate sensitivity*, **29**, 288–298.

Darby, D. A., J. F. Bischof, R. F. Spielhagen, S. A. Marshall, and S. W. Herman, 2002: Arctic ice export events and their potential impact on global climate during the late Pleistocene. *Paleoceanography*, **17**, 15–1.

De Boer, B., R. Van de Wal, L. Lourens, R. Bintanja, and T. Reerink, 2013: A continuous simulation of global ice volume over the past 1 million years with 3-D ice-sheet models. *Climate Dynamics*, **41**, 1365–1384.

DeConto, R. M. and D. Pollard, 2016: Contribution of Antarctica to past and future sea-level rise. *Nature*, **531**, 591–597, doi:10.1038/nature17145.

Dowdeswell, J. A., J. Evans, and C. Ó. Cofaigh, 2010: Submarine landforms and shallow acoustic stratigraphy of a 400 km-long fjord-shelf-slope tran-

sect, Kangerlussuaq margin, East Greenland. *Quaternary Science Reviews*, **29**, 3359–3369.

Dutrieux, P., D. G. Vaughan, H. F. Corr, A. Jenkins, P. R. Holland, I. Joughin, and A. Fleming, 2013: Pine Island glacier ice shelf melt distributed at kilometre scales. *The Cryosphere*, **7**, 1543–1555, doi:10.5194/tc-7-1543-2013.

Dutton, A., A. Carlson, A. Long, G. Milne, P. Clark, R. DeConto, B. Horton, S. Rahmstorf, and M. Raymo, 2015: Sea-level rise due to polar ice-sheet mass loss during past warm periods. *Science*, **349**, aaa4019.

Eldrett, J. S., I. C. Harding, P. A. Wilson, E. Butler, and A. P. Roberts, 2007: Continental ice in Greenland during the Eocene and Oligocene. *Nature*, **446**, 176.

Enderlin, E. M. and I. M. Howat, 2013: Submarine melt rate estimates for floating termini of Greenland outlet glaciers (2000-2010). *Journal of Glaciology*, **59(213)**, 67–75, doi:10.3189/2013JoG12J049.

Favier, L., G. Durand, S. L. Cornford, G. H. Gudmundsson, O. Gagliardini, F. Gillet-Chaulet, T. Zwinger, A. Payne, and A. M. Le Brocq, 2014: Retreat of Pine Island Glacier controlled by marine ice-sheet instability. *Nature Climate Change*, **4**, 117–121, doi:10.1038/NCLIMATE2094.

Favier, L., F. Pattyn, S. Berger, and R. Drews, 2016: Dynamic influence of pinning points on marine ice-sheet stability: a numerical study in Dronning Maud Land, East Antarctica. *The Cryosphere*, **10**, 2623–2635, doi:10.5194/tc-10-2623-2016.

Fettweis, X., B. Franco, M. Tedesco, J. Van Angelen, J. Lenaerts, M. Van den Broeke, and H. Gallée, 2013: Estimating Greenland ice sheet surface mass balance contribution to future sea level rise using the regional atmospheric climate model MAR. *The Cryosphere*, **7**, 469489, doi:10.5194/tc-7-469-2013.

Fleming, K. and K. Lambeck, 2004: Constraints on the Greenland Ice Sheet since the Last Glacial Maximum from sea-level observations and glacial-rebound models. *Quaternary Science Reviews*, **23(9)**, 1053–1077, doi:10.1016/j.quascirev.2003.11.001.

Fried, M., G. Catania, T. Bartholomaus, D. Duncan, M. Davis, L. Stearns, J. Nash, E. Shroyer, and D. Sutherland, 2015: Distributed subglacial discharge

drives significant submarine melt at a Greenland tidewater glacier. *Geophysical Research Letters*, **42(21)**, 9328–9336, doi:10.1002/2015GL065806.

Funder, S., K. K. Kjeldsen, K. H. Kjær, and C. Cofaigh, 2011: The Greenland Ice Sheet during the past 300,000 years: A review. *Developments in Quaternary Sciences*, **15**, 699–713, doi:10.1016/B978-0-444-53447-7.00050-7.

Fürst, J. J., H. Goelzer, and P. Huybrechts, 2013: Effect of higher-order stress gradients on the centennial mass evolution of the Greenland ice sheet. *The Cryosphere*, **7**, 183–199, doi:10.5194/tc-7-183-2013.

Fürst, J. J., H. Goelzer, and P. Huybrechts, 2015: Ice-dynamic projections of the Greenland ice sheet in response to atmospheric and oceanic warming. *The Cryosphere*, **9**, 1039–1062, doi:10.5194/tc-9-1039-2015.

Ganopolski, A. and S. Rahmstorf, 2001: Rapid changes of glacial climate simulated in a coupled climate model. *Nature*, **409**, 153.

Gladstone, R., A. Payne, and S. Cornford, 2010: Parameterising the grounding line in flow-line ice sheet models. *The Cryosphere*, **4**, 605–619.

Gladstone, R. M., V. Lee, J. Rougier, A. J. Payne, H. Hellmer, A. Le Brocq, A. Shepherd, T. L. Edwards, J. Gregory, and S. L. Cornford, 2012: Calibrated prediction of Pine Island Glacier retreat during the 21st and 22nd centuries with a coupled flowline model. *Earth and Planetary Science Letters*, **333**, 191–199.

Gladstone, R. M., R. C. Warner, B. K. Galton-Fenzi, O. Gagliardini, T. Zwinger, and R. Greve, 2017: Marine ice sheet model performance depends on basal sliding physics and sub-shelf melting. *The Cryosphere*, **2017**, 319–329, doi:10.5194/tc-11-319-2017.

Golledge, N. R., C. J. Fogwill, A. N. Mackintosh, and K. M. Buckley, 2012: Dynamics of the last glacial maximum Antarctic ice-sheet and its response to ocean forcing. *Proceedings of the National Academy of Sciences*, **109(40)**, 16052–16056, doi:10.1073/pnas.1205385109.

Gottschalk, J., L. C. Skinner, S. Misra, C. Waelbroeck, L. Menviel, and A. Timmermann, 2015: Abrupt changes in the southern extent of North Atlantic Deep Water during Dansgaard–Oeschger events. *Nature Geoscience*, **8**, 950.

Grant, K., E. Rohling, C. B. Ramsey, H. Cheng, R. Edwards, F. Florindo, D. Heslop, F. Marra, A. Roberts, M. E. Tamisiea, et al., 2014: Sea-level variability over five glacial cycles. *Nature Communications*, **5**, 5076, doi:10.1038/ncomms6076.

Greve, R. and H. Blatter, 2009: *Dynamics of ice sheets and glaciers.*. Springer Science & Business Media.

Grootes, P. M., M. Stuiver, J. White, S. Johnsen, and J. Jouzel, 1993: Comparison of oxygen isotope records from the GISP2 and GRIP Greenland ice cores. *Nature*, **366**, 552.

Grousset, F. E., C. Pujol, L. Labeyrie, G. Auffret, and A. Boelaert, 2000: Were the North Atlantic Heinrich events triggered by the behavior of the European ice sheets? *Geology*, **28**, 123–126.

Hall, D. K., R. S. Williams, S. B. Luthcke, and N. E. Digirolamo, 2008: Greenland ice sheet surface temperature, melt and mass loss: 2000-06. *Journal of Glaciology*, **54 (184)**, 81–93.

Hanna, E., P. Huybrechts, K. Steffen, J. Cappelen, R. Huff, C. Shuman, T. Irvine-Fynn, S. Wise, and M. Griffiths, 2008: Increased runoff from melt from the Greenland Ice Sheet: a response to global warming. *Journal of Climate*, **21**, 331–341, doi:10.1175/2007JCLI1964.1.

Hanna, E., F. J. Navarro, F. Pattyn, C. M. Domingues, X. Fettweis, E. R. Ivins, R. J. Nicholls, C. Ritz, B. Smith, S. Tulaczyk, P. L. Whitehouse, and H. J. Zwally, 2013: Ice-sheet mass balance and climate change. *Nature*, **498**, 51–59, doi:10.1038/nature12238.

Helsen, M., W. Van De Berg, R. Van De Wal, M. Van Den Broeke, and J. Oerlemans, 2013: Coupled regional climate-ice-sheet simulation shows limited Greenland ice loss during the Eemian. *Climate of the Past*, **9(4)**, 1773, doi:10.5194/cp-9-1773-2013.

Hemming, S. R., 2004: Heinrich events: Massive late Pleistocene detritus layers of the North Atlantic and their global climate imprint. *Reviews of Geophysics*, **42**.

Henry, L., J. F. McManus, W. B. Curry, N. L. Roberts, A. M. Piotrowski, and L. D. Keigwin, 2016: North Atlantic ocean circulation and abrupt climate change during the last glaciation. *Science*, **353**, 470–474.

Hill, E. A., J. R. Carr, and C. R. Stokes, 2017: A review of recent changes in major marine-terminating outlet glaciers in Northern Greenland. *Frontiers in Earth Science*, **4**, 1–24, doi:10.3389/feart.2016.00111.

Hodell, D. A., H. F. Evans, J. E. Channell, and J. H. Curtis, 2010: Phase relationships of North Atlantic ice-rafted debris and surface-deep climate proxies during the last glacial period. *Quaternary Science Reviews*, **29**, 3875–3886.

Hogg, A. E. and G. H. Gudmundsson, 2017: Impacts of the Larsen-C Ice Shelf calving event. *Nature Climate Change*, **7**, 540–542, doi:10.1038/nclimate3359.

Holland, D. M., R. H. Thomas, B. De Young, M. H. Ribergaard, and B. Lyberth, 2008a: Acceleration of Jakobshavn Isbrae triggered by warm subsurface ocean waters. *Nature Geoscience*, **1**, 659–664, doi:10.1038/ngeo316.

Holland, P., A. Brisbourne, H. Corr, D. Mcgrath, K. Purdon, J. Paden, H. Fricker, F. Paolo, and A. Fleming, 2015: Oceanic and atmospheric forcing of Larsen C Ice-Shelf thinning. *The Cryosphere*, **9**, 1005–1024, doi:10.5194/tc-9-1005-2015.

Holland, P. R., A. Jenkins, and D. M. Holland, 2008b: The response of ice shelf basal melting to variations in ocean temperature. *Journal of Climate*, **21**, 2558–2572, doi:10.1175/2007JCLI1909.1.

Howat, I. M., I. Joughin, and T. A. Scambos, 2007: Rapid changes in ice discharge from Greenland outlet glaciers. *Science*, **315**, 1559–1561, doi:10.1126/science.1138478.

Howat, I. M., I. Joughin, S. Tulaczyk, and S. Gogineni, 2005: Rapid retreat and acceleration of Helheim Glacier, east Greenland. *Geophysical Research Letters*, **32**, L22502, doi:10.1029/2005GL024737.

Hutter, K., 1983: Theoretical Glaciology: Material Science of Ice and the Mechanics of Glaciers and Ice Sheets (Mathematical Approaches to Geophysics).

Huybrechts, P., 2002: Sea-level changes at the LGM from ice-dynamic reconstructions of the Greenland and Antarctic ice sheets during the glacial cycles. *Quaternary Science Reviews*, **21**, 203–231, doi:10.1016/S0277-3791(01)00082-8.

Jansen, D., A. J. Luckman, A. Cook, S. Bevan, B. Kulessa, B. Hubbard, and P. Holland, 2015: Brief Communication: Newly developing rift in Larsen C

Ice Shelf presents significant risk to stability. *The Cryosphere*, **9**, 1223–1227, doi:10.5194/tc-9-1223-2015.

Jansen, E., T. Fronval, F. Rack, and J. E. Channell, 2000: Pliocene-Pleistocene ice rafting history and cyclicity in the Nordic Seas during the last 3.5 Myr. *Paleoceanography and Paleoclimatology*, **15**, 709–721.

Jenkins, A., 2011: Convection-driven melting near the grounding line of ice shelves and tidewater glaciers. *Journal of Physical Oceanography*, **41**, 2279–2294, doi:10.1175/JPO-D-11-03.1.

Jenkins, A. and C. Doake, 1991: Ice-ocean interaction on Ronne Ice Shelf, Antarctica. *Journal of Geophysical Research: Oceans*, **96**, 791–813.

Jennings, A. E., J. T. Andrews, C. Ó. Cofaigh, G. S. Onge, C. Sheldon, S. T. Belt, P. Cabedo-Sanz, and C. Hillaire-Marcel, 2017: Ocean forcing of Ice Sheet retreat in central west Greenland from LGM to the early Holocene. *Earth and Planetary Science Letters*, **472**, 1–13.

Jensen, M. F., A. Nummelin, S. B. Nielsen, H. Sadatzki, E. Sessford, B. Risebrobakken, C. Andersson, A. Voelker, W. H. G. Roberts, J. Pedro, and A. Born, 2018: A spatiotemporal reconstruction of sea-surface temperatures in the North Atlantic during Dansgaard–Oeschger events 5–8. *Climate of the Past*, **14**, 901–922, doi:10.5194/cp-14-901-2018.
URL https://www.clim-past.net/14/901/2018/

Johnsen, S. J., D. Dahl-Jensen, N. Gundestrup, J. P. Steffensen, H. B. Clausen, H. Miller, V. Masson-Delmotte, A. E. Sveinbjörnsdottir, and J. White, 2001: Oxygen isotope and palaeotemperature records from six Greenland ice-core stations: Camp Century, Dye-3, GRIP, GISP2, Renland and NorthGRIP. *Journal of Quaternary Science: Published for the Quaternary Research Association*, **16**, 299–307.

Jonkers, L., M. Moros, M. A. Prins, T. Dokken, C. A. Dahl, K. Dijkstra, N.and Perner, and G. J. A. Brummer, 2010: Irregular glacial interstadials recorded in a new Greenland ice core. *Quaternary Science Reviews*, **29**, 1791–1800.

Joughin, I., W. Abdalati, and M. Fahnestock, 2004: Large fluctuations in speed on Greenland's Jakobshavn Isbrae glacier. *Nature*, **432**, 608.

Joughin, I., R. B. Alley, and D. M. Holland, 2012a: Ice-sheet response to oceanic forcing. *Science*, **338**, 1172–1176, doi:10.1126/science.1226481.

Joughin, I., M. Fahnestock, D. MacAyeal, J. L. Bamber, and P. Gogineni, 2001: Observation and analysis of ice flow in the largest Greenland ice stream. *Journal of Geophysical Research: Atmospheres*, **106**, 34021–34034.

Joughin, I., B. E. Smith, I. M. Howat, D. Floricioiu, R. B. Alley, M. Truffer, and M. Fahnestock, 2012b: Seasonal to decadal scale variations in the surface velocity of Jakobshavn Isbrae, Greenland: Observation and model-based analysis. *Journal of Geophysical Research*, **117**, F02030, doi:10.1029/2011JF002110.

Joughin, I., B. E. Smith, and B. Medley, 2014: Marine ice sheet collapse potentially under way for the Thwaites Glacier Basin, West Antarctica. *Science*, **344**, 735–738, doi:10.1126/science.1249055.

Kanner, L. C., S. J. Burns, H. Cheng, and R. L. Edwards, 2012: High-latitude forcing of the South American summer monsoon during the last glacial. *Science*, 1213397.

Khan, S. A., K. H. Kjær, M. Bevis, J. L. Bamber, J. Wahr, K. K. Kjeldsen, A. A. Bjørk, N. J. Korsgaard, L. A. Stearns, and M. R. van den Broeke, 2014: Sustained mass loss of the northeast Greenland ice sheet triggered by regional warming. *Nature*, **4(4)**, 292–299, doi:10.1038/nclimate2161.

Kindler, P., M. Guillevic, M. Baumgartner, J. Schwander, A. Landais, and M. Leuenberger, 2014: Temperature reconstruction from 10 to 120 kyr b2k from the NGRIP ice core. *Climate of the Past*, **10**, 887–902, doi:10.5194/cp-10-887-2014.

Kissel, C., C. Laj, L. Labeyrie, T. Dokken, A. Voelker, and D. Blamart, 1999: Rapid climatic variations during marine isotopic stage 3: magnetic analysis of sediments from Nordic Seas and North Atlantic. *Earth and Planetary Science Letters*, **171**, 489–502.

Kleiven, H. F., E. Jansen, T. Fronval, and T. Smith, 2002: Intensification of Northern Hemisphere glaciations in the circum Atlantic region (3.5–2.4 Ma)–ice-rafted detritus evidence. *Palaeogeography, Palaeoclimatology, Palaeoecology*, **184**, 213–223.

Kleppin, H., M. Jochum, B. Otto-Bliesner, C. A. Shields, and S. Yeager, 2015: Stochastic atmospheric forcing as a cause of Greenland climate transitions. *Journal of Climate*, **28**, 7741–7763.

Krabill, W., W. Abdalati, E. Frederick, S. Manizade, C. Martin, J. Sonntag, R. Swift, R. Thomas, W. Wright, and J. Yungel, 2000: Greenland ice sheet: High-elevation balance and peripheral thinning. *Science*, **289**, 428–430.

Krabill, W., E. Frederick, S. Manizade, C. Martin, J. Sonntag, R. Swift, R. Thomas, W. Wright, and J. Yungel, 1999: Rapid thinning of parts of the southern Greenland ice sheet. *Science*, **283**, 1522–1524.

Kuhlbrodt, T., A. Griesel, M. Montoya, A. Levermann, M. Hofmann, and S. Rahmstorf, 2007: On the driving processes of the Atlantic meridional overturning circulation. *Reviews of Geophysics*, **45**.

Landais, A., J. Barnola, V. Masson-Delmotte, J. Jouzel, J. Chappellaz, N. Caillon, C. Huber, M. Leuenberger, and S. J. Johnsen, 2004: A continuous record of temperature evolution over a sequence of Dansgaard-Oeschger events during Marine Isotopic Stage 4 (76 to 62 kyr BP). *Geophysical Research Letters*, **31**.

Langebroek, P. M. and K. H. Nisancioglu, 2016: Moderate Greenland ice sheet melt during the last interglacial constrained by present-day observations and paleo ice core reconstructions. *The Cryosphere Discussions*, 1–35, doi:10.5194/tc-2016-15.

Langehaug, H. R., I. Medhaug, T. Eldevik, and O. H. Otterå, 2012: Arctic/Atlantic exchanges via the subpolar gyre. *Journal of Climate*, **25**, 2421–2439.

Larsen, N. K., L. B. Levy, A. E. Carlson, C. Buizert, J. Olsen, A. Strunk, A. A. Bjørk, and D. S. Skov, 2018: Instability of the Northeast Greenland Ice Stream over the last 45,000 years. *Nature Communications*, **9**, 1872.

Larsen, S. H., S. A. Khan, A. P. Ahlstrøm, C. S. Hvidberg, M. J. Willis, and S. B. Andersen, 2016: Increased mass loss and asynchronous behavior of marine-terminating outlet glaciers at Upernavik Isstrøm, NW Greenland. *Journal of Geophysical Research: Earth Surface*, **121**, 241–256.

Laske, G. and G. Masters, 1997: A global digital map of sediment thickness. *EOS Transactions American Geophysical Union*, **78**, F483.

URL https://igppweb.ucsd.edu/~gabi/sediment.html

Le Meur, E. and P. Huybrechts, 1996: A comparison of different ways of dealing with isostasy: examples from modeling the Antarctic ice sheet during the last glacial cycle. *Annals of Glaciology*, **23**, 309–317.

Lea, J. M., D. W. Mair, F. M. Nick, B. R. Rea, A. Weidick, K. H. Kjaer, M. Morlighem, D. Van As, and J. E. Schofield, 2014: Terminus-driven retreat of a major southwest Greenland tidewater glacier during the early 19th century: insights from glacier reconstructions and numerical modelling. *Journal of Glaciology*, **60**, 333–344.

Lecavalier, B. S., D. A. Fisher, G. A. Milne, B. M. Vinther, L. Tarasov, P. Huybrechts, D. Lacelle, B. Main, J. Zheng, J. Bourgeois, and A. S. Dyke, 2017: High Arctic Holocene temperature record from the Agassiz ice cap and Greenland ice sheet evolution. *Proceedings of the National Academy of Sciences*, **1**, 1–6, doi:10.1073/pnas.1616287114.

Lecavalier, B. S., G. A. Milne, M. J. Simpson, L. Wake, P. Huybrechts, L. Tarasov, K. K. Kjeldsen, S. Funder, A. J. Long, S. Woodroffe, A. S. Dykei, and N. K. Larsen, 2014: A model of Greenland ice sheet deglaciation constrained by observations of relative sea level and ice extent. *Quaternary Science Reviews*, **102**, 54–84, doi:10.1016/j.quascirev.2014.07.018.

Li, C., D. S. Battisti, and C. M. Bitz, 2010: Can North Atlantic sea ice anomalies account for Dansgaard–Oeschger climate signals? *Journal of Climate*, **23**, 5457–5475.

Li, C., D. S. Battisti, D. P. Schrag, and E. Tziperman, 2005: Abrupt climate shifts in Greenland due to displacements of the sea ice edge. *Geophysical Research Letters*, **32**.

Lisiecki, L. E. and M. E. Raymo, 2005: A Pliocene-Pleistocene stack of 57 globally distributed benthic δ^{18}O records. *Paleoceanography*, **20**.

Little, C. M., D. Goldberg, A. Gnanadesikan, and M. Oppenheimer, 2012: On the coupled response to ice-shelf basal melting. *Journal of Glaciology*, **58**, 203–215.

Liu, Y., J. C. Moore, X. Cheng, R. M. Gladstone, J. N. Bassis, H. Liu, J. Wen, and F. Hui, 2015: Ocean-driven thinning enhances iceberg calving and retreat

of Antarctic ice shelves. *Proceedings of the National Academy of Sciences*, 201415137.

Liu, Z., B. Otto-Bliesner, F. He, E. Brady, R. Tomas, P. Clark, A. Carlson, J. Lynch-Stieglitz, W. Curry, E. Brook, et al., 2009: Transient simulation of last deglaciation with a new mechanism for Bølling-Allerød warming. *Science*, **325**, 310–314.

Loulergue, L., A. Schilt, R. Spahni, V. Masson-Delmotte, T. Blunier, B. Lemieux, J.-M. Barnola, D. Raynaud, T. F. Stocker, and J. Chappellaz, 2008: Orbital and millennial-scale features of atmospheric CH_4 over the past 800,000 years. *Nature*, **453**, 383.

Luckman, A. and T. Murray, 2005: Seasonal variation in velocity before retreat of Jakobshavn Isbræ, Greenland. *Geophysical Research Letters*, **32**.

Lunt, D. J., G. L. Foster, A. M. Haywood, and E. J. Stone, 2008: Late Pliocene Greenland glaciation controlled by a decline in atmospheric CO_2 levels. *Nature*, **454**, 1102.

Lynch-Stieglitz, J., 2017: The Atlantic meridional overturning circulation and abrupt climate change. *Annual review of marine science*, **9**, 83–104.

Mac Ayeal, D. R., 1989: Large-scale ice flow over a viscous basal sediment: theory and application to ice stream B, Antarctica. *Journal of Geiphysical Research*, **94**, 4071–4087.

Marcott, S. A., P. U. Clark, L. Padman, G. P. Klinkhammer, S. R. Springer, Z. Liu, B. L. Otto-Bliesner, A. E. Carlson, A. Ungerer, J. Padman, et al., 2011: Ice-shelf collapse from subsurface warming as a trigger for Heinrich events. *Proceedings of the National Academy of Sciences*, **108**, 13415–13419.

MARGO, P. m., 2009: Constraints on the magnitude and patterns of ocean cooling at the Last Glacial Maximum. *Nature Geoscience*, **2**, 127–132, doi:10.1038/ngeo411.

Marshall, S. J. and M. R. Koutnik, 2006: Ice sheet action versus reaction: Distinguishing between Heinrich events and Dansgaard-Oeschger cycles in the North Atlantic. *Paleoceanography*, **21**.

Mayer, C., J. Schaffer, T. Hattermann, D. Floricioiu, L. Krieger, P. A. Dodd, T. Kanzow, C. Licciulli, and C. Schannwell, 2018: Large ice loss variability at

Nioghalvfjerdsfjorden Glacier, Northeast-Greenland. *Nature Communications*, **9**, 2768.

McFarlin, J. M., Y. Axford, M. R. Osburn, M. A. Kelly, E. C. Osterberg, and L. B. Farnsworth, 2018: Pronounced summer warming in northwest Greenland during the Holocene and Last Interglacial. *Proceedings of the National Academy of Sciences*, 201720420.

McKay, M. D., R. J. Beckman, and W. J. Conover, 1979: Comparison of three methods for selecting values of input variables in the analysis of output from a computer code. *Technometrics*, **21**, 239–245.

Menviel, L., A. Timmermann, T. Friedrich, and M. England, 2014: Hindcasting the continuum of Dansgaard–Oeschger variability: mechanisms, patterns and timing. *Climate of the Past*, **10**, 63–77.

Mignot, J., A. Ganopolski, and A. Levermann, 2007: Atlantic subsurface temperatures: Response to a shutdown of the overturning circulation and consequences for its recovery. *Journal of Climate*, **20**, 4884–4898.

Mikkelsen, T. B., A. Grinsted, and P. Ditlevsen, 2018: Influence of temperature fluctuations on equilibrium ice sheet volume. *The Cryosphere*, **12**, 39–47.

Millan, R., E. Rignot, J. Mouginot, M. Wood, A. A. Bjørk, and M. Morlighem, 2018: Vulnerability of Southeast Greenland Glaciers to Warm Atlantic Water From Operation IceBridge and Ocean Melting Greenland Data. *Geophysical Research Letters*.

Mitrovica, J. X., M. E. Tamisiea, J. L. Davis, and G. A. Milne, 2001: Recent mass balance of polar ice sheets inferred from patterns of global sea-level change. *Nature*, **409**, 1026.

Montoya, M. and A. Levermann, 2008: Surface wind-stress threshold for glacial Atlantic overturning. *Geophysical Research Letters*, **35**, L03608, doi:10.1029/2007GL032560.

Moon, T. and I. Joughin, 2008: Changes in ice front position on Greenland's outlet glaciers from 1992 to 2007. *Journal of Geophysical Research: Earth Surface*, **113**.

Moon, T., I. Joughin, and B. Smith, 2015: Seasonal to multiyear variability of glacier surface velocity, terminus position, and sea ice/ice mélange in northwest

Greenland. *Journal of Geophysical Research: Earth Surface*, **120**, 818–833.

Morland, L., 1984: Thermomechanical balances of ice sheet flows. *Geophysical & Astrophysical Fluid Dynamics*, **29**, 237–266.

Morlighem, M., J. Bondzio, H. Seroussi, E. Rignot, E. Larour, A. Humbert, and S. Rebuffi, 2016: Modeling of Store Gletscher's calving dynamics, West Greenland, in response to ocean thermal forcing. *Geophysical Research Letters*, **43**, 6, doi:10.1002/2016GL067695.

Morlighem, M., C. N. Williams, E. Rignot, L. An, J. E. Arndt, J. L. Bamber, G. Catania, N. Chauché, J. A. Dowdeswell, B. Dorschel, et al., 2017: BedMachine v3: Complete bed topography and ocean bathymetry mapping of Greenland from multibeam echo sounding combined with mass conservation. *Geophysical Research Letters*, **44**.

Motyka, R. J., M. Truffer, M. Fahnestock, J. Mortensen, S. Rysgaard, and I. Howat, 2011: Submarine melting of the 1985 Jakobshavn Isbrae floating tongue and the triggering of the current retreat. *Journal of Geophysical Research*, **116**, F01007, doi:10.1029/2009JF001632.

Mouginot, J., E. Rignot, B. Scheuchl, I. Fenty, A. Khazendar, M. Morlighem, A. Buzzi, and J. Paden, 2015: Fast retreat of Zachariæ Isstrøm, northeast Greenland. *Science*, **350**, 1357–1361.

Münchow, A., L. Padman, and H. A. Fricker, 2014: Interannual changes of the floating ice shelf of Petermann Gletscher, North Greenland, from 2000 to 2012. *Journal of Glaciology*, **60**, 489–499, doi:10.3189/2014JoG13J135.

Murray, T., K. Scharrer, N. Selmes, A. Booth, T. James, S. Bevan, J. Bradley, S. Cook, L. C. Llana, Y. Drocourt, et al., 2015: Extensive retreat of Greenland tidewater glaciers, 2000–2010. *Arctic, Antarctic, and Alpine research*, **47**, 427–447.

NEEM, 2013: Eemian interglacial reconstructed from a Greenland folded ice core. *Nature*, **493**, 489–494, doi:10.1038/nature11789.

Nick, F. M., A. Vieli, I. M. Howat, and I. Joughin, 2009: Large-scale changes in Greenland outlet glacier dynamics triggered at the terminus. *Nature Geoscience*, **2**, 110–114, doi:10.1038/ngeo394.

Nowicki, S., R. A. Bindschadler, A. Abe-Ouchi, A. Aschwanden, E. Bueler, H. Choi, J. Fastook, G. Granzow, R. Greve, and G. Gutowski, 2013: Large-scale changes in Greenland outlet glacier dynamics triggered at the terminus. *Journal of Geophysical Research: Earth Surface*, **118**, 1025–1044, doi:10.1002/jgrf.20076.

Oeschger, H., J. Beer, U. Siegenthaler, B. Stauffer, W. Dansgaard, and C. Langway, 1983: Late-glacial climate history from ice cores. *Palaeoclimatic Research and Models*, Springer, 95–107.

Otto-Bliesner, B. L., S. J. Marshall, J. T. Overpeck, G. H. Miller, A. Hu, et al., 2006: Simulating Arctic climate warmth and icefield retreat in the last interglaciation. *Science*, **311**, 1751–1753.

Paillard, D., 2015: Quaternary glaciations: from observations to theories. *Quaternary Science Reviews*, **107**, 11–24.

Pattyn, F., 2017: Sea-level response to melting of antarctic ice shelves on multi-centennial time scales with the fast Elementary Thermomechanical Ice Sheet model (f.ETISh v1.0). *The Cryosphere*, **8**, 1–52, doi:10.5194/tc-2017-8.

Pattyn, F., C. Schoof, L. Perichon, R. Hindmarsh, E. Bueler, B. De Fleurian, G. Durand, O. Gagliardini, R. Gladstone, D. Goldberg, et al., 2012: Results of the marine ice sheet model intercomparison project, MISMIP. *The Cryosphere*, **6**, 573–588.

Peano, D., F. Colleoni, A. Quiquet, and S. Masina, 2017: Ice flux evolution in fast flowing areas of the Greenland ice sheet over the 20th and 21st centuries. *Journal of Glaciology*, **63**, 499–513.

Peltier, W. R. and G. Vettoretti, 2014: Dansgaard-Oeschger oscillations predicted in a comprehensive model of glacial climate: A kicked salt oscillator in the Atlantic. *Geophysical Research Letters*, **41**, 7306–7313.

Petersen, S. V., D. P. Schrag, and P. U. Clark, 2013: A new mechanism for Dansgaard-Oeschger cycles. *Paleoceanography*, **28**, 24–30.

Peyaud, V., C. Ritz, and G. Krinner, 2007: Modelling the Early Weichselian Eurasian Ice Sheets: role of ice shelves and influence of ice-dammed lakes. *Climate of the Past*, **3**, 375–386.

Philippon, G., G. Ramstein, S. Charbit, M. Kageyama, C. Ritz, and C. Dumas, 2006: Evolution of the Antarctic ice sheet throughout the last deglaciation: A study with a new coupled climatenorth and south hemisphere ice sheet model. *Earth and Planetary Science Letters*, **248**, 750–758, doi:10.1016/j.epsl.2006.06.017.

Piotrowski, A. M., S. L. Goldstein, R. H. Sidney, R. G. Fairbanks, and D. R. Zylberberg, 2008: Oscillating glacial northern and southern deep water formation from combined neodymium and carbon isotopes. *Earth and Planetary Science Letters*, **272**, 394–405.

Pollard, D., W. Chang, M. Haran, P. Applegate, and R. DeConto, 2016: Large ensemble modeling of the last deglacial retreat of the West Antarctic Ice Sheet: comparison of simple and advanced statistical techniques. *Geoscientific Model Development*, **9**, 1697–1723, doi:10.5194/gmd-9-1697-2016.

Pollard, D. and R. M. DeConto, 2012: Description of a hybrid ice sheet-shelf model, and application to Antarctica. *Geoscientific Model Development*, **5**, 1273–1295, doi:10.5194/gmd-5-1273-2012.

Pritchard, H. D., S. R. M. Ligtenberg, H. A. Fricker, D. G. Vaughan, M. R. Van den Broeke, and L. Padman, 2012: Antarctic ice-sheet loss driven by basal melting of ice shelves. *Nature*, **484**, 502–505, doi:10.1038/nature10968.

Quiquet, A., H. Punge, C. Ritz, X. Fettweis, M. Kageyama, G. Krinner, D. Salas y Mélia, and J. Sjolte, 2012: Sensitivity of a Greenland ice sheet model to atmospheric forcing fields. *The Cryosphere*, **6**, 999–1018, doi:10.5194/tc-6-999-2012.

Quiquet, A., C. Ritz, H. J. Punge, and D. Salas y Mélia, 2013: Greenland Ice Sheet contribution to sea level rise during the last geoscientific interglacial period: a modelling study driven and instrumentation constrained by methods and ice core data. *Climate of the Past*, **9**, 353–366, doi:10.5194/cp-9-353-2013.

Rahmstorf, S., 2002: Ocean circulation and climate during the past 120,000 years. *Nature*, **419**, 207.

Rasmussen, T. L. and E. Thomsen, 2004: The role of the North Atlantic Drift in the millennial timescale glacial climate fluctuations. *Palaeogeography, Palaeoclimatology, Palaeoecology*, **210**, 101–116.

Rasmussen, T. L., E. Thomsen, L. Labeyrie, and T. C. van Weering, 1996: Circulation changes in the Faeroe-Shetland Channel correlating with cold events during the last glacial period (58–10 ka). *Geology*, **24**, 937–940.

Rasmussen, T. L., E. Thomsen, and M. Moros, 2016: North Atlantic warming during Dansgaard-Oeschger events synchronous with Antarctic warming and out-of-phase with Greenland climate. *Scientific Reports*, **6**, 20535.

Rathmann, N., C. Hvidberg, A. Solgaard, A. Grinsted, G. H. Gudmundsson, P. L. Langen, K. Nielsen, and A. Kusk, 2017: Highly temporally resolved response to seasonal surface melt of the Zachariae and 79N outlet glaciers in northeast Greenland. *Geophysical Research Letters*, **44**, 9805–9814.

Reeh, N., 1989: Parameterization of melt rate and surface temperature on the Greenland ice sheet. *Polarforschung*, **59**, 113–128.

Reese, R., T. Albrecht, M. Mengel, X. Asay-Davis, and R. Winkelmann, 2018: Antarctic sub-shelf melt rates via PICO. *The Cryosphere*, **12**, 1969–1985.

Rhodes, R. H., E. J. Brook, J. C. Chiang, T. Blunier, O. J. Maselli, J. R. McConnell, D. Romanini, and J. P. Severinghaus, 2015: Enhanced tropical methane production in response to iceberg discharge in the North Atlantic. *Science*, **348**, 1016–1019.

Rignot, E., G. Casassa, P. Gogineni, W. Krabill, A. u. Rivera, and R. Thomas, 2004: Accelerated ice discharge from the Antarctic Peninsula following the collapse of Larsen B ice shelf. *Geophysical Research Letters*, **31**, L18401, doi:10.1029/2004GL020697.

Rignot, E., S. Jacobs, J. Mouginot, and B. Scheuchl, 2013: Ice-shelf melting around Antarctica. *Science*, **341(6143)**, 266–270, doi:10.1126/science.1235798.

Rignot, E. and S. S. Jacobs, 2002: Rapid bottom melting widespread near Antarctic Ice Sheet grounding lines. *Science*, **296**, 2020–2023, doi:10.1126/science.1070942.

Rignot, E. and P. Kanagaratnam, 2006: Changes in the velocity structure of the Greenland Ice Sheet. *Science*, **311(5763)**, 986–990, doi:10.1126/science.1121381.

Rignot, E., M. Koppes, and I. Velicogna, 2010: Rapid submarine melting of the calving faces of West Greenland glaciers. *Nature Geoscience*, **3**, 187–191, doi:10.1038/ngeo765.

Rignot, E. and J. Mouginot, 2012: Ice flow in Greenland for the international polar year 2008–2009. *Geophysical Research Letters*, **39**.

Rignot, E., J. Mouginot, M. Morlighem, H. Seroussi, and B. Scheuchl, 2014: Widespread, rapid grounding line retreat of Pine Island, Thwaites, Smith, and Kohler glaciers, West Antarctica, from 1992 to 2011. *Geophysical Research Letters*, **41, 10**, 3502–3509, doi:10.1002/2014GL060140.

Rignot, E. and K. Steffen, 2008: Channelized bottom melting and stability of floating ice shelves. *Geophysical Research Letters*, **35**, L02503.

Rignot, E., I. Velicogna, M. R. Van den Broeke, A. Monaghan, and J. T. M. Lenaerts, 2011: Acceleration of the contribution of the Greenland and Antarctic ice sheets to sea level rise. *Geophysical Research Letters*, **38**, L05503, doi:10.1029/2011GL046583.

Rignot, E., Y. Xu, D. Menemenlis, J. Mouginot, B. Scheuchl, X. Li, M. Morlighem, H. Seroussi, M. v. Broeke, I. Fenty, C. Cai, L. An, and B. de Fleurian, 2016: Modeling of ocean-induced ice melt rates of five west Greenland glaciers over the past two decades. *Geophysical Research Letters*, **43**, 6374–6382, doi:10.1002/2016GL068784.

Ritz, C., A. Fabre, and A. Letréguilly, 1996: Sensitivity of a greenland ice sheet model to ice flow and ablation parameters: consequences for the evolution through the last climatic cycle. *Climate Dynamics*, **13**, 11–23.

Ritz, C., V. Rommelaere, and C. Dumas, 2001: Modeling the evolution of Antarctic Ice Sheet over the last 420,000 years. implications for altitude changes in the Vostok region. *Journal of Geophysical Research*, **106(D23)**, 31943–31964, doi:10.1029/2001JD900232.

Robinson, A., J. Alvarez-Solas, R. Calov, A. Ganopolski, and M. Montoya, 2017: MIS-11 duration key to disappearance of the Greenland ice sheet. *Nature Communications*, **8**, 16008.

Robinson, A., R. Calov, and A. Ganopolski, 2011: Greenland ice sheet model parameters constrained using simulations of the Eemian Interglacial. *Climate*

of the Past, **7**, 381–396, doi:10.5194/cp-7-381-2011.

Robinson, A. and H. Goelzer, 2014: The importance of insolation changes for paleo ice sheet modeling. *The Cryosphere*, **8**, 1419–1428, doi:10.5194/tc-8-1419-2014.

Ruddiman, W. F., 1977: Late Quaternary deposition of ice-rafted sand in the subpolar North Atlantic (lat 40 to 65 N). *Geological Society of America Bulletin*, **88**, 1813–1827.

Sachs, J. P. and S. J. Lehman, 1999: Subtropical North Atlantic temperatures 60,000 to 30,000 years ago. *Science*, **286**, 756–759.

Sasgen, I., M. van den Broeke, J. L. Bamber, E. Rignot, L. S. Sørensen, B. Wouters, Z. Martinec, I. Velicogna, and S. B. Simonsen, 2012: Timing and origin of recent regional ice-mass loss in Greenland. *Earth and Planetary Science Letters*, **333-334**, 293–303, doi:10.1016/j.epsl.2012.03.033.

Schaffer, J., R. Timmermann, J. E. Arndt, S. S. Kristensen, C. Mayer, M. Morlighem, and D. Steinhage, 2016: A global, high-resolution data set of ice sheet topography, cavity geometry, and ocean bathymetry. *Earth Systm Scientific Data*, **8**, 543–557.

Schaffer, J., W.-J. von Appen, P. A. Dodd, C. Hofstede, C. Mayer, L. de Steur, and T. Kanzow, 2017: Warm water pathways toward Nioghalvfjerdsfjorden Glacier, northeast Greenland. *Journal of Geophysical Research: Oceans*, **122**, 4004–4020.

Schmittner, A., O. Saenko, and A. Weaver, 2003: Coupling of the hemispheres in observations and simulations of glacial climate change. *Quaternary Science Reviews*, **22**, 659–671.

Schoof, C., 2007: Ice sheet grounding line dynamics: steady states, stability, and hysteresis. *Journal of Geophysical Research*, **112**, F03S28, doi:10.1029/2006JF000664.

Schulz, M., 2002: On the 1470-year pacing of Dansgaard-Oeschger warm events. *Paleoceanography*, **17**, 4–1.

Schüpbach, S., U. Federer, P. Kaufmann, S. Albani, C. Barbante, T. Stocker, and H. Fischer, 2013: High-resolution mineral dust and sea ice proxy records from the Talos Dome ice core. *Climate of the Past*, **9**, 2789–2807.

Schüpbach, S., H. Fischer, M. Bigler, T. Erhardt, G. Gfeller, D. Leuenberger, O. Mini, R. Mulvaney, N. J. Abram, L. Fleet, et al., 2018: Greenland records of aerosol source and atmospheric lifetime changes from the Eemian to the Holocene. *Nature Communications*, **9**, 1476.

Sciascia, R., F. Straneo, C. Cenedese, and P. Heimbach, 2013: Seasonal variability of submarine melt rate and circulation in an East Greenland fjord. *Journal of Geophysical Research: Oceans*, **118**, 2492–2506, doi:10.1002/jgrc.20142.

Scourse, J. D., I. R. Hall, I. N. McCave, J. R. Young, and C. Sugdon, 2000: The origin of Heinrich layers: evidence from H_2 for European precursor events. *Earth and Planetary Science Letters*, **182**, 187–195.

Sévellec, F. and A. V. Fedorov, 2015: Unstable AMOC during glacial intervals and millennial variability: The role of mean sea ice extent. *Earth and Planetary Science Letters*, **429**, 60–68.

Shackleton, N. J., M. A. Hall, and E. Vincent, 2000: Phase relationships between millennial-scale events 64,000–24,000 years ago. *Paleoceanography*, **15**, 565–569.

Shaffer, G., S. M. Olsen, and C. J. Bjerrum, 2004: Ocean subsurface warming as a mechanism for coupling Dansgaard-Oeschger climate cycles and ice-rafting events. *Geophysical Research Letters*, **31**.

Shapiro, N. M. and M. H. Ritzwoller, 2004: Inferring surface heat flux distributions guided by a global seismic model: particular application to Antarctica. *Earth and Planetary Science Letters*, **223**, 213–224, doi:10.1016/j.epsl.2004.04.011.

Shepherd, A., E. R. Ivins, A. Geruo, V. R. Barletta, M. J. Bentley, S. Bettadpur, K. H. Briggs, D. H. Bromwich, R. Forsberg, N. Galin, M. Horwath, S. Jacobs, I. Joughin, M. A. King, J. T. M. Lenaerts, J. Li, S. R. M. Ligtenberg, A. Luckman, S. B. Luthcke, M. McMillan, R. Meister, G. Milne, J. Mouginot, A. Muir, J. P. Nicolas, J. Paden, A. J. Payne, H. Pritchard, E. Rignot, H. Rott, L. Sandberg Sorensen, T. A. Scambos, B. Scheuchl, E. J. O. Schrama, B. Smith, A. V. Sundal, J. H. van Angelen, W. J. van de Berg, M. R. van den Broeke, D. G. Vaughan, I. Velicogna, J. Wahr, P. L. Whitehouse, D. J. Wingham, D. Yi, D. Young, and H. J. Zwally, 2012: A reconciled estimate of ice sheet mass

balance. *Science*, **338**, 1183–1189, doi:10.1126/science.1228102.

Shepherd, A., D. Wingham, and E. Rignot, 2004: Warm ocean is eroding West Antarctic ice sheet. *Geophysical Research Letters*, **31**, L23402, doi:10.1029/2004GL021106.

Simpson, M. J. R., G. A. Milne, P. Huybrechts, and A. J. Long, 2009: Calibrating a glaciological model of the greenland ice sheet from the Last Glacial Maximum to present-day using field observations of relative sea level and ice extent. *Quat. Science Rev.*, **28(17)**, 1631–1657, doi:10.1016/j.quascirev.2009.03.004.

Skinner, L. and H. Elderfield, 2007: Rapid fluctuations in the deep North Atlantic heat budget during the last glacial period. *Paleoceanography*, **22**.

Slater, D. A., F. Straneo, S. B. Das, T. J. W. Richards, C. G.and Wagner, and P. W. Nienow, 2018: Localized plumes drive front-wide ocean melting of a Greenlandic tidewater glacier. *Geophysical Research Letters*, doi:10.1029/2018gl080763.

Stearns, L. A. and G. S. Hamilton, 2007: Rapid volume loss from two East Greenland outlet glaciers quantified using repeat stereo satellite imagery. *Geophysical Research Letters*, **34**, L05503, doi:10.1029/2006GL028982.

Steffensen, J. P., K. K. Andersen, M. Bigler, H. B. Clausen, D. Dahl-Jensen, H. Fischer, K. Goto-Azuma, M. Hansson, S. J. Johnsen, J. Jouzel, et al., 2008: High-resolution Greenland ice core data show abrupt climate change happens in few years. *Science*, **321**, 680–684.

Stein, R., S.-i. Nam, H. Grobe, and H. Hubberten, 1996: Late Quaternary glacial history and short-term ice-rafted debris fluctuations along the East Greenland continental margin. *Geological Society, London, Special Publications*, **111**, 135–151.

Stocker, T. F. and S. J. Johnsen, 2003: A minimum thermodynamic model for the bipolar seesaw. *Paleoceanography*, **18**.

Stockhecke, M., M. Sturm, I. Brunner, H.-U. Schmincke, M. Sumita, R. Kipfer, D. Cukur, O. Kwiecien, and F. S. Anselmetti, 2014: Sedimentary evolution and environmental history of Lake Van (Turkey) over the past 600000 years. *Sedimentology*, **61**, 1830–1861.

Stommel, H., 1961: Thermohaline convection with two stable regimes of flow. *Tellus*, **13**, 224–230.

Stone, E., D. Lunt, J. Annan, and J. Hargreaves, 2013: Quantification of the Greenland ice sheet contribution to Last Interglacial sea level rise. *Climate of the Past*, **9**, 621–639, doi:10.5194/cp-9-621-2013.

Stone, E. J., D. J. Lunt, I. C. Rutt, and E. Hanna, 2010: Investigating the sensitivity of numerical model simulations of the modern state of the Greenland ice-sheet and its future response to climate change. *The Cryosphere*, **4**, 397–417, doi:10.5194/tc-4-397-2010.

Stouffer, R. J., J. Yin, J. Gregory, K. Dixon, M. Spelman, W. Hurlin, A. Weaver, M. Eby, G. Flato, H. Hasumi, et al., 2006: Investigating the causes of the response of the thermohaline circulation to past and future climate changes. *Journal of Climate*, **19**, 1365–1387.

Straneo, F., G. S. Hamilton, L. A. Stearns, and D. A. Sutherland, 2016: Connecting the Greenland Ice Sheet and the ocean: a case study of Helheim Glacier and Sermilik Fjord. *Oceanography*, **29 (4)**, 22–33, doi:10.5670/oceanog.2016.97.

Straneo, F., G. S. Hamilton, D. A. Sutherland, L. A. Stearns, F. Davidson, M. O. Hammill, G. B. Stenson, and A. Rosing-Asvid, 2010: Rapid circulation of warm subtropical waters in a major glacial fjord in East Greenland. *Nature Geoscience*, **3**, 182–186, doi:10.1038/ngeo764.

Straneo, F. and P. Heimbach, 2013: North Atlantic warming and the retreat of Greenlands outlet glaciers. *Nature*, **504**, 36–43, doi:10.1038/nature12854.

Straneo, F., D. A. Sutherland, D. Holland, C. Gladish, G. S. Hamilton, H. L. Johnson, E. Rignot, Y. Xu, and M. Koppes, 2012: Characteristics of ocean waters reaching Greenland's glaciers. *Annnual of Glaciology*, **53(60)**, 202–210, doi:10.3189/2012AoG60A059.

Sutherland, D. A. and F. Straneo, 2012: Estimating ocean heat transports and submarine melt rates in Sermilik Fjord, Greenland, using lowered acoustic Doppler current profiler (LADCP) velocity profiles. *Annuals of Glaciology*, **53(60)**, 50–58, doi:10.3189/2012AoG60A050.

Tabone, I., J. Blasco, A. Robinson, J. Alvarez-Solas, and M. Montoya, 2018a: The sensitivity of the Greenland Ice Sheet to glacial–interglacial oceanic forcing.

Climate of the Past, **14**, 455–472, doi:https://doi.org/10.5194/cp-14-455-2018.

Tabone, I., A. Robinson, J. Alvarez-Solas, and M. Montoya, 2018b: Impact of millennial-scale oceanic variability on the Greenland Ice Sheet evolution throughout the Last Glacial Period. *Climate of the Past Discussions*, doi:https://doi.org/10.5194/cp-2018-129, in review.

Tabone, I., A. Robinson, J. Alvarez-Solas, and M. Montoya, 2018c: Submarine melt rate as a potential trigger of grounding-line retreat during Marine Isotope Stage 3. *submitted to The Cryosphere*.

Tarasov, L. and R. W. Peltier, 2002: Greenland glacial history and local geodynamic consequences. *Geophysical Journal International*, **150**, 198–229.

Tedesco, M., S. Doherty, X. Fettweis, P. Alexander, J. Jeyaratnam, and J. Stroeve, 2016: The darkening of the Greenland ice sheet: trends, drivers, and projections (1981-2100). *The Cryosphere*, **10**, 477–496, doi:10.5194/tc-10-477-2016.

Tedesco, M., X. Fettweis, M. Van den Broeke, R. Van de Wal, C. Smeets, W. J. van de Berg, M. Serreze, and J. Box, 2011: The role of albedo and accumulation in the 2010 melting record in Greenland. *Environmental Research Letters*, **6**, 014005.

van den Broeke, M. R., E. M. Enderlin, I. M. Howat, and B. P. Y. Noël, 2016: On the recent contribution of the Greenland ice sheet to sea level change. *The Cryosphere*, **10**, 1933–1946, doi:10.5194/tc-2016-123.

Van Kreveld, S., M. Sarnthein, H. Erlenkeuser, P. Grootes, S. Jung, M. Nadeau, U. Pflaumann, and A. Voelker, 2000: Potential links between surging ice sheets, circulation changes, and the dansgaard-oeschger cycles in the irminger sea, 60–18 kyr. *Paleoceanography*, **15**, 425–442.

Vasskog, K., P. M. Langebroek, J. T. Andrews, J. E. Nilsen, and A. Nesje, 2015: The greenland ice sheet during the last glacial cycle: Current ice loss and contribution to sea-level rise from a palaeoclimatic perspective. *Earth-Science Reviews*, **150**, 45–67.

Vaughan, D. G., J. C. Comiso, I. Allison, J. Carrasco, G. Kaser, R. Kwok, P. Mote, T. Murray, F. Paul, J. Ren, E. Rignot, O. Solomina, K. Steffen, and T. Zhang, 2013: Observations: cryosphere. *Climate Change 2013: The Physi-*

cal Science Basis. Contribution of Working Group I to the Fifth Assessment Report of the Intergovernmental Panel on Climate Change .

Velicogna, I., T. Sutterley, and M. Van Den Broeke, 2014: Regional acceleration in ice mass loss from Greenland and Antarctica using GRACE time-variable gravity data. *Geophysical Research Letters*, **41**, 8130–8137.

Vellinga, M. and R. A. Wood, 2002: Global climatic impacts of a collapse of the Atlantic thermohaline circulation. *Climatic Change*, **54**, 251–267.

Verplanck, E. P., G. L. Farmer, J. Andrews, G. Dunhill, and C. Millo, 2009: Provenance of Quaternary glacial and glacimarine sediments along the southeast Greenland margin. *Earth and Planetary Science Letters*, **286**, 52–62.

Vettoretti, G. and W. R. Peltier, 2015: Interhemispheric air temperature phase relationships in the nonlinear Dansgaard-Oeschger oscillation. *Geophysical Research Letters*, **42**, 1180–1189.

Vettoretti, G. and W. R. Peltier, 2016: Thermohaline instability and the formation of glacial North Atlantic super polynyas at the onset of Dansgaard-Oeschger warming events. *Geophysical Research Letters*, **43**, 5336–5344.

Vettoretti, G. and W. R. Peltier, 2018: Fast Physics and Slow Physics in the Nonlinear Dansgaard–Oeschger Relaxation Oscillation. *Journal of Climate*, **31**, 3423–3449.

Vieli, A. and F. M. Nick, 2011: Understanding and modelling rapid dynamic changes of tidewater outlet glaciers: issues and implications. *Surveys in Geophysics*, **32**, 437–458, doi:10.1007/s10712-011-9132-4.

Vinther, B. M., S. L. Buchardt, H. B. Clausen, D. Dahl-Jensen, S. J. Johnsen, D. Fisher, R. Koerner, D. Raynaud, V. Lipenkov, K. Andersen, et al., 2009: Holocene thinning of the Greenland ice sheet. *Nature*, **461**, 385–388, doi:10.1038/nature08355.

Voelker, A. H., 2002: Global distribution of centennial-scale records for Marine Isotope Stage (MIS) 3: a database. *Quaternary Science Reviews*, **21**, 1185–1212.

Voelker, A. H. and H. Haflidason, 2015: Refining the Icelandic tephrachronology of the last glacial period–the deep-sea core PS2644 record from the southern Greenland Sea. *Global and Planetary Change*, **131**, 35–62.

Voelker, A. H., M. Sarnthein, P. M. Grootes, H. Erlenkeuser, C. Laj, A. Mazaud, M.-J. Nadeau, and M. Schleicher, 1997: Correlation of marine ^{14}C ages from the Nordic Seas with the GISP2 isotope record: Implications for ^{14}C calibration beyond 25 ka BP. *Radiocarbon*, **40**, 517–534.

Waelbroeck, C., L. Labeyrie, E. Michel, J. C. Duplessy, J. McManus, K. Lambeck, E. Balbon, and M. Labracherie, 2002: Sea-level and deep water temperature changes derived from benthic foraminifera isotopic records. *Quaternary Science Reviews*, **21**, 295–305.

Wagner, J. D., J. E. Cole, J. W. Beck, P. J. Patchett, G. M. Henderson, and H. R. Barnett, 2010: Moisture variability in the southwestern United States linked to abrupt glacial climate change. *Nature Geoscience*, **3**, 110.

Wang, Z., X. Zhang, Z. Guan, B. Sun, X. Yang, and C. Liu, 2015: An atmospheric origin of the multi-decadal bipolar seesaw. *Scientific Reports*, **5**, 8909.

Weber, M., L. A. Mayer, C. Hillaire-Marcel, G. Bilodeau, F. Rack, R. Hiscott, and A. Aksu, 2001: Derivation of δ^{18}O from sediment core log data: Implications for millennial-scale climate change in the Labrador Sea. *Paleoceanography and Paleoclimatology*, **16**, 503–514.

Wilson, N., F. Straneo, and P. Heimbach, 2017: Submarine melt rates and mass balance for Greenlands remaining ice tongues. *The Cryosphere Discussions*, 1–17, doi:10.5194/tc-2017-99.

Winkelmann, D., W. Jokat, L. Jensen, and H.-W. Schenke, 2010: Submarine end moraines on the continental shelf off NE Greenland–Implications for Lateglacial dynamics. *Quaternary Science Reviews*, **29**, 1069–1077.

Winkelmann, R., M. A. Martin, M. Haseloff, T. Albrecht, E. Bueler, C. Khroulev, and A. Levermann, 2011: The Potsdam parallel ice sheet model (PISM-PIK)–Part 1: Model description. *The Cryosphere*, **5**, 715–726.

Winsor, K., A. E. Carlson, B. M. Welke, and B. Reilly, 2015: Early deglacial onset of southwestern Greenland ice-sheet retreat on the continental shelf. *Quaternary Science Reviews*, **128**, 117–126.

Wood, M., E. Rignot, I. Fenty, D. Menemenlis, R. Millan, M. Morlighem, J. Mouginot, and H. Seroussi, 2018: Ocean-induced melt triggers glacier retreat in Northwest Greenland. *Geophysical Research Letters*, **45**, 8334–8342.

Wouters, B., A. Martin-Español, V. Helm, T. Flament, J. van Wessem, S. Ligtenberg, M. van den Broeke, and J. Bamber, 2015: Dynamic thinning of glaciers on the Southern Antarctic Peninsula. *Science*, **348**, 899–903, doi:10.1126/science.aaa5727.

Xu, Y., E. Rignot, I. Fenty, D. Menemenlis, and M. Flexas, 2013: Subaqueous melting of Store Glacier, west Greenland from three-dimensional, high-resolution numerical modeling and ocean observations. *Geophysical Research Letters*, **40**, 4648–4653, doi:10.1002/grl.50825.

Xu, Y., E. Rignot, D. Menemenlis, and M. Koppes, 2012: Numerical experiments on subaqueous melting of Greenland tidewater glaciers in response to ocean warming and enhanced subglacial discharge. *Annals of Glaciology*, **53**, 229–234, doi:10.3189/2012AoG60A139.

Yau, A. M., M. L. Bender, T. Blunier, and J. Jouzel, 2016a: Setting a chronology for the basal ice at Dye-3 and GRIP: implications for the long-term stability of the Greenland Ice Sheet. *Earth and Planetary Science Letters*, **451**, 1–9.

Yau, A. M., M. L. Bender, A. Robinson, and E. J. Brook, 2016b: Reconstructing the last interglacial at Summit, Greenland: Insights from GISP2. *Proceedings of the National Academy of Sciences*, **113(35)**, 9710–9715, doi:10.1073/pnas.1524766113.

Yi, S., W. Sun, K. Heki, and A. Qian, 2015: An increase in the rate of global mean sea level rise since 2010. *Geophysical Research Letters*, **42**, 3998–4006, doi:10.1002/2015GL063902.

Zhang, X., G. Knorr, G. Lohmann, and S. Barker, 2017: Abrupt North Atlantic circulation changes in response to gradual CO_2 forcing in a glacial climate state. *Nature Geoscience*, **10**, 518.

Zhang, X., G. Lohmann, and C. Knorr, G.and Purcell, 2014a: Abrupt glacial climate shifts controlled by ice sheet changes. *Nature*, **3512**, 290.

Zhang, X., M. Prange, U. Merkel, and M. Schulz, 2014b: Instability of the Atlantic overturning circulation during Marine Isotope Stage 3. *Nature*, **3512**, 290.

Zwally, H. J., L. I. Jun, A. C. Brenner, M. Beckley, H. G. Cornejo, J. DiMarzio, M. B. Giovinetto, T. A. Neumann, J. Robbins, J. L. Saba, D. Yi, and W. Wang, 2011: Greenland ice sheet mass balance: distribution of increased mass loss with

climate warming; 2003-07 versus 1992-2002. *Journal of Glaciology*, **57(201)**, 88–102, doi:10.3189/002214311795306682.